uOttawa

L'Université canadienne
Canada's university

FACULTÉ DES ÉTUDES SUPÉRIEURES ET POSTOCTORALES

uOttawa

L'Université canadienne
Canada's university

FACULTY OF GRADUATE AND POSDOCTORAL STUDIES

Steven Horvath
AUTEUR DE LA THÈSE / AUTHOR OF THESIS

M.Sc. (Chemistry)
GRADE / DEGREE

Department of Chemistry
FACULTÉ, ÉCOLE, DÉPARTEMENT / FACULTY, SCHOOL, DEPARTMENT

Synthesis of Chromium Guanidinate Complexes and their Activity in Ethylene Oligomerization/Polymerization

TITRE DE LA THÈSE / TITLE OF THESIS

Sandro Gambarotta
DIRECTEUR (DIRECTRICE) DE LA THÈSE / THESIS SUPERVISOR

CO-DIRECTEUR (CO-DIRECTRICE) DE LA THÈSE / THESIS CO-SUPERVISOR

D. Fogg

M. Murugesu

Gary W. Slater
Le Doyen de la Faculté des études supérieures et postdoctorales / Dean of the Faculty of Graduate and Postdoctoral Studies

Synthesis of chromium guanidinate complexes and their activity in ethylene oligomerization/polymerization.

Steven Horvath

Candidate

Steven Horvath

Supervisor

Professor Sandro Gambarotta

Library and Archives Canada

Published Heritage Branch

395 Wellington Street
Ottawa ON K1A 0N4
Canada

Bibliothèque et Archives Canada

Direction du Patrimoine de l'édition

395, rue Wellington
Ottawa ON K1A 0N4
Canada

Your file Votre référence
ISBN: 978-0-494-66236-6
Our file Notre référence
ISBN: 978-0-494-66236-6

NOTICE:

The author has granted a non-exclusive license allowing Library and Archives Canada to reproduce, publish, archive, preserve, conserve, communicate to the public by telecommunication or on the Internet, loan, distribute and sell theses worldwide, for commercial or non-commercial purposes, in microform, paper, electronic and/or any other formats.

The author retains copyright ownership and moral rights in this thesis. Neither the thesis nor substantial extracts from it may be printed or otherwise reproduced without the author's permission.

AVIS:

L'auteur a accordé une licence non exclusive permettant à la Bibliothèque et Archives Canada de reproduire, publier, archiver, sauvegarder, conserver, transmettre au public par télécommunication ou par l'Internet, prêter, distribuer et vendre des thèses partout dans le monde, à des fins commerciales ou autres, sur support microforme, papier, électronique et/ou autres formats.

L'auteur conserve la propriété du droit d'auteur et des droits moraux qui protège cette thèse. Ni la thèse ni des extraits substantiels de celle-ci ne doivent être imprimés ou autrement reproduits sans son autorisation.

In compliance with the Canadian Privacy Act some supporting forms may have been removed from this thesis.

While these forms may be included in the document page count, their removal does not represent any loss of content from the thesis.

Conformément à la loi canadienne sur la protection de la vie privée, quelques formulaires secondaires ont été enlevés de cette thèse.

Bien que ces formulaires aient inclus dans la pagination, il n'y aura aucun contenu manquant.

Canada

©Steven Horvath, Ottawa, Canada, 2010

In memory of my Grandfather
Josef Horvath
Whose love for his family, compassion for others, and thirst for knowledge has been truly inspirational

Acknowledgement

There are many people I have to thank over the course of this thesis. First and foremost would be my supervisor Sandro Gambarotta. His immense knowledge of chemistry is amazing and his wit has made working in his lab an enjoyable experience.

There are other professors whom I also have to give the appropriate acknowledgement. First and foremost I would like to thank Dr. Serge Gorelsky for the tremendous amount of help he gave in doing DFT calculations and explaining them. I would also like to thank Dr. Darren Richeson whose knowledge of molecular orbital theory and classes he taught were invaluable and Dr. Muralee Murugesu for his advice and insight into molecular magnetism.

In addition to the professors a number of individuals about the department have helped me immeasurably. Glenn Facey must be thanked for the help in performing some NMR experiments and in interpreting of spectra. Annette and Linda in the office must be thanked as well for their assistance in cutting through the miles of red tape that are a part of any university.

I am incredibly thankful for the help and assistance given to me by the post-doctoral fellows of the laboratory, specifically Ilia Korobkov and Grigory Nikiforov. Without their experimental knowledge I would probably still be setting up my schlenck line.

Finally I would like to thank all the other graduate students I have had the pleasure to encounter. Specifically my friends Vladimir, Malcolm, Ian, Jessica, Dominic and all the people I played softball with this summer. A special thank you to my close friends Chris and Indu with whom I've spend countless hours working alongside and who have been great friends while I've lived in Ottawa.

This would not be complete without a huge thanks to my family. Who have always supported me in all my efforts and whom I am forever indebted. My father has to be thanked for the hours he's spent in driving back and forth from Ottawa and the work he's done in helping me along the way with any struggles I have faced. My stepmother, Shirley, has to be thanked for her support and patience in taking the time to listen when I've needed someone to. Finally my mother has to be thanked for all the love and advice she has offered and without whom I would be lost.

Abstract

The overall objective in this body of work was to synthesize a new class of chromium complexes containing a bound guanidinate ligand (Chapter 2) and ultimately test these complexes for catalytic activity in ethylene oligomerization/polymerization reactions (Chapter 4). A number of reactions between the chromium guanidinate complexes and alkyl aluminum reagents (Chapter 3) were attempted to gain insight into the nature of the active species in the catalytic cycle. A large majority of the complexes presented in this thesis have been characterized using x-ray crystallography. Additionally a number of dimeric Cr^{II} complexes were obtained with bridging guanidinate and alkyl groups. One such complex had an ultra short Cr^{II}-Cr^{II} distance of 1.773 Å (Steven Horvath, Serge I. Gorelsky, Sandro Gambarotta, Ilia Korobkov *Angew. Chem* **2008**, 47, 9937) and a thorough DFT study was performed on the complex (Chapter 3). The catalytic testing of this new class of chromium guanidinate complexes was very promising and a thorough investigation of the factors that affect the selectivity and activity of the catalysts was performed (Chapter 4).

Publications

Steven Horvath, Serge I. Gorelsky, Sandro Gambarotta, Ilia Korobkov. *Angew. Chem. Int. Ed. Engl.* 47 (2008) 9937.

Contents

1 Introduction

Table of Contents

Chapter 1

1.1 Background on Ethylene Oligo/Polymerization

Ethylene polymerization and oligomerization are very important industrial processes producing enormous amount of commodity chemicals central to our modern lifestyle. Given the large worldwide demand for polyethylene and α-olefins and the financial viability of their production, there is no surprise that considerable research effort has been invested to discover new and better performing catalytic systems. Central to these discoveries is of course a deep understanding of these two processes.

Polymerization and oligomerization of ethylene belong to the same class of C-C bond forming reactions. However, these processes are believed to proceed through completely different mechanisms (oxidative addition followed by ring expansion for oligomerization[1] versus migratory insertion for polymerization[2]). The process is referred to as polymerization when saturated chains are formed as a product. When chains with a vinylic terminal are produced the process is commonly referred to as oligomerization. At first glance both are essentially the same process the only difference being the type of chain-growth termination process. However, a survey of the experimental and theoretical data leads to the conclusion that the two processes are fundamentally different.[1-2] This is particularly true for oligomerization processes affording a statistical distribution of light α-olefins (S-F distribution).[3]

The importance of linear α-olefins as commodity chemicals resides in their use as precursors for the preparation of detergents, co-polymers, synthetic lubricants and plasticizers.[4] A variety of marketed products can be attained through the use of the different chain length of industrially manufactured α-olefin. The highest market demand is by far for 1-butene, 1-hexene, and 1-octene since these species are essential ingredients for the production of LLDPE (Linear Low Density PolyEthylene).[4] These α-olefins were traditionally obtained by distillation of a statistical distribution of α-olefins known as a Shultz-Flory distribution as generated by the SHELL-SHOP process and which typically

contains α-olefins in the range of C4-C20.[3] The extensive distillation needed to efficiently separate the components from each other makes this process expensive and inconvienent. This provides in turn a major stimulus for the design of selective catalysts capable of specifically and selectively producing the desired product with high activity. Currently there are only a few routes for obtaining linear α-olefins in high selectivity. 1-Butene is made in the Middle East by dimerizing ethylene. 1-Hexene is made by ethylene trimerization by the Chevron-Phillips company by using a proprietary catalytic system. 1-Hexene and 1-octene are also obtained through extraction in the Synthol streams in South Africa by Sasol.[5] The C10-C14 chain length α-olefins are used for producing poly-α-olefin (PAO) synthetic lubricants which are used in car, motor, and gear oils. These are an improvement over traditional oils as they reduce engine wear and need changing less often. The heavier α-olefins, C14-C26, are used as intermediates in a large number of consumer products, such as surfactants, detergents and lubricant additives.[6] They are also used in surface technologies, such as industrial coatings, decorative paints, printing inks, adhesives and sealants. Large amounts of α-olefins are also used in the cosmetics industry where easy spreading, quick drying, fast penetration, long term stability and non-greasy feel are needed.

A process which thus far unavoidably accompanies oligomerization is polymerization. Industrial chemists continually face the challenge of trying to prevent reactor fouling. This is when small unwanted quantities of polyethylene deposit on the walls of the reactor during an oligomerization reaction and interfere with the correct operation of the mechanic. This requires shutting down the reactor and cleaning the polymer in a labor intensive task. Hence high selectivity in the oligomerization process is even more desirable. However, the development of selective catalysts would require acquisition of a solid grasp on the factors that determine the catalyst behavior (either polymerizing ethylene into a long chain polymer or oligomerize into short chain α-olefin) and which instead remain limited.[7]

Polyethylene formed by a catalyst can have many different uses depending on its macroscopic and microscopic properties. Two highly sought after types of polymer are low-density and high-density polyethylene (LDPE and HDPE). The major uses of LDPE is in film wraps, such as those used for wrapping food, extrusion coatings, and trays. This

versatility is due to the lack of strength of the low density polymer and which is in turn related to the presence of highly branched chains. The employments of 1-octene in the preparation process greatly improve the rheology of the polymer. On the other hand, HDPE as generated by the presence of highly linear chains with little or no branching has the advantage of greater strength than LDPE. Therefore, HDPE is used in more demanding devices such as bottles, fences, pipes, bags and chairs.

Imperial Chemical Industries (ICI) initiated the commercial production of polyethylene in the 1930's by using high pressure, radical polymerization.[6] With the discovery of chromium oxide on silica gel (also known as Phillips catalyst), Hogan and Banks commercialised the production of polyethylene at low pressures.[8] Currently, around 40% of the worldwide manufacture of polyethylene is performed by this catalytic system.[9] The advantages in using the Phillips catalyst are that the manufacturing cost of the catalyst is low, and that the catalytic activity is very high (about 60,000,000 g of polyethylene per 1g of metal).[10]

The saga of the search for catalytic systems for ethylene polymerization started with the independent discovery by Ziegler and Natta in the 1960's of the Ti-AlR_3 catalyzed polymerization process and which opened the door to the modern era of polymer technology. In 1980, Sinn and Kaminsky discovered the co-catalyst methylalumoxane (MAO).[11] This activator changed the whole perspective on ethylene polymerization, due to the fact that this co-catalyst increases the activity by several orders of magnitude. The exact structure and role that MAO plays is still largely unknown and debated in the literature, but one can speculate that, based on the fact that commercially available MAO contains 30% $AlMe_3$, some sort of alkylation or ligand abstraction and cationization is taking place. The discovery of the so-called "cationic Ziegler Natta process" has further revolutionized catalyst technology by allowing a tighter control of polymer formation and rheology.

New catalysts are typically compared to the ziegler and metallocene catalytic system developed in the 80s. The search for new catalytic systems that are better performing and give more control over the resulting polymer has not ended. A few of these catalytic systems are shown below. [12]

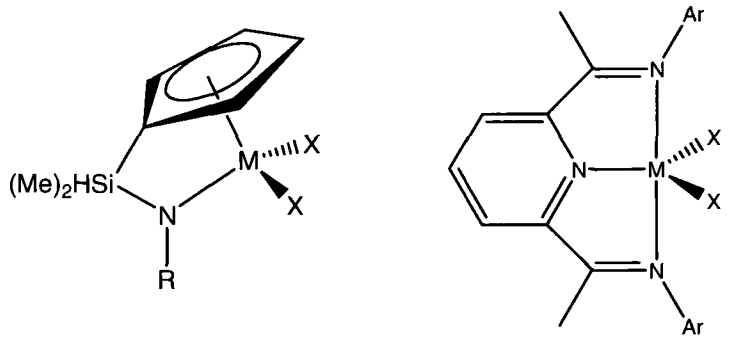

Figure 1.1.1 Polymerization catalysts

1.2 Polymerization Mechanism

During the 1950's, Ziegler and Natta discovered that a mixture of MCl_x, where M = Ti, Zr or V and X = 3 or 4, $AlEt_3$ (TEAL), and $MgCl_2$ polymerized ethylene.[13] This opened the doorway for modern day catalyst research. Research has focussed on extending the catalyst lifetime, increasing activity, and control over the molecular weight of the polymer produced. As mentioned above, this has partly been achieved through the development and use of co-catalysts such as Methylalumoxane (MAO) or trimethylaluminum (TMA).[14] The role of these species has never been conclusively demonstrated but it is commonly believed that it is both to alkylate and cationize the metal centre, as shown in Figure 1.2.1.

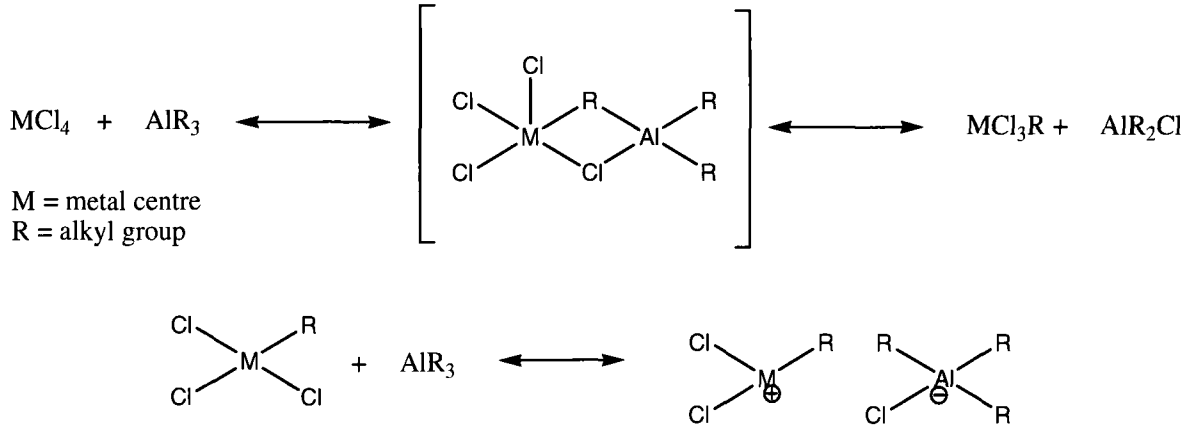

Figure 1.2.1 Alkylation and cationization of metal center by AlR_3.

The commonly accepted mechanism in Ziegler-Natta polymerization process is generally referred to as the Cossee-Arlman mechanism. [15] This mechanism is shown below in Figure 1.2.2. A transition metal complex, in this case $TiCl_4$, and co-catalyst, in this case $AlEt_3$, undergo a ligand substitution reaction thus alkylating the transition metal center. This new complex, the "active species", can then coordinate ethylene to a vacant coordination site and insert the coordinated molecule of ethylene into the M-C bond, thus elongating by two carbons the alkyl chain on the transition metal. The resulting species, complex **3** in Figure 1.2.2, can then coordinate another molecule of ethylene, insert it into

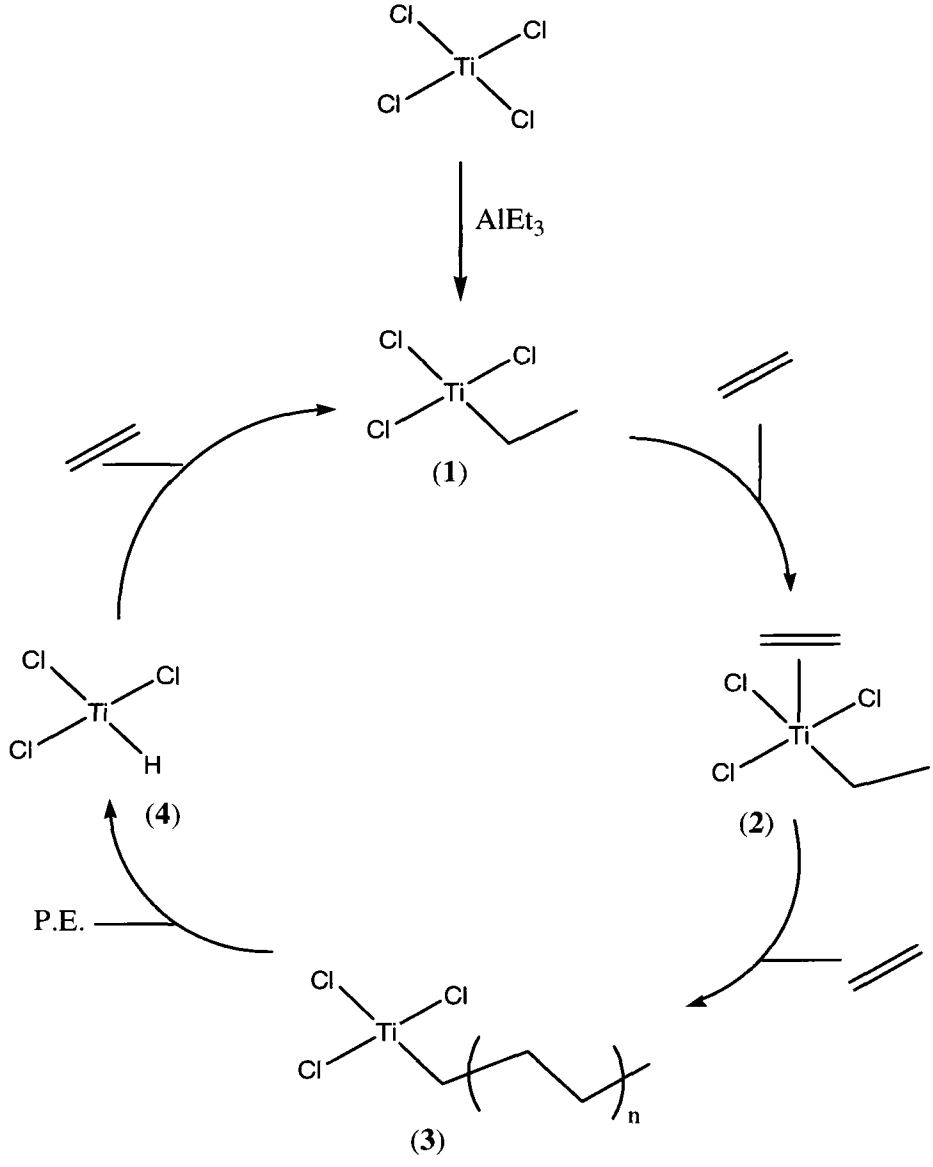

Figure 1.2.2 Cossee-Arlman mechanism of ethylene polymerization using $TiCl_4$ and AlR_3

the M-C bond and, by repeating several time the same event, extends the alkyl chain further. This process may continue until a termination process (β-hydride elimination, chain transfer to Al, C-H bond metathesis, etc.) occurs releasing a long chain polymer of *n* length, where *n* represents the number of ethylene molecules that coordinate and insert into the M-C bond. The metal hydride complex, **4** in Figure 1.2.2, can then coordinate a molecule of ethylene and insert it into the M-H bond thus reforming the M-C bond and the process may restart until irreversible catalyst decomposition occurs. If the catalyst continues to polymerize ethylene with no decomposition, the process is commonly referred to as a "living polymerization catalysis".[16] Relevant to the following discussion is that the metal oxidation state does not change during any of the steps of the polymerization process. *Ethylene polymerization typically is a non-redox process.*

1.3 Oligomerization Mechanism

The factors that control selective oligomerization are still unknown and are the center of much debate.[17] Whether the same or different mechanisms are at work during selective and non-selective oligomerization is a challenging question to answer. Although both belonging to the same type of C-C bond forming reaction, the mechanisms of polymerization and oligomerization are believed to be quite distinct. The oxidation state of the metal center and steric tension around the metal center both play important roles in dictating catalyst performance. The current level of understanding on the process may be simplified into two mechanistic proposals.

The first mechanism is in essence a polymerization terminated at its early stages and was published by Cossee in 1964 to explain observations from Ziegler-Natta polymerization.[2a-b] A quickly terminated polymerization could occur when the rate of β-hydride elimination is competitive with the rate of chain growth. The factors that control the selectivity would be the same that determine the rate of β-hydride elimination, such as steric tension around the metal center and strength of the M-C bond.

The second mechanism is currently the most widely accepted mechanistic proposal for selective oligomerization. It is known as the metallacycle ring expansion mechanism, commonly referred to as the "metallacyclic mechanism" (Figure 1.3.1).[18]

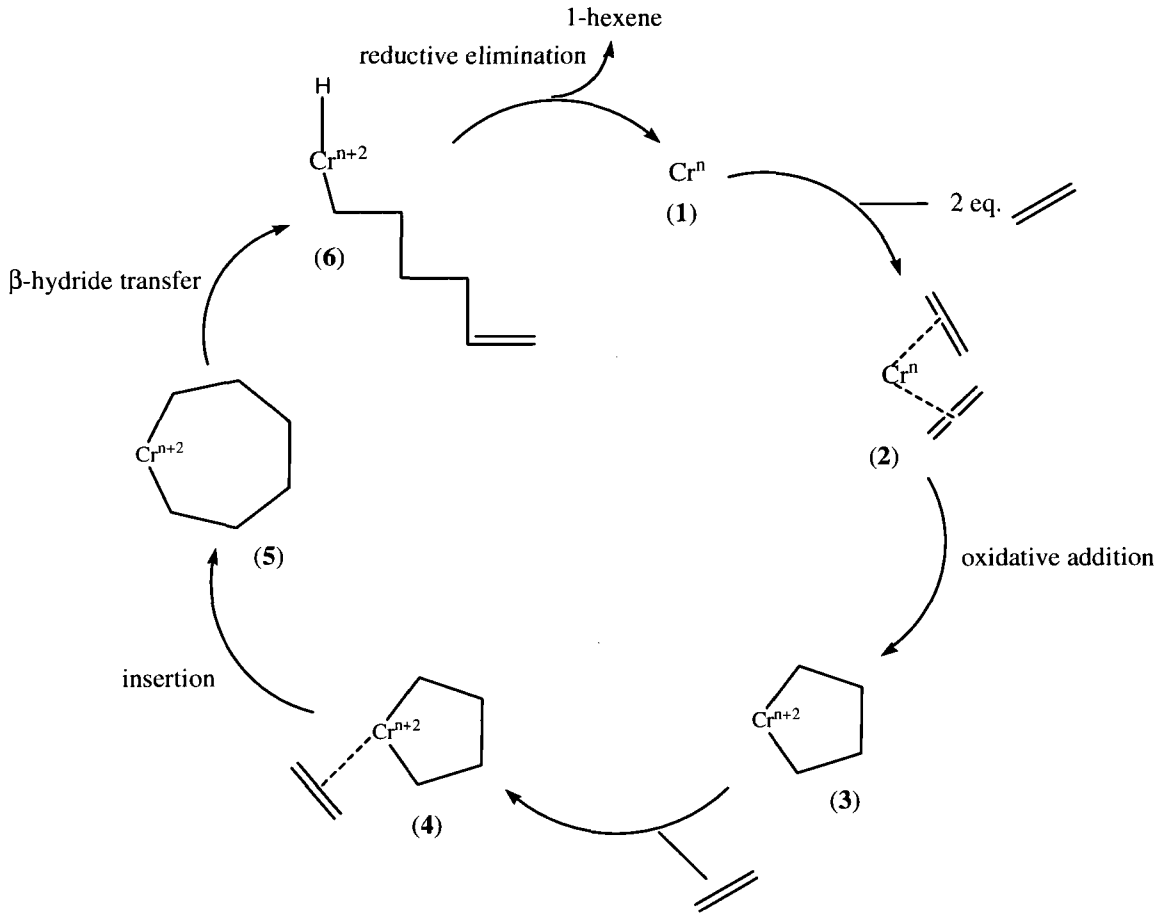

Figure 1.3.1 Metallacycle mechanism.

In the metallacycle mechanism the first step consists of the coordination of two molecules of ethylene to a metal center. The coordinatively unsaturated metal center is commonly generated by co-catalysts such as MAO or AlR_3 as illustrated in Figure 1.2.1. The two coordinated molecules of ethylene undergo reductive coupling forming a metallacyclopentane (**3**) with simultaneous two-electron oxidation of the metal center (Figure 1.3.1). At this point in the cycle one of two events may occur. If the rate of β-hydride transfer is competitive with coordination of another molecule of ethylene and

subsequent insertion, reductive elimination to form 1-butene and the reduced Cr starting compound (**1** in Figure 1.3.1) will take place. Otherwise another molecule of ethylene will coordinate and insert into the M-C bond to form a metallocycloheptane (**5**). Once again the same two events are possible at this point: β-hydride transfer and reductive elimination to form 1-hexene and the starting material, or coordination of another molecule of ethylene and subsequent expansion of the metallacycle.

A number of quantum chemical calculations have been carried out on this system to elucidate the mechanism, many of them using different transition metals.[19] It has been found that there is a significant energy barrier for the β-hydride transfer and elimination from a metallocyclopentane to form 1-butene. The calculations show that coordination and insertion of another molecule of ethylene requires much less energy and is thus the preferred pathway.[18a-b] Computational studies have also revealed that the two-step process of β–hydride transfer followed by reductive elimination to yield an alkene actually is a one-step concerted hydride transfer illustrated in Figure 1.3.2.[18c] This supports the finding that simple dimerization is energetically disfavored because the ring strain prevents a concerted hydride transfer pathway within the metallacyclopentane. While the 7-membered ring leading to 1-hexene is particularly favorable for that purpose, further insertion to form a 9-membered ring (and eventually 1-octene) is highly unlikely. Thus this mechanism does not well account for the formation of 1-octene.

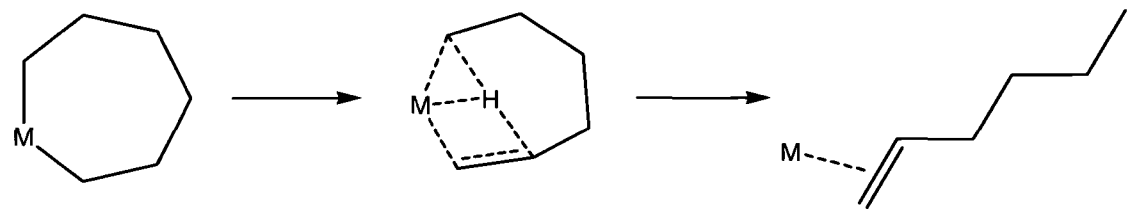

Figure 1.3.2 Concerted hydride transfer pathway

The major difference of the oligomerization mechanism with respect to polymerization is that the oligomerization *involves a two-electron redox couple.* Oxidative coupling and reductive elimination are the crucial steps of the catalytic cycle.

As far as the oligomerization process is concern, chromium is by far the element of preference. Chromium accounts for over 90% of the examples present in both patent

and academic literature. In turn this raises fascinating questions about the chromium oxidation states which may be responsible for polymerization versus statistical and selective oligomerizations. If selective oligomerization truly is a two electron process, the question must be asked what oxidation state of chromium is sufficiently reactive to perform reversible oxidative addition to ethylene. To this end, evidence has been reported for a number of redox couples Cr(0)-Cr(II)[20], Cr(I)-Cr(III)[21], Cr-(II)-Cr(IV)[22], Cr(III)-Cr(V)[23] which might be involved in the catalytic cycle.

The large number of variables that must be considered during one of these catalytic cycles (pressure, temperature, solvent, reaction time, etc.) makes determination of the oxidation state even more challenging. There can be no certainty that the oxidation state of the metal precursor is preserved during the catalytic cycle as reduction or oxidation *in situ* to form the active species is always possible through reaction with co-catalyst or through a disproportionation pathway.[7, 24]

1.4 Research Rationale

As mentioned above, chromium is the most widely used metal among all the known catalytic oligomerization systems. Other metals have been used but none compares in activity and selectivity to the chromium systems that have been developed. For this reason chromium was chosen as the most likely candidate to obtain a highly active and selective catalyst system. Additionally, we had hoped to answer the question of which oxidation of chromium is responsible for polymerization, selective oligomerization and non-selective oligomerization.

Given the tremendous activity of the amidinate chromium systems in ethylene oligomerization[25], we had hoped that the guanidinate ligands (somewhat related to the amidinates) discussed in detail in Chapter 2, may also provide highly active catalysts. The structural resemblance of the guanidinate ligand to many well known oligomerization catalysts makes this system very promising as well. Some of these catalysts are shown below along with the guanidinate ligand. Another interesting feature

of the guanidinate anion is the possibility of coordinating further alkyl aluminum residues. This coordination is expected to introduce a zwitterionic type of structure deemed beneficial for the preparation of single component catalysts.

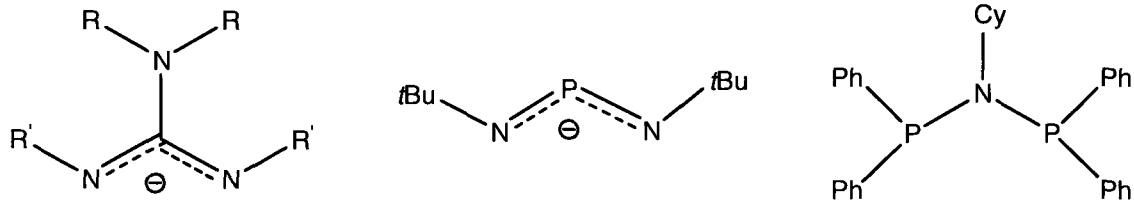

Guanidinate ligand NPN system[26] BP/Sasol PNP[27]

Figure 1.4.1 Comparision of guanidinate ligand (left) to two well known oligomerization catalysts the NPN system (middle) and PNP (right).

The strategy adopted for testing this system is quite straightforward and is shown in Figure 1.4.2. First a number of Cr(II) and Cr(III) guanidinate complexes were synthesized through salt metathesis reaction of the metal halide with the lithium guanidinates. These complexes were then tested for their oligomerization/polymerization activity using a co-catalyst as activator. The Cr(II) and Cr(III) guanidinate complexes were also reacted with a number of alkyl aluminums in hope of gaining insight in to the nature of the catalytically active species. Additional reactions were also carried out in an attempt to alkylate the metal center. These chromium alkyls could then be used as self-activating oligomerization/polymerization catalysts also referred to as single component catalysts. Catalysts that are self-activated and do not require the use of co-catalysts are highly desirable because of the cost and danger associated with the alkyl aluminum co-catalysts.

After reaction of the chromium guanidinate complexes with alkyl aluminums the complexes obtained from these reactions were also tested for their activity in oligomerization/polymerization. The testing of all the complexes obtained was performed for gaining insight as to the nature of the active species and how the different variables affect the product distribution and yield.

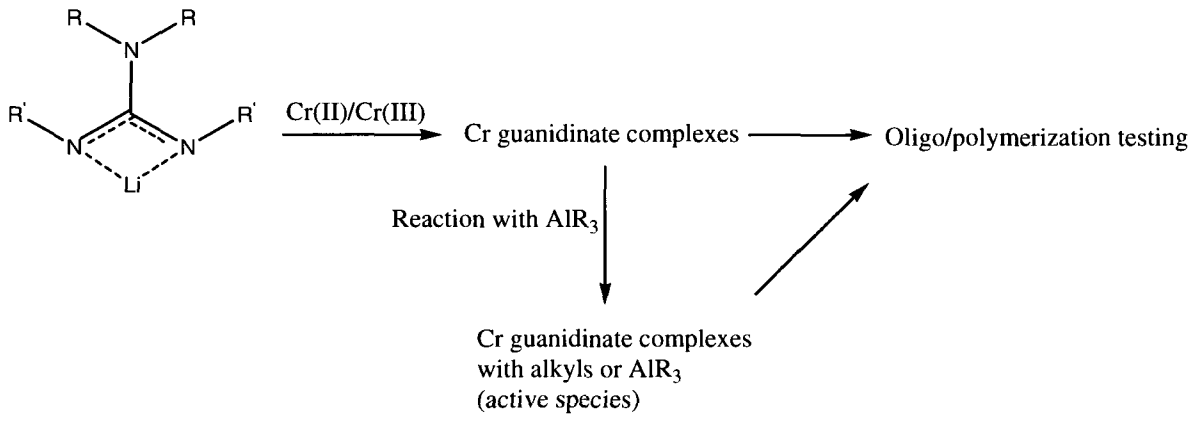

Figure 1.4.2 Catalyst synthesis and testing strategy

From this research we hope that a better understanding of the factors that control oligomerization and polymerization reactions may stem. Additionally, it has laid the groundwork for further exploration into this system for optimization and potential commercialization. It should also be noted that due to the goodness of the results obtained within this thesis a new project has been started aiming at the immobilization of these catalysts. The goal was a further increase of the catalyst lifetime and possibly improvement of the selectivity.

1.5 References

1. a) J. X. McDermott, J. F.White, G. M.Whitesides, *J. Am. Chem. Soc.* **1973**, *95*, 4451; b) J. X. McDermott, J. F. White, G. M. Whitesides, *J. Am. Chem. Soc.* **1976,** *98*, 6521; c) R. M. Manyik, W. E. Walker, T. P. Wilson, *J. Catal.* **1977**, *47*, 197; d) M. P. McDaniel, *Adv. Catal.* **1985**, *33*, 47; e) J. R. Briggs, *Chem. Commun.* **1989**, 674; f) N. Meijboom, C. J. Schaverien, A. G. Orpen, *Organometallics* **1990**, *9*, 774; g) R. Emrich, O. Heinemann, P. W. Jolly, KrGger, G. P. J. Verhovnik, *Organometallics* **1997**, *16*, 1511.

2. a) P. Cossee, *J. Catal.* **1964**, *3*, 80; b) E. J. Arlman, P. Cossee, *J. Catal.* **1964**, *3*, 99; c) J. Skupinska, *Chem. Rev.* **1991**, *91*, 613.

3. a) Flory, P. J. *J. Am. Chem. Soc.* **1940**, *61,* 1561. b) Schulz. G. V. Z. *Phys. Chem. Abt. B.* **1939**, *43*, 25. c) Schulz, G. V. Z. *Phys. Chem. Abt. B.* **1935**, *30*, 379.

4. Weissermal, K.; Arpe, J.-J. *Industrial Organic Chemistry: Important Raw Materials and Intermediates*, Verlag Chemie, New York, **1978**.

5. J.T. Dixon, M.J. Green, F.M. Hess, D.H. Morgan. *Journal of Organometallic Chemistry* **2004**, *689*, 3641.

6. R.B.Seymour, T.C., *History of polyolefins.* D. Riedel Publ. Co., Dordrecht, **1986**.

7. Amir Jabri, Chris B. Mason, Yan Sim, Sandro Gambarotta, Tara J. Burchell, and Robbert Duchateau *Angew. Chem. Int. Ed.* **2008**, *47*, 9717.

8. J.P.Hogan and R.L.Banks, *Phillips Petroleum Co.* Belg. Pat., **1955**. 530617.

9. Whiteley, K.S. and T.G. Heggs, *Ullmann's Encyclopedia of Industrial Chemistry*. Vol. A21. p.387, **1992**: VCH Weinheim.

10. Dr.S.Palackal and D.A. Raqabah, *Metallocene Catalysts for Ethylene Polymerisation*: Sabic R&D,Riyadh, Kingdom of Saudi Arabia, Available from: http://www.kfupm.edu.sa/catsymp/Symp12th/Data%5CSabic-20.pdf.

11. Aulbach, M. and F. Küber, *Chem. Unserer Zeit*, **1994**, *4*, 197.

12. a) George J. P. Britovsek, Vernon C. Gibson, and Duncan F. Wass *Angew. Chem. Int. Ed.* **1999**, *38*, 428. b) J. A. M. Canich, H. W. Turner *Chem. Abstr.* **1993**, *118*, 8161. c) Y.-X. Chen, T. J. Marks, *Organometallics* **1997**, *16*, 3649. d) G. J. P. Britovsek, V. C. Gibson, B. S. Kimberley, P. J. Maddox, S. J. McTavish, G. A. Solan, A. J. P. White, D. J. Williams, *Chem. Commun.* **1998**, 849. e) B. L. Small, M. Brookhart, A. M. A. Bennett, *J. Am. Chem. Soc.* **1998**, *120*, 4049.

13. Ziegler, K., H. Martin, and J. Stedefeder, *Tetrahedron Letters*, **1959**, *1*, 12.

14. Brookhart, M., B. Grant, and A.F. Volpe, *Organometallics*, **1992**, *11*, 3920.

15. Atkins, P., *Shriver and Atkins, Inorganic Chemistry*. **1999**, 105.

16. Halasa, A. F. *Rubber Chem. Technol.*, **1981**, *54*, 627.

17. (a) de Bruin, T. J. M.; Magna, L.; Raybaud, P.; Toulhoat, H. *Organometallics* **2003**, *4*, 3404. (b) Tobisch, S.; Ziegler, T. *Organometallics* **2005**, *26*, 256 and referencess therein. (c) Blok, A. N. J.; Budzelaar, P. H. M.; Gal, A. W. *Organometallics* **2003**, *22*, 2564. (d) van Rensburg, W. J.; Grove, C.; Steynberg, J. P.; Stark, K. B.; Huyser, J. J.; Steynberg, P. J. *Organometallics* **2004**, *23*, 1207. (e) Tobisch, S.; Ziegler, T. *J. Am. Chem. Soc.* **2004**, *126*, 9059. (f) Jolly, P. W. *Acc. Chem. Res.* **1996**, *29*, 544. (g) Morgan, D. H.; Schwikkard, S. L.; Dixon, J. T.; Nair, J. J.; Hunter, R. *Ad*V. *Synth. Catal.* **2003**, 939. (h) Yang, Y.; Kim, H.; Lee, J.; Paik, H.; Jang, H. G. *Appl. Catal. A* **2000**, *193*, 29. (i) Bercaw, J. E. *The 15th International Symposium on Olefin Metathesis and Related Chemistry,* (ISOM XV) July 28-Aug 1, **2003**, Kyoto, Japan. (j) Theopold, K. H. *Eur. J. Inorg. Chem.* **1998**, 15. (k) Meijboom, N.; Schaverien, C. J.; Orpen, A. G. *Organometallics* **1990**, *9*, 774. (l) Fang, Y.; Liu, Y.; Ke, Y.; Cuo, C.; Zhu, N.; Mi, X.; Ma, Z.; Hu, Y. *Appl. Catal. A. Gen.* **2002**, *235*, 33. (m) Ko¨hn, R. D.; Haufe, M.; Mihan, S.; Lilge, D. *Chem. Commun.* **2000**, 1927. (n) Agapie, T.; Schofer, S. J.; Labinger, J.; Bercaw, J. E. *J. Am. Chem. Soc.* **2004**, *126*, 1304.

18. (a) Briggs, J. R. *J. Chem. Soc., Chem. Commun.*, **1989**, 674. (b) Jolly, P.W. *Acc. Chem. Res.* **1996**, *29*, 544. (c) Emrich, R.; Heinemann, O.; Jolly, P. W.; Kruger, C.; Verhovnik, G. P. J.; *Organometallics*, **1997**, *16*, 1511.

19. a) van Rensburg, W. J.; Grove, C.; Steynberg, J. P.; Stark, K. B.; Huyser, J. J.; Steynberg, P. J *Organometallics,* **2004**, *23*, 1207. b) Yu, Z.-X.; Houk, K. N. *Angew. Chem. Int. Ed.* **2003**, *42*, 808. (c) Blok, A. N. J.; Budzelaar, P. H. M.; Gal, A. W. *Organometallics* **2003**, *22*, 2564.

20. a) Mimura, H.; Oguri, M.; Yamamoto, T.; Murakita, H.; Okada, H.; Yoshida, T. US Pat. 6 337 297 (Tosoh Corporation), **2002**. b) Mimura, H.; Oguri, M.; Yamamoto, T.; Okada, H.; Osamu, Y. Jap. Pat. 2001002724 (Tosoh Corporation), **2001**. c) Mimura, H.; Oguri, M.; Okada, H.; Yoshida, T. Jap. Pat. 2000176291 (Tosoh Corporation), **2000**. d) Oguri, M.; Mimura, H.; Okada, H.; Yoshida, T. Jap. Pat. 2000202299 (Tosoh Corporation), **2000**.

21. a) Fang, Y.; Liu, Y.; Ke, Y.; Guo, C.; Zhu, N.; Mi, X.; Ma, Z.; Hu, Y. *J. Appl. Catal. A,* **2002**, *193*, 33. b) Kohn, R. D.; Haufe, M.; Mihan, S.; Lilge, D. *Chem. Commun.* **2000**, 1927.

22. a) van Rensburg, W. J.; Grove, C.; Steynberg, K. B.; Stark, K. B.; Huyser, J. J.; Steynberg, K. B. *Organometallics* **2004**, *23*, 1207. b) Morgan, D. H.; Schwikkard, S.

L.; Dixon, J. T.; Nair, J. J.; Hunter, R. *Adv. Synth. Catal.* **2003**, *345*, 939. c) Theopold, K. H. *Eur. J. Inorg. Chem.* **1998**, 15.

23. Meijboom, N.; Schaverien, C. J.; Orpen, A. G. *Organometallics*, **1990**, *9*, 774.

24. (a) C. Temple, A. Jabri, P. Crewdson, S. Gambarotta, I. Korobkov, R. Duchateau, *Angew. Chem.* **2006**, *118*, 7208; *Angew. Chem. Int. Ed.* **2006**, *45*, 7050

25. Pat Crewdson, *Chromium catalyzed ethylene oligomerization* Chapter 7 (PhD thesis) **2006**.

26. K. Albahily, S. Gambarotta, et al. *Angew. Chem. Int. Ed.* **2008**, *47*, 5816.

27. a) Bollmann, A.; Blann, K.; Dixon, J. T.; Hess, F. M.; Killian, E.; Maumela, H.; McGuinness, D. S.; Morgan, D. H.; Neveling, A.; Otto, S.; Overett, M.; Slawin, A. M. Z.; Wasserscheid, P.; Kuhlmann, S. *J. Am. Chem. Soc.* **2004**, *126*, 14712. b) Overett, M. J.; Blann, K.; Bollmann, A.; Dixon, J. T.; Hess, F.; Killian, E.; Maumela, H.; Morgan, D. H.; Neveling, A.; Otto, S. *Chem. Commun.* **2005**, 622.

2 Guanidinato Complexes of Chromium

Table of Contents

Chapter 2

2.1 Introduction

Guanidinates belong to the general class of 1,3-nitrogen ligands and offer interesting steric and electronic flexibility to stabilize transition metal complexes.[1] These anions contain a Y-shaped NC_3 core and can be thought of as a more versatile alternative to the well known three-center chelating ligands (e.g. amidinate[2] or triazenide[3] shown in Figure 2.1.1). While the steric bulk of the substituents may adjust the ligand bite to the

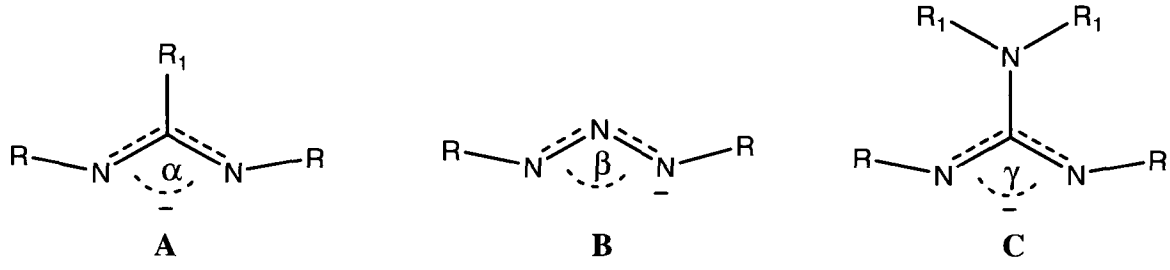

Figure 2.1.1 **A**) Amidinate, **B**) triazenate, and **C**) guanidinate anions.

extent of controlling the nuclearity of the complexes,[4] the third nitrogen atom of the guanidinate ligand can bear at least one hydrogen atom. In turn this may allow for further deprotonation affording the dianionic species such as shown in figure 2.1.2. The double negative charge may exhibit π delocalization (Y conjugation) making the dianion an analogue of the trimethylene methane dianion.[5]

The neutral guanidine (0) $[(R_2N)_2CN{=}R]$, the monoanionic guanidinate (-1) $[(RN)_2CNR_2]^-$, and the dianionic guanidinate (-2) $[(RN)_2C{=}NR]^{2-}$ are all capable of exhibiting a variety of coordination modes.[1] The ease with which a variety of guanidinate ligands bearing different combinations of substituents may be synthesized makes them very attractive for a range of transition and even non-transition metals.[1a] The monoanionic lithium salt of guanidinate is a common and useful starting material as it

can be synthesized in one step and may be used in salt metathesis reactions with a number of metal halides.[1]

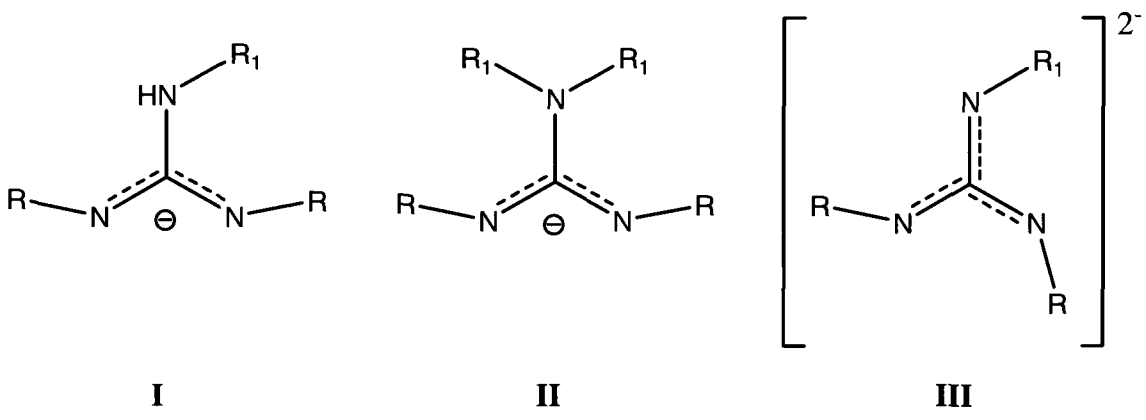

I II III

Figure 2.1.2 **I**) N,N',N''-Trisubstituted Guanidinate **II**) N,N,N',N''-Tetrasubstituted Guanidinate **III**) Dianionic Guanidinate displaying "Y conjugation"

Tuning the properties of a three-center chelating ligand, such as amidinate, is restricted to changing the substituents on the carbon and nitrogen atoms thus altering the steric tension around the metal centre. As mentioned above, with the guanidinate monoanion instead both the steric and electronic properties can be adjusted more readily. Changing the substituents at the R^1 position alters the steric crowding around the metal center. The ligand geometry can also be altered at the R position thus modifying the bite angle γ (Figure 2.1.1). The electron donating properties can be somewhat controlled due to the presence of a third, "zwitterionic", resonance structure. The possible resonance structures of the generic guanidinate monoanion $[(R'N)_2CNR_2]^-$ are shown in Figure 2.1.3.[6] The degree to which resonance structure **C** contributes to the overall bonding is depending on the angle between the "R_2N-" and "NCN" moieties. The maximum contribution from resonance structure C occurs when this angle is equal to zero and all R and R' substituents lay in the same plane. This allows for the correct orbital alignment for a π-overlap to occur between the nitrogen lone pair and *p*-orbital of the sp^2-carbon atom.[6]

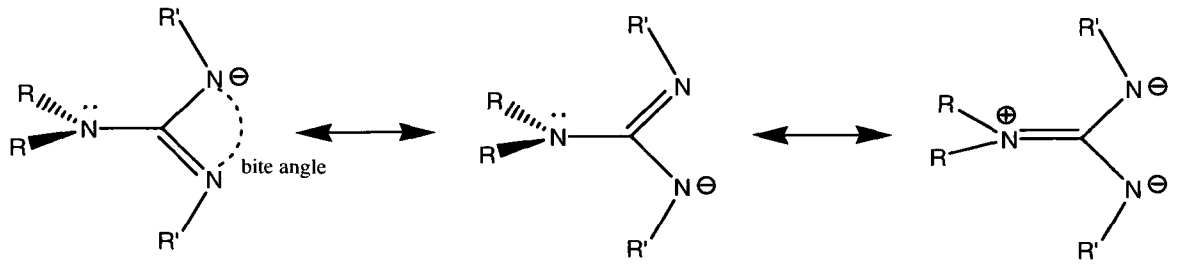

Figure 2.1.3 Resonance structures of monoanionic guanidinate $[(R'N)_2CNR_2]^-$.

A good indication of the relative contribution from resonance structure **C** comes from an analysis of the C-N bonds in the CN_3 core of the coordinated guanidinate ligand. Clearly the shorter the C-N bond to the uncoordinated N, the greater the contribution from resonance structure **C**.[7]

Only a few guanidinato complexes of chromium have been characterized crystallographically and reported in the literature [8a-g] and some of these are shown in Figure 2.1.4. The majority of these have been made in an attempt to obtain complexes with exceedingly short metal-metal bonds. The ability of the guanidinate ligand to stabilize such complexes will be discussed in chapter 3. It should also be noted that a number of the crystallographically characterized compounds have been obtained as hydrated salts.

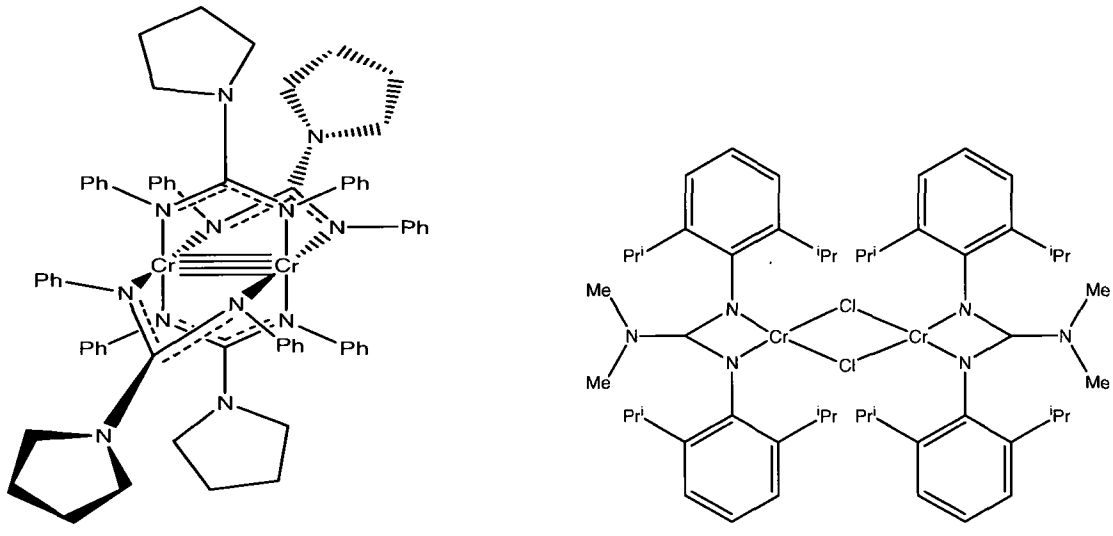

2.1.4 Molecular structures of 3 chromium guanidinate complexes **A** [8c] **B** [8g].

One modification to the guanidinate ligand that can be made is to replace one or more of the nitrogen atoms with sulfur atoms. The effect of changing from a hard nitrogen donor atom to a much softer sulfur atom can induce substantial electronic change at the metal center. This substitution is easy to achieve as potassium and sodium dithiocarbamate salts, shown in Figure 2.1.5 are readily synthesized and can undergo the same salt metathesis reactions as the lithium guanidinates.[9]

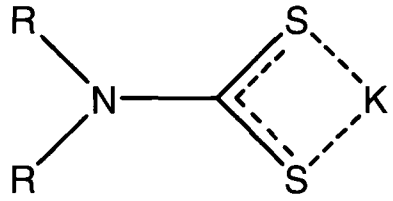

2.1.5 Potassium salt of dithiocarbamate ligands

As abundantly explained in the introduction, chromium was the metal of preference for this thesis work aiming at the preparation of new oligomerization and polymerization catalysts. However, one nickel guanidinate complex was also synthesized and included in this chapter. Divalent nickel was selected because of the electronic analogies generated by the square planar ligand field with the d^8 electronic configuration of Ni(II) and the half-filled d^4 of divalent chromium. Because of this, same geometry and bonding modes were anticipated. Additionally, there are a number of cases where Ni(II) has been shown to dimerize ethylene to 1-butene with high selectivity and activity.[10] The results obtained in ethylene oligomerization with the chromium guanidinate ligand system, which will be discussed in chapter 4, encouraged the synthesis and catalytic testing of other transition metal guanidinate complexes.

2.2 Experimental Section

All reactions were carried out under a dry nitrogen atmosphere. Solvents were dried using an aluminum oxide solvent purification system. $CrCl_2THF_2$ and $CrCl_3THF_3$ were synthesized according to standard procedure. The ligands, $(Me_3Si)_2NC(NCy)_2Li$ and $(Me_3Si)_2NC(N^iPr)_2Li$, were prepared according to literature methods[11] using starting materials supplied by Aldrich. The 3 other guanidinate ligands were prepared by deprotonating either cyclohexylamine, dicyclohexylamine, or 2,6-dimethylaniline with ^nBuLi in THF and allowing the reaction to stir for 4 hours. Either diisopropylcarbodiimide or dicyclohexylcarbodiimide dissolved in THF was added and the solution stirred for 24 hours. The product was isolated by removal of the solvent under reduced pressure. The white or beige powder was washed with hexanes and dried under vacuum before use. Infrared spectra were recorded on an ABB Bomem FTIR instrument from Nujol mulls prepared in a drybox. Samples for magnetic susceptibility were pre-weighed inside a drybox equipped with an analytical balance and measured on a Johnson Matthey Magnetic Susceptibility balance. NMR data was collected on an INOVA Varian 300 or 500 MHz instrument in the deuterated solvent of choice. Elemental analysis was carried out with a Perkin-Elmer 2400 CHN analyzer. Data for X-ray crystal structure determination were obtained with a Bruker diffractometer equipped with a 1K Smart CCD area detector.

Synthesis of $[(Me_3Si)_2NC(NCy)_2CrCl]_4$(II) (1): Solid $(Me_3Si)_2NC(NCy)_2Li$ (373 mg, 1 mmol) was added to $CrCl_2(THF)_2$ (266 mg, 1 mmol) in toluene (20 mL). The color of the solution changed from purple to blue over a period of two hours. The reaction mixture was stirred for 24 hours and centrifuged to remove LiCl. After two days at -37 °C small blue crystals, suitable for X-ray crystallography, precipitated out of the solution (1.108 g, 0.61mmol, 61%). Additional product may be obtained by reduction of the mother liquor *in vacuo*. IR (Nujol, cm^{-1}): 1468 (w), 1376 (m), 1360 (m), 1345 (m), 1305 (m), 1252 (m), 1212 (m), 1143 (s), 1085 (m), 1047 (s), 1011 (m), 970 (s), 943 (m), 890 (m), 865 (m), 838 (w), 756 (m), 727 (s), 677 (m), 641 (s). Elemental Analysis calcd (found) for $C_{76}H_{160}Cl_4Cr_4N_{12}Si_8$: C 50.25 (50.88), H 8.88 (9.33), N 9.25 (9.10). (μ_{eff} = 8.79 μ_B)

Synthesis of $[(Me_3Si)_2NC(N^iPr)_2CrCl]_4$(II) (2): Solid $(Me_3Si)_2NC(N^iPr)_2Li$ (293 mg, 1 mmol) was added to $CrCl_2(THF)_2$ (266 mg, 1 mmol) in toluene (20 mL). The color of the solution turned from purple to blue over two hours. The mixture was stirred for additional 24 hours and centrifuged to remove LiCl. The solution was allowed to stand for two days at -37 °C. Blue crystals of insufficient quality for X-ray crystallography precipitated out of solution (825 mg, 0.57 mmol, 57%). An additional crop of product may be obtained by reduction of the mother liquor *in vacuo*. IR (Nujol, cm^{-1}): 1458 (w), 1359 (s), 1327 (m), 1253 (m), 1228 (m), 1168 (s), 1149 (m), 1118 (s), 1070 (m), 1047 (m), 945 (w), 838 (w), 757 (s), 702 (s), 680 (s), 659 (s). Elemental Analysis calcd (found) for C_{48} H_{128} Cl_4 Cr_4 N_{12} Si_8: C 39.81 (39.98), H 8.91 (8.34), N 11.61 (10.52). (μ_{eff} = 8.78 μ_B)

Synthesis of $[(Me_3Si)_2NC(NCy)_2]_2Cr$(II) (3): Solid $(Me_3Si)_2NC(NCy)_2Li$ (746 mg, 2 mmol) was added to $CrCl_2(THF)_2$ (266 mg, 1 mmol) in toluene (20 mL). The color of the solution turned from purple to red over 30 minutes. The mixture was stirred for 24 hours and centrifuged to remove LiCl. After standing two days at -37 °C, red needle crystals precipitated from the solution (350 mg, 0.45 mmol, 45 %). Crystals suitable for X-ray crystallography were grown by re-crystallization from hot toluene. An additional crop of product may be obtained by reduction of the mother liquor *in vacuo*. IR (Nujol mull, cm-1): 1464 (w), 1404 (m), 1377 (s), 1354 (s), 1344 (s), 1304 (s), 1252 (m), 1193 (m), 1141 (s), 1077 (s), 1007 (s), 964 (s), 946 (m), 886 (s), 864 (m), 839 (w), 758 (m), 700 (s), 665 (s), 641 (s). Elemental Analysis calcd (found) for C_{38} H_{80} Cr N_6 Si_4: C 58.11 (57.10), H 10.27 (10.44), N 10.70 (10.80). (μ_{eff} = 4.77 μ_B)

Synthesis of $[(Me_3Si)_2NC(N^iPr)_2]_2Cr$(II) (4): Solid $(Me_3Si)_2NC(N^iPr)_2Li$ (586 mg, 2 mmol) was added to $CrCl_2(THF)_2$ (266 mg, 1 mmol) in toluene (20 mL). The solution turned from purple to red over 30 minutes. The mixture was stirred for 24 hours and centrifuged to remove LiCl. After two days at -37 °C red block crystals, suitable for X-ray crystallography, precipitated out of the solution (262 mg, 0.42 mmol, 42 %). An additional crop of product may be obtained by reduction of the mother liquor *in vacuo*. IR (Nujol, cm^{-1}): 1424 (m), 1389 (s), 1357 (m), 1309 (s), 1263 (m), 1197 (m), 1072 (s), 1027

(m), 1005 (m), 949 (m), 898 (m), 869 (m), 845 (w), 732 (m), 710 (s), 643 (s). Elemental Analysis calcd (found) for $C_{26}H_{64}CrN_6Si_4$: C 49.95 (50.35), H 10.32 (10.94), N 13.44 (13.22). ($\mu_{eff} = 4.76\ \mu_B$)

Synthesis of $[(Cy)_2NC(NCy)_2CrCl]_4$(II) (5): Solid $(Cy)_2NC(NCy)_2Li$ (393 mg, 1 mmol) was added to $CrCl_2(THF)_2$ (266 mg, 1 mmol) in toluene (20 mL). The solution turned from purple to blue over two hours. The mixture was stirred for 24 hours and centrifuged to remove LiCl. Toluene was removed under reduced pressure and replaced with 15 mL of THF. This solution was layered with hexanes and after 2 days at -37 °C small blue microcrystals, of insufficient quality for X-ray crystallography, precipitated out of the solution (1.259 g, 0.66 mmol, 66%). An additional crop of product may be obtained by reduction *in vacuo* of the volume of the mother liquor. IR (Nujol, cm^{-1}): 1392 (w), 1369 (m), 1299 (m), 1245 (s), 1215 (m), 1150(s), 1063 (m), 1004 (m), 964 (s), 938 (m), 889(m), 857 (w), 832 (m), 751 (m), 672 (m), 648 (s). Elemental Analysis calcd (found) for $C_{100}H_{176}Cl_4Cr_4N_{12}$: C 63.34 (64.23), H 9.36 (9.85), N 8.86 (8.97). ($\mu_{eff} = 8.83\ \mu_B$)

Synthesis of $[(Cy)_2NC(NCy)_2]_2Cr$(II) (6): Solid $(Cy)_2NC(NCy)_2Li$ (786 mg, 2 mmol) was added to $CrCl_2(THF)_2$ (266 mg, 1 mmol) in toluene (20 mL). The solution turned to purple over 30 minutes. The mixture was stirred for 24 hours and centrifuged to remove LiCl. After twodays at -37 °C, purple crystals, of insufficient quality for X-ray crystallography, precipitated out of the solution (648 mg, 0.79 mmol, 79%). An additional crop of product may be obtained by reduction of the mother liquor *in vacuo*. IR (Nujol mull, cm-1): 1450 (m), 1399 (s), 1386 (s), 1365 (m), 1302 (m), 1253 (m), 1203 (s), 1150 (s), 1142 (s), 1087 (w), 987 (m), 941 (s), 878 (s), 834 (s), 787 (m), 748 (s), 697 (m), 666 (s), 644 (s). Elemental Analysis calcd (found) for $C_{50}H_{88}CrN_6$: C 72.77 (73.23), H 10.75 (10.98), N 10.18 (10.20). ($\mu_{eff} = 4.73\ \mu_B$)

Synthesis of $[(HNCy)C(NCy)_2CrCl]_4$(II) (7): Solid $(HNCy)C(NCy)_2Li$ (310 mg, 1 mmol) was added to $CrCl_2(THF)_2$ (266 mg, 1 mmol) in toluene (20 mL). The solution turned from purple to blue over two hours. The mixture was stirred for 24 hours and

centrifuged to remove LiCl. Toluene was removed under reduced pressure and replaced with of THF (15 mL). This solution was layered with hexanes and after 2 days at -37 °C small blue microcrystals, of insufficient quality for X-ray crystallography, precipitated out of solution (905 mg, 0.58 mmol, 58%). An additional crop of product may be obtained by reduction of the mother liquor *in vacuo*. IR (Nujol, cm^{-1}): 1497 (m), 1420 (m), 1387 (s), 1355 (m), 1276 (m), 1205 (s), 1139 (m), 1109 (s), 1086 (m), 979 (s), 938 (m), 872 (s), 798 (m), 748 (s), 688 (s), 654 (s), 639 (s). Elemental Analysis calcd (found) for C_{76} H_{136} Cl_4 Cr_4 N_{12}: C 58.22 (59.19), H 8.74 (9.10), N 10.72 (10.93). ($\mu_{eff} = 8.79\ \mu_B$)

Synthesis of [(HNCy)C(NCy)$_2$]$_2$Cr(II) (8): Solid (CyNH)C(NCy)$_2$Li (623 mg, 2 mmol) was added to $CrCl_2(THF)_2$ (266 mg, 1 mmol) in toluene (20 mL). The solution turned purple over 1 hour. The contents stirred for 24 hours and centrifuged to remove LiCl. After 4 days at -37 °C, purple needle crystals, suitable for X-ray diffraction, precipitated out of solution (437 mg, 0.66 mmol, 66 %). Additional product may be obtained by reduction of the mother liquor *in vacuo*. IR (Nujol, cm^{-1}): 1487 (m), 1432 (w), 1364 (m), 1283 (s), 1257 (s), 1248 (m), 1204 (m), 1181 (s), 1133 (m), 1087 (m), 980 (s), 920 (m), 869 (s), 852 (s), 837 (m), 799 (m), 764 (m), 721 (s), 694 (s), 657 (m), 641 (s). Elemental Analysis calcd. (found) for C_{38} N_6 Cr H_{68} : C 69.05 (69.82), H 10.37 (10.49), N 12.71 (12.80). ($\mu_{eff} = 4.77\ \mu_B$)

Synthesis of [(HN^{i}Pr)C(ArN)(N^{i}Pr)]$_2$Cr(II) (9): Solid (HN^{i}Pr)C(ArN)(N^{i}Pr)Li (506 mg, 2 mmol) was added to $CrCl_2(THF)_2$ (266 mg, 1 mmol) in toluene (20 mL). The solution turned purple after 1 hour. The mixture was stirred for 24 hours and centrifuged to remove LiCl. After two days at -37 °C, purple crystals suitable for X-ray crystallography, precipitated out of the solution (406 mg, 0.75 mmol, 75%). An additional crop of product may be obtained by reduction of the mother liquor *in vacuo*. IR (Nujol, cm^{-1}): 1456 (s), 1429 (s), 1421 (s), 1397 (m), 1275 (m), 1233 (m), 1174 (s), 1135 (m), 1022 (m), 957 (m), 932 (m), 886 (s), 832 (s), 791 (m), 723 (m), 699 (m), 657 (m), 641 (m). Elemental Analysis calcd (found) for C_{30} H_{48} Cr N_6: C 66.15 (66.23), H 8.88 (9.14), N 15.43 (15.74). ($\mu_{eff} = 4.79\ \mu_B$)

Synthesis of $[(Me_3Si)_2NC(NCy)_2]_2CrCl(III)$ (10): Solid $(Me_3Si)_2NC(NCy)_2Li$ (746 mg, 2 mmol) was added to $CrCl_3(THF)_3$ (374 mg, 1 mmol) in toluene (20 mL). The solution turned dark red over two hours. The mixture was stirred for 24 hours and centrifuged to remove LiCl. The solvent was removed *in vacuo* and replaced with hexane. After two days at -37 °C, red plate crystals suitable for X-ray diffraction precipitated out of the solution (624 mg, 0.76 mmol, 76%). IR (Nujol, cm^{-1}): 1668 (m), 1637 (m), 1469 (w), 1345 (m), 1308 (m), 1251 (w), 1200 (w), 1142 (s), 1074 (m), 1012 (m), 970 (s), 940 (w), 823 (w), 757 (m), 678 (m), 640 (s). Elemental Analysis calcd (found) for $C_{38}H_{80}ClCrN_6Si_4$: C 55.60 (54.65), H 9.82 (10.41), N 10.24 (10.31). ($\mu_{eff} = 3.49\ \mu_B$)

Synthesis of $[(Me_3Si)_2NC(N^iPr)_2]_2CrCl(III)$ (11): Solid $(Me_3Si)_2NC(N^iPr)_2Li$ (586 mg, 2 mmol) was added to $CrCl_3(THF)_3$ (374 mg, 1 mmol) in toluene (20 mL). The solution turned dark red over two hours. The mixture was stirred for 24 hours and centrifuged to remove LiCl. The solvent was removed *in vacuo* and replaced with hexane. After two days at -37 °C, red plate crystals suitable for X-ray diffraction, precipitated out of solution. (487 mg, 0.74 mmol, 74%) IR (Nujol, cm^{-1}): 1654 (m), 1598 (m), 1475 (w), 1350 (s), 1310 (m), 1231 (w), 1110 (s), 1093 (m), 992 (m), 960 (s), 938 (m), 840 (m), 790 (w), 681 (m), 641 (s). Elemental Analysis calcd (found) for $C_{26}H_{64}ClCrN_6Si_4$: C 47.27 (46.56), H 9.76 (9.66), N 12.72 (12.68). ($\mu_{eff} = 3.51\ \mu_B$)

Synthesis of $[(Me_3Si)_2NC(NCy)_2]_3Cr(III)$ (12): Solid $(Me_3Si)_2NC(NCy)_2Li$ (1.119 g, 3 mmol) was added to $CrCl_3(THF)_3$ (374 mg, 1 mmol) in toluene (20 mL). The solution turned dark blue over twohours. The mixture was stirred for 24 hours and centrifuged to remove LiCl. After 4 days at -37 °C, blue microcrystals of insufficient quality for X-ray diffraction, precipitated out of the solution (609 mg, 0.53 mmol, 53%). IR (Nujol, cm^{-1}): 1622 (w), 1587 (m), 1563 (m), 1531 (s), 1499 (m), 1463 (s), 1413 (m), 1377 (s), 1320 (w), 1282 (m), 1255 (m), 1203 (s), 1137 (m), 1061 (m), 989 (s), 911 (m), 873 (m), 812 (s), 773 (m), 743 (m), 721 (s), 679 (m), 643 (s). Elemental Analysis calcd (found) for $C_{57}H_{120}CrN_9Si_6$: C 59.42 (60.13), H 10.50 (10.78), N 10.94 (10.99). ($\mu_{eff} = 3.79\ \mu_B$)

Synthesis of $[(Me_3Si)_2NC(N^iPr)_2]_3Cr(III)$ (13): Solid $(Me_3Si)_2NC(N^iPr)_2Li$ (879 mg, 3 mmol) was added to $CrCl_3(THF)_3$ (374 mg, 1 mmol) in toluene (20 mL). The solution turned dark blue over two hours. The mixture was stirred for 24 hours and centrifuged to remove LiCl. After four days at -37 °C, blue microcrystals of insufficient quality for X-ray diffraction, precipitated out of the solution (572 mg, 0.63 mmol, 63%). IR (Nujol, cm^{-1}): 1692 (w), 1562 (m), 1538 (s), 1505 (m), 1471 (s), 1397 (m), 1361 (m), 1319 (s), 1272 (m), 1199(s), 1138 (m), 1084 (m), 1023 (m), 1008 (m), 978 (m), 934 (s), 876 (m), 853 (s), 819 (m), 788 (s), 723 (m), 689 (m), 650 (s). Elemental Analysis calcd (found) for C_{39} H_{96} Cr N_9 Si_6: C 51.38 (53.02), H 10.61 (10.78), N 13.83 (13.91). (μ_{eff} = 3.73 μ_B)

Synthesis of $((Et)_2NCS_2)CrCl_2(THF)_2$(III) (14) (Method A): Tetraethylthiuram disulfide (296 mg, 1 mmol) was added to $CrCl_2(THF)_2$ (532 mg, 2 mmol) in THF (20 mL). The solution turned immediately blue. The mixture was stirred for 24 hours. From a slow evaporation of the solution blue block crystals formed after 5 days (638 mg, 1.582 mmol, 79%). An additional crop of product may be obtained by reduction of the mother liquor *in vacuo*. IR (Nujol, cm^{-1}): 1515 (s), 1456 (m), 1376 (s), 1286 (s), 1205 (s), 1149 (m), 1074 (s), 1020 (s), 918 (m), 863 (m), 718 (m), 663 (s). Elemental Analysis calcd (found) for C_{13} H_{26} Cl_2 Cr N O_2 S_2: C 37.59 (36.55), H 6.31 (6.30), N 3.37 (3.37). (μ_{eff} = 3.70 μ_B)

Synthesis of $((Et)_2NCS_2)CrCl_2(THF)_2$(III) (14) (Method B): Solid $(Et)_2NC(S)_2K$ (746 mg, 2 mmol) was added to $CrCl_3(THF)_3$ (374 mg, 1 mmol) in THF (15 mL). The solution turned dark blue over two hours. The mixture was stirred for 24 hours and centrifuged to remove KCl. After four days at -37 °C, blue microcrystals precipitated out of the solution (398 mg, 0.96 mmol, 96%). IR, EA and magnetic moment measurements confirmed the identity of the product as **14**.

Synthesis of $[(Me_3Si)_2NC(NCy)_2]_2Ni(II)$ (15): To a suspension of $NiCl_2THF_2$ (274 mg, 1 mmol) in toluene (15 mL) $(Me_3Si)_2NC(NCy)_2Li$ (746 mg, 2 mmol) was added. The color of the solution turned brown and stirring was continued for additional 24 hours. The solution was then centrifuged to remove LiCl. After 3 days at -37 °C, brown needle

crystals of sufficient quality for X-ray diffraction precipitated out of the solution (621 mg, 0.78 mmol, 78%). IR (Nujol mull, cm-1): 1587 (m), 1520 (m), 1489 (s), 1475 (m), 1432 (s), 1398 (w), 1339 (m), 1286 (s), 1257 (s), 1209 (m), 1180 (m), 1103 (m), 1071 (m), 988 (s), 952 (m), 899 (w), 823 (m), 765 (s), 690 (m), 645 (s). Elemental Analysis calcd (found) for C_{38} H_{80} N_6 Ni Si_4: C 57.62 (58.12), H 10.18 (10.46), N 10.61 (10.74). ($\mu_{eff} = 2.84\ \mu_B$)

2.3 Crystal Structure Descriptions

The structure of complex **1** consists of four chromium and four chlorine atoms each occupying one corner of a cubic arrangement (Figure 2.4.1). Each chromium atom is surrounded by two nitrogen atoms of one chelating guanidinate ligand and three chlorine atoms. The chromium atoms adopt distorted trigonal bipyramidal geometries with each corner of the cube being generated by symmetry operation. The internal bond angles [C1(1)-Cr(1)-Cl(1a) and Cl(1)-Cr(1)-Cl(1b) = 92.66(7)°, Cr(1)-Cl(1)-Cr(1b) = 96.91(7)°, N(2)-Cr(1)-Cl(1) = 100.38(15)°, N(1)-Cr(1)-Cl(1) = 166.68(19)°] clearly show the distortion in the trigonal bypramidal geometry introduced by the small bite angle of the ligand [N(1)-C(1)-N(2) = 111.2(6)°]. The Cr-N bond lengths [Cr(1)-N(1) = 2.034(5) Å, Cr(1)-N(2) = 2.030(5) Å] are comparable to other known guanidinate chromium complexes.[8] The Cr-Cl bond lengths [Cr(1)-Cl(1) = 2.4301(19) Å, Cr(1)-Cl(1a) and Cr(1)-Cl(1b) = 2.441(2) Å] are in the normal range.[8] The C(1)-N(1) and C(1)-N(2) bond lengths average to 1.3465 Å while the C(1)-N(3) bond length is significantly longer [1.445(8) Å]. This indicates that little π conjugation is taking place between the C(1) and N(3) atoms, most likely being the result of the presence of bulky trimethylsilyl and cyclohexyl substituents on the nitrogen atoms of the guanidinate ligand.

Complex **3** (Figure 2.4.2) consists of two bidentate guanidinate ligands surrounding one chromium metal center in a distorted square planar arrangement. The guanidinate ligand binds to the chromium through two nitrogen atoms [Cr(1)-N(1) = 2.084(3) Å, Cr-N(2) = 2.077(3) Å] to yield a planar 4-membered ring with sp^2 hybridized N and C centers [N(1)-Cr(1)-N(2) and N(1a)-Cr(1)-N(2a) = 64.08(11)°, N(1)-Cr(1)-N(1a) = 117.17(16)°, N(2)-Cr(1)-N(2a) = 115.96(17)°]. The narrow bite angle of the chelating ligand [N(2)-C(19)- N(3) = 112.5(3)°] again is the cause of the distortion. The distance between the chromium atom and the central carbon atom of the guanidinate ligand although short is still outside the bonding range [Cr(1)-C(19) = 2.501(3) Å]. The partial double bond character of the N-C-N ligand backbone is reflecting in the average bond lengths [N(1)-C(19) = 1.323(4) Å, N(2)-C(19) = 1.332(4) Å]. Similar to **1** the trimethylsilyl groups attached to the N(3) atom are out of the plane defined by the metal with cyclohexyl groups attached to the N(1) and N(2) atoms.

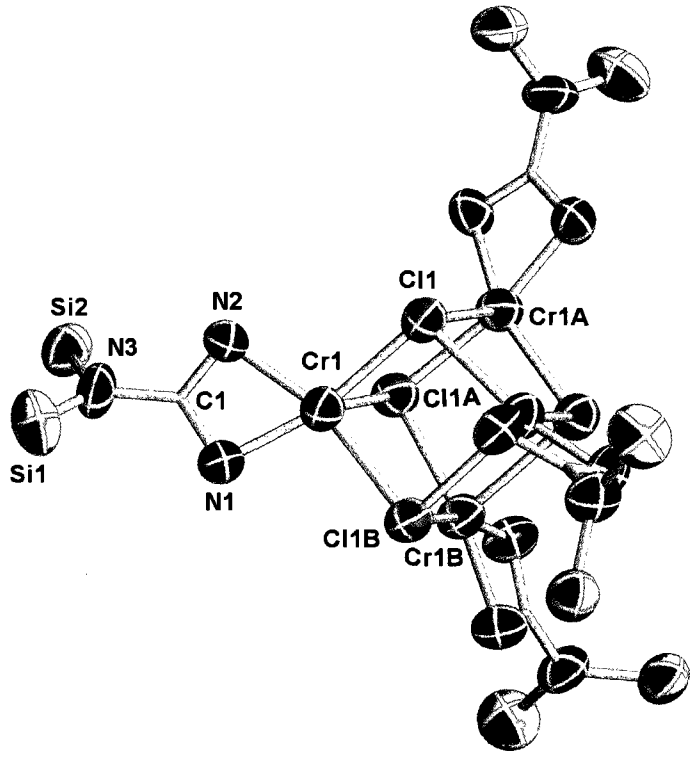

Figure 2.3.1. ORTEP representation of **1**, with thermal ellipsoids set at 50% probability. Hydrogen atoms, cyclohexyl groups and trimethylsilyl groups have been emitted for clarity. Atoms labeled with "a" are generated by the symmetry operation. Selected bond lengths (Å) and angles (°): Cr(1)-N(1) 2.034(5), Cr(1)-N(2) 2.030(5), Cr(1)-Cl(1) 2.4301(19), Cr(1)-Cl(1)a and Cr(1)-Cl(1)b 2.441(2), C(1)-N(3) 1.445(8), N(1)-C(1)-N(2) 111.2 (6).

Complex **4** has structural features very similar to those of **3**. The only difference is the presence on the ligand of isopropyl groups in place of the cyclohexyl groups. Even in this case, the chromium metal center is surrounded by two chelating guanidinate ligands and adopts a distorted square planar geometry. The bite angle of the chelating ligand [N(1)-C(1)-N(2) = 112.1(3)°] is similar to that found in **3.** The isopropyl groups on adjacent guanidinate ligands are oriented so that the methyl groups are not pointed directly at each other. The Cr-N bonds [Cr(1)-N(1) = 2.075(3) Å, Cr(1)-N(2) = 2.066(3) Å] are slightly shorter than in complex **3**. The partial double bond character of the C-N bonds in the N-C-N ligand backbone gives the expected bond lengths [N(1)-C(1) = 1.332(5) Å, N(2)-C(1) = 1.334(5) Å]. The C-N bond to the non-coordinated nitrogen

atom [N(3)-C(1) = 1.423(5) Å] is also as expected due to the presence of bulky isopropyl and trimethylsilyl groups attached to the nitrogen atoms.

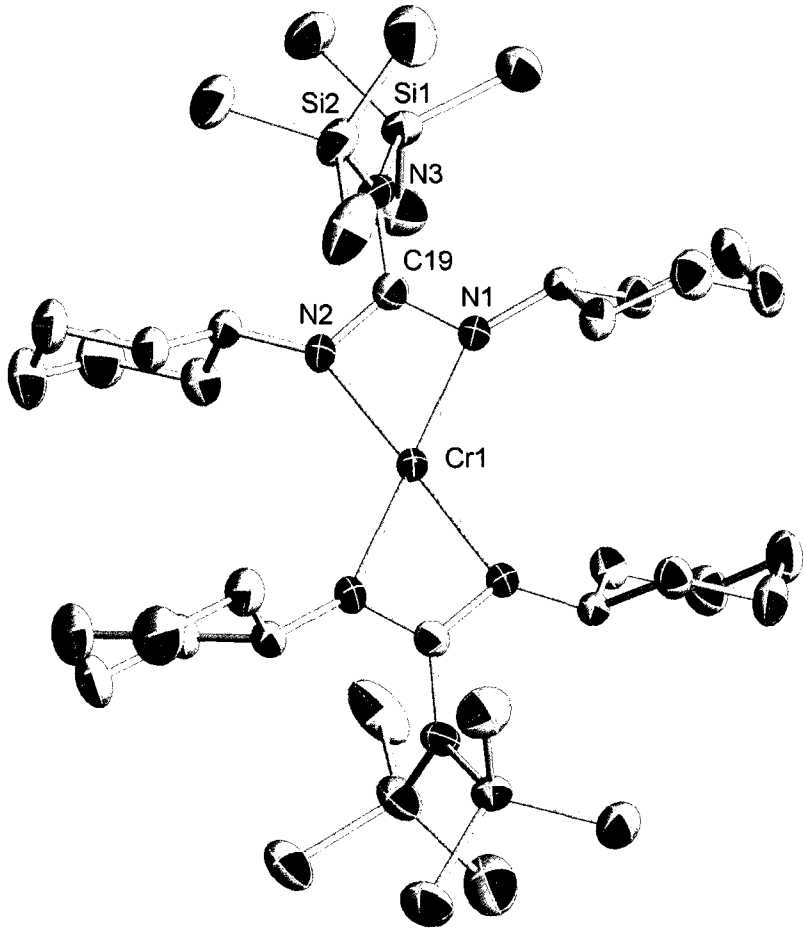

Figure 2.2.2 ORTEP representation of **3**, with thermal ellipsoids set at 50% probability and hydrogen atoms emitted for clarity. Atoms labeled with "a" are generated by the symmetry operation. Selected bond lengths (Å) and angles (°): Cr(1)-N(1) 2.084(3), Cr(1)-N(2) 2.077(3), C(19)-N(3) 1.437(4), N(1)-C(19)-N(2) 112.5(3).

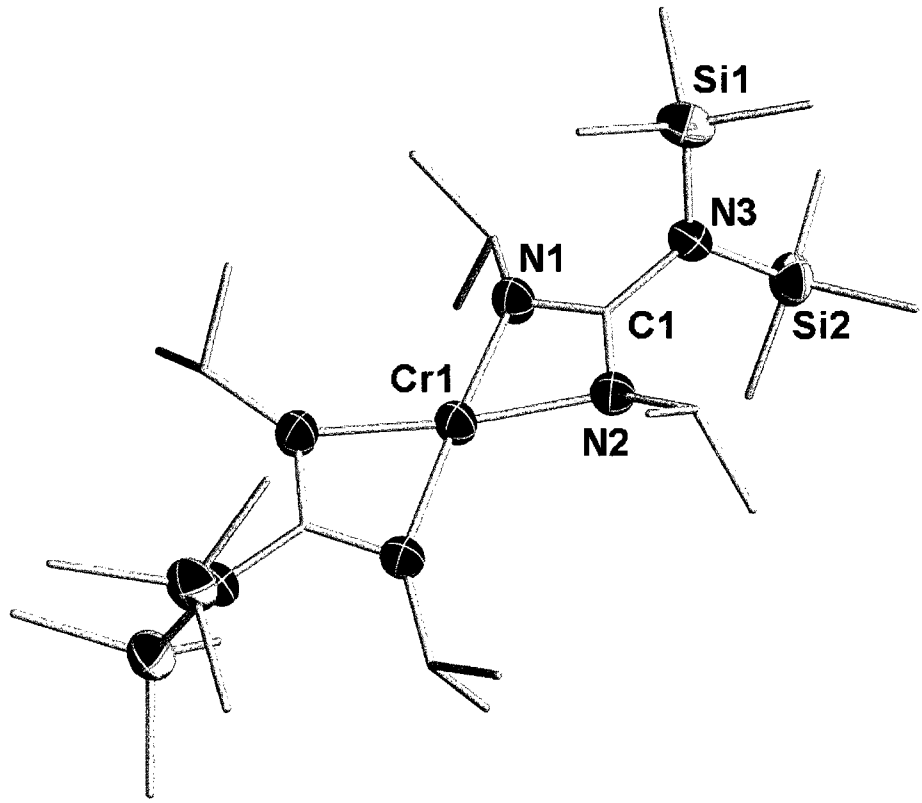

Figure 2.3.3 ORTEP representation of **4**, with thermal ellipsoids set at 50% probability and hydrogen atoms emitted for clarity. Atoms labeled with "a" are generated by the symmetry operation. Selected bond lengths (Å) and angles (°): Cr(1)-N(1) 2.075(3), Cr(1)-N(2) 2.066(3), C(1)-N(3) 1.423(5), N(1)-C(1)-N(2) 112.1(3).

The structure of **8**, shown in Figure 2.4.4, is very similar to the other two previously characterized bis-guanidinato complexes of chromium. The Cr metal center is surrounded by two guanidinate ligands in a distorted square planar geometry. The flanking nitrogen atom, N(1) in this case, is now bonded to a cyclohexyl group and hydrogen atom as opposed to two trimethylsilyl groups. This allows the N(1)-C(1) bond to rotate more freely and, as a result, the cyclohexy group attached to N(1) becomes coplanar with the other cyclohexyl groups attached to N(2) and N(3). The bite angle of the ligand [N(2)-C(1)-N(3) = 112.0(2)°] is very similar to those found in complexes **3** and **4**. The Cr-N bond lengths [Cr(1)-N(2) = 2.082(2) Å, Cr(1)-N(3) = 2.058(2) Å] are also as to be expected. Examining the bonds within the CN_3 unit [N(2)-C(1) = 1.332(3) Å, N(3)-C(1) = 1.335(3) Å, N(1)-C(1) = 1.379(3) Å] reveals that the C-N bond to the non-

coordinated nitrogen atom is significantly shorter than in the previously characterized guanidinate complexes. The shortening of this bond is clearly caused by decreasing the steric bulk of the alkyl groups attached to the non-coordinated nitrogen atom of the guanidinate ligand.

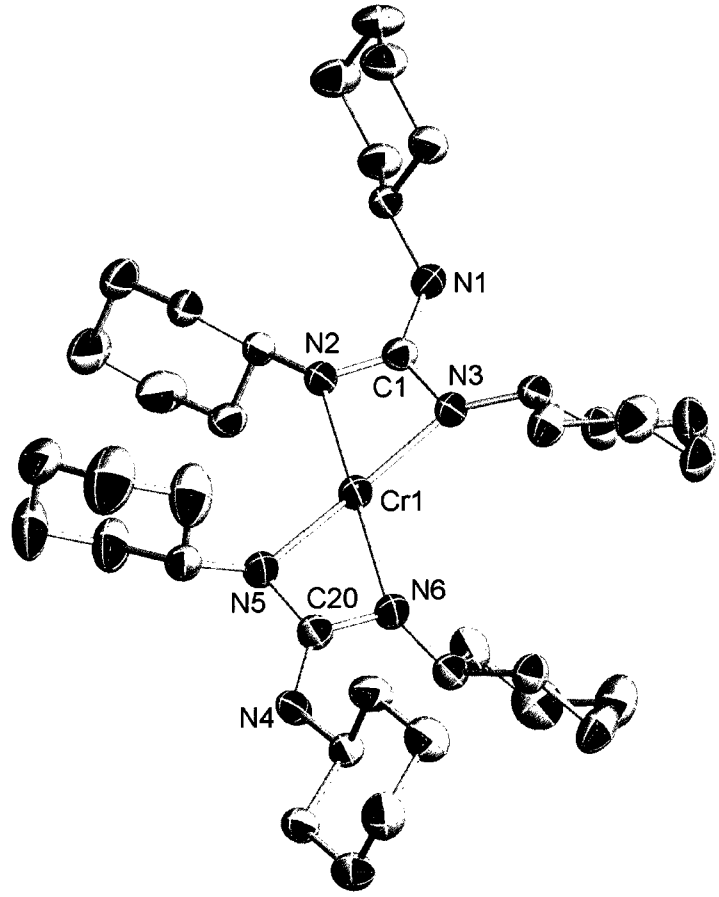

Figure 2.3.4 ORTEP representation of **8**, with thermal ellipsoids set at 50% probability and hydrogen atoms emitted for clarity. Atoms labeled with "a" are generated by the symmetry operation. Selected bond lengths (Å) and angles (°): Cr(1)-N(2) 2.082(2), Cr(1)-N(3) 2.058(2), C(1)-N(1) 1.379(3), N(2)-C(1)-N(3) 112.0(2).

Complex **9** features two guanidinate ligands surrounding one chromium atom in a distorted square planar geometry (Figure 2.4.5). The bite angle of the chelating ligand [N(3)-C(7)-N(5a) = 111.6(3)°] causes the deviation of the geometry from the ideal trigonal planar. The Cr-N bond lengths [Cr(1)-N(3) = 2.047(3) Å, Cr(1)-N(5a) = 2.073(3)

Å] compare well with those of the other compounds reported in this work. The C-N bonds within the CN_3 core [N(3)-C(7) = 1.322(4) Å, N(5a)-C(7) = 1.345(4) Å, N(4)-C(7) = 1.370(5) Å] show that the replacement of sterically encumbered cyclohexyl or isopropyl groups on one of the nitrogen atoms of the ligand for the less bulky 2,6-dimethylphenyl group has allowed for a larger extent of hybridization of the amido nitrogen and carbon atom. The bond to the non-coordinated nitrogen atom is the shortest in all the chromium guanidinato complexes characterized in these studies.

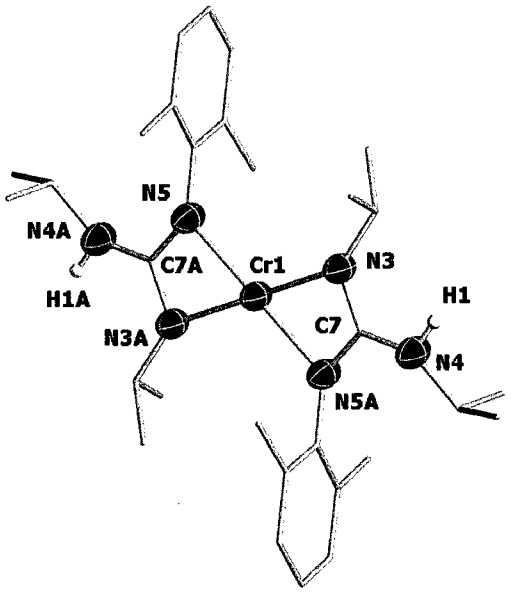

Figure 2.3.5 ORTEP representation of **9**, with thermal ellipsoids set at 50% probability and hydrogen atoms emitted for clarity. Atoms labeled with "a" are generated by the symmetry operation. Selected bond lengths (Å) and angles (°): Cr(1)-N(3) 2.047(3), Cr(1)-N(5)a 2.073(3), C(7)-N(4) 1.370(5), N(3)-C(7)-N(5)a 111.6(3).

Complex **10** (Figure 2.4.6) consists of one chromium atom surrounded by two guanidinate ligands and one chlorine atom in a distorted trigonal bipyramidal geometry. The chlorine atom and one nitrogen atom occupy the axial positions while the other three nitrogen atoms occupy the equatorial positions. The bite angles of the two guanidinate ligands [N(1)-C(2)-N(2) = 110.7(4)°, N(3)-C(1)-N(4) = 109.9(4)°] are comparable to the other guanidinato complexes of chromium. The Cr-N bond lengths [Cr(1)-N(1) = 2.050(4) Å, Cr(1)-N(2) = 2.008(4) Å, Cr(1)-N(3) = 2.072(3) Å, Cr(1)-N(4) = 1.970(4) Å] are all similar except for the bond to the N(4) atom which is in the axial position. The Cr-

Cl bond [Cr(1)-Cl(1) = 2.2900(13) Å] is within the expected range. The trimethylsilyl groups and cyclohexyl groups are oriented on the opposite sites of the plane defined by the three ligand nitrogen atoms. The C-N bond lengths of the CN_3 units [N(1)-C(2) = 1.329(6) Å, N(2)-C(2) = 1.321(6) Å, N(3)-C(1) = 1.329(6) Å, N(4)-C(1) = 1.337(6) Å, N(5)-C(2) = 1.427(6) Å, N(6)-C(1) = 1.420(6) Å] are similar to the other Cr(II) guanidinato complexes bearing the same ligand.

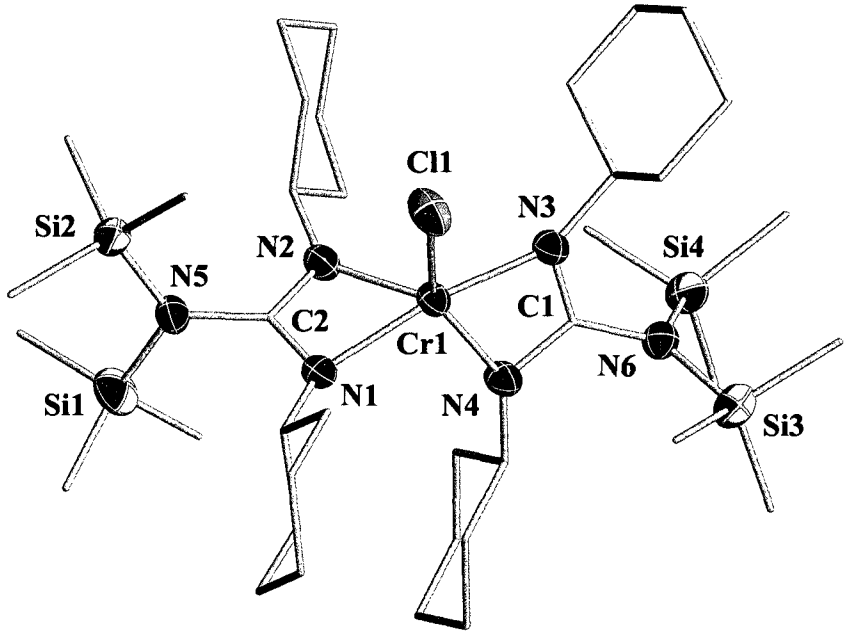

Figure 2.3.6 ORTEP representation of **10**, with thermal ellipsoids set at 50% probability and hydrogen atoms emitted for clarity. Atoms labeled with "a" are generated by the symmetry operation. Selected bond lengths (Å) and angles (°): Cr(1)-Cl(1) 2.2900(13), Cr(1)-N(1) 2.050(4), Cr(1)-N(2) 2.008(4), Cr(1)-N(3) 2.072(3), Cr(1)-N(4) 1.970(4), N(1)-C(2)-N(2) 110.7(4), N(3)-C(1)-N(4) 109.9(4).

Complex **11** is isostructural with **10** (Figure 2.4.7). The complex consists of one chromium atom surrounded by two guanidinate ligands and one chlorine atom in a distorted trigonal bipyramidal geometry. The chlorine atom and one nitrogen atom occupy the axial positions while the other three nitrogen atoms occupy the equatorial positions, the same as in complex **10**. The only difference between the two complexes is the substitution of the cyclohexyl substituents on the "NCN" moiety with isopropyl

substituents. The bite angles of the chelating ligands [N(1)-C(1)-N(2) = 109.5(3)°, N(4)-C(2)-N(5) = 110.5(3)°] are nearly identical to that of complex **10**. The Cr-N bond lengths [Cr(1)-N(1) = 1.971(3) Å, Cr(1)-N(2) = 2.049(3) Å, Cr(1)-N(4) = 2.027(3) Å, Cr(1)-N(5) = 2.030(3) Å] are similar to those of complex (**10**) except for the fact that the Cr-N to the axial nitrogen atom is not the shortest. The Cr-Cl bond [Cr(1)-Cl(1) = 2.2875(14) Å] is as expected. The C-N bond lengths of the two CN_3 units [N(1)-C(1) = 1.329(5) Å, N(2)-C(1) = 1.325(5) Å, N(4)-C(2) = 1.323(5) Å, N(5)-C(2) = 1.342(5) Å, N(3)-C(1) = 1.431(5) Å, N(6)-C(2) = 1.424(5) Å] imply that no significant π conjugation is taking place between the N(3) or N(6) atoms and the C(1) and C(2) atoms respectively.

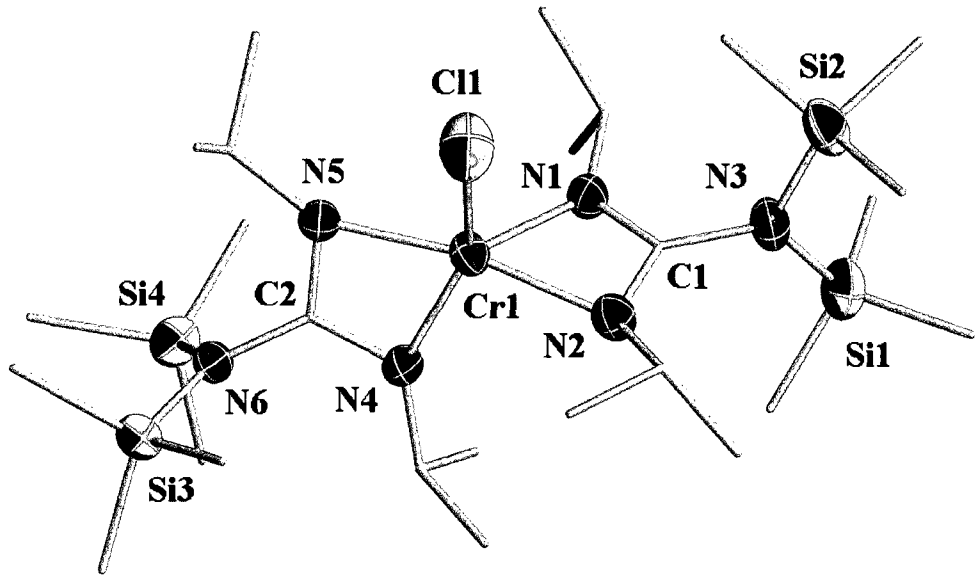

Figure 2.3.7 ORTEP representation of **11**, with thermal ellipsoids set at 50% probability and hydrogen atoms emitted for clarity. Atoms labeled with "a" are generated by the symmetry operation. Selected bond lengths (Å) and angles (°): Cr(1)-Cl(1) 2.2875(14), Cr(1)-N(1) 1.971(3), Cr(1)-N(2) 2.049(3), Cr(1)-N(3) 2.027(3), Cr(1)-N(4) 2.030(3), N(1)-C(1)-N(2) 109.5(3), N(4)-C(2)-N(5) 110.5(3).

The structure of complex **14**, shown in Figure 2.3.7, consists of one Cr atom surrounded by the two sulfur atoms of the chelating ligand, two chlorine atoms, and two oxygen atoms from two molecules of THF. The overall geometry of the complex is distorted octahedral. The THF molecules are located *trans* to each other while the sulfur atoms and chlorine atoms are in *cis*. The deviation from trigonal planar angle arises from

the small bite angle of the thiocarbamate ligand [S(1)-C(1)-S(2) = 113.4(2)°]. This is larger by about 3° than the bite angle found in the guanidinato complexes of chromium. An inspection of the internal angles [S(1)-Cr(1)-S(2) = 74.04(6)°, Cl(1)-Cr(1)-Cl(2) = 100.79(7)°, S(2)-Cr(1)-Cl(1) = 92.81(7)°, S(1)-Cr(1)-Cl(2) = 92.37(6)°] reveals the distortions being caused by the small bite angle of the ligand and the repulsions between the lone pairs of electrons on the chlorine atoms. The Cr-O bond lengths are the expected length for a coordinated THF molecule [Cr(1)-O(1) = 2.047(3) Å, Cr(1)-O(2) = 2.061(3) Å].[12] The Cr-Cl bond lengths [Cr(1)-Cl(1) = 2.3294(16) Å, Cr(1)-Cl(2) = 2.3293(15) Å] are as expected and the Cr-S bond lengths [Cr(1)-S(1) = 2.4015(17) Å, Cr(1)-S(2) = 2.3970(16) Å] are comparable to the hitherto known chromium dithiocarbamate complexes.[13] The S(1)-C(1) and S(2)-C(1) bonds, 1.727(4) Å and 1.729(4) Å respectively, differ by only 0.002 Å. The C-N bond length [N(1)-C(1) = 1.321(5) Å] is significantly shorter than those found in the guanidinato complexes of chromium.

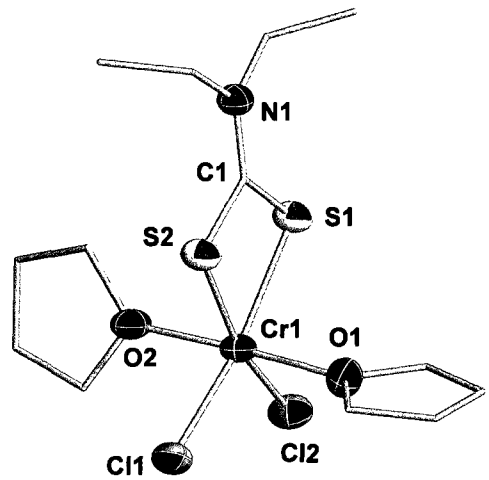

Figure 2.3.8 ORTEP representation of **14**, with thermal ellipsoids set at 50% probability and hydrogen atoms emitted for clarity. Atoms labeled with "a" are generated by the symmetry operation. Selected bond lengths (Å) and angles (°): Cr(1)-S(1) 2.4015(17), Cr(1)-S(2) 2.3970(16), Cr(1)-Cl(1) 2.3294(16), Cr(1)-Cl(2) 2.3293(15), Cr(1)-O(1) 2.047(3), Cr(1)-O(2) 2.061(3), S(1)-C(1)-S(2) 113.4(2).

Complex **15** consist of a single Ni atom surrounded by two guanidinate ligands in a tetrahedral geometry (Figure 2.3.9). The guanidinate ligand binds to the nickel through two nitrogen atoms to yield a planar 4-membered ring with sp^2 hybridized N and C

centers, the same as in the chromium guanidinate complexes. All four Ni-N bond lengths [Ni(1)-N(1) = 1.975(5) Å] are equivalent. The Ni(1)-C(1) distance although short [2.408(8) Å] is still too long for any bonding interaction. The C-N bond lengths within the CN_3 core [N(1)-C(1) = 1.323(6) Å, N(2)-C(1) = 1.416(10) Å] show that there is little π conjugation occurring between the N(2) and C(1) atoms.

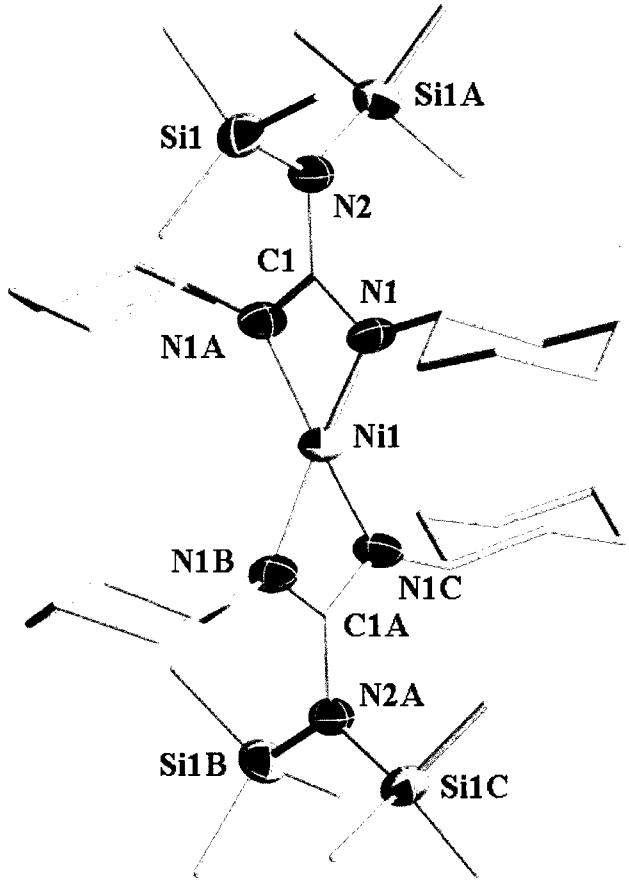

Figure 2.3.9 ORTEP representation of **15**, with thermal ellipsoids set at 50% probability and hydrogen atoms emitted for clarity. Atoms labeled with "a" are generated by the symmetry operation. Selected bond lengths (Å) and angles (°): Ni(1)-N(1) 1.975(5), Ni(1)-C(1) 2.408(8), N(1)-C(1) 1.323(6), N(2)-C(1) 1.416(10), N(1)-C(1)-N(1)a 110.2(7).

2.4 Results and Discussion

The lithium salts of a number of guanidinate monoanions were synthesized. The only ligands that will be discussed are those for which a chromium complex was obtained and fully characterized. These ligands are highlighted in Figure 2.4.1.

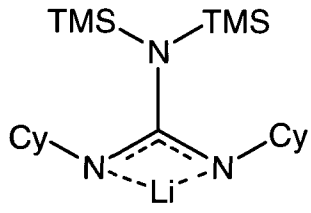

$(Me_3Si)_2NC(NCy)_2Li$

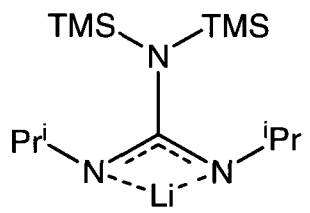

$(Me_3Si)_2NC(N^iPr)_2Li$

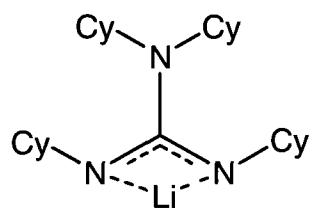

$(Cy)_2NC(NCy)_2Li$

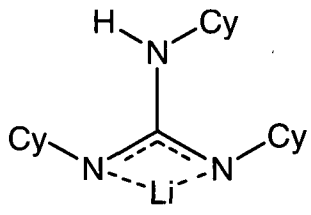

$(HNCy)C(NCy)_2Li$

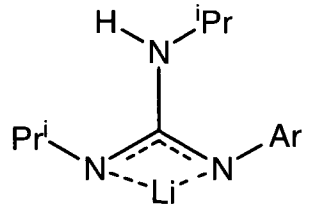

Ar = 2,6-dimethylphenyl

$(HN^iPr)C(ArN)(N^iPr)Li$

Figure 2.4.1 Lithium salts of the guanidinates used.

The lithium salts $(Me_3Si)_2NC(NR)_2Li$, [R = Cy,^{i}Pr] were synthesized according to a literature procedure.[9] A commercially obtained solution of $LiN(Me_3Si)_2$ was added to dicyclohexylcarbodiimide or diisopropylcarbodiimide in diethyl ether and removal of the solvent under reduced pressure yielded the pure lithium guanidinates. The other three lithium guanidinates were obtained by the same standard procedure shown in Figure 2.4.2. Dicyclohexylamine, cyclohexylamine or 2,6-dimethylaniline was deprotonated using ^{n}BuLi in THF. To this solution was added either dicyclohexylcarbodiimide or

diisopropylcarbodiimide. The solution was stirred overnight and solvent removed under reduced pressure to yield the pure lithium guanidinate salts.

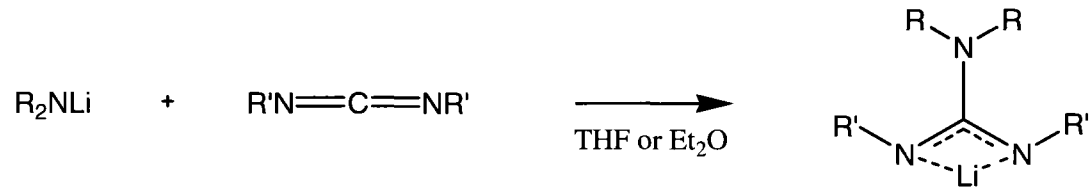

Figure 2.4.2 Synthesis of lithium guanidinate salts.

The lithium guanidinate salts were reacted directly through a metathesis reaction with either $CrCl_2THF_2$ or $CrCl_3THF_3$. The reaction mixtures were usually stirred overnight, or until the color of the solution remained constant. The solution was then centrifuged to remove LiCl which precipitates readily out of toluene. Crystallizations were attempted by cooling the reaction mother liquors at -37 °C for a week. If no crystals had formed a number of different techniques were used to try to induce crystallization. Some of these included, layering with hexanes, slow evaporation, changing of solvent, and hot recrystallization from a minimum amount of solvent. In some cases crystals of the product were obtained and a thorough and conclusive characterization of the compound was performed. In the other cases, where no crystals were obtained a structure was assumed and characterization was carried out via magnetic moment, elemental analysis, and IR. NMR analysis could not be performed as all complexes obtained in this chapter were paramagnetic.

The reaction of one equivalent of lithium guanidinate with $CrCl_2THF_2$ in toluene provided good yields of tetrameric cluster complexes **1**, **2**, **5**, and **7** (Figure 2.4.3). The reaction of two equivalents of lithium guanidinate with $CrCl_2THF_2$ in toluene provided instead the expected square planar chromium complexes **3**, **4**, **6**, and **8** (Figure 2.4.4).

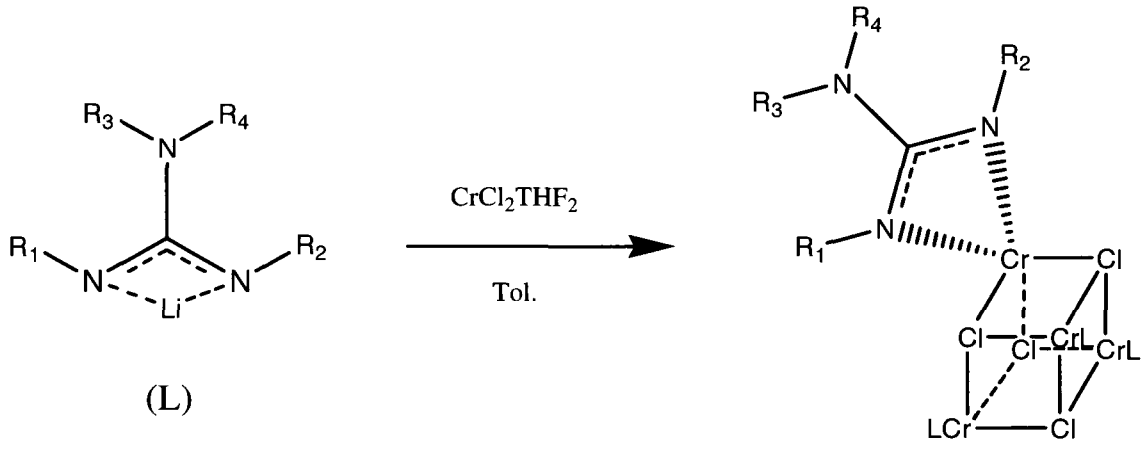

1: $R_1 = R_2 = Cy$, $R_3 = R_4 = TMS$
2: $R_1 = R_2 = {}^{i}Pr$, $R_3 = R_4 = TMS$
5: $R_1 = R_2 = R_3 = R_4 = Cy$
7: $R_1 = R_2 = R_3 = Cy$, $R_4 = H$

L = Guanidinate ligand

Figure 2.4.3 Synthesis of Monoguanidinate Chromium (II) Chloride complexes.

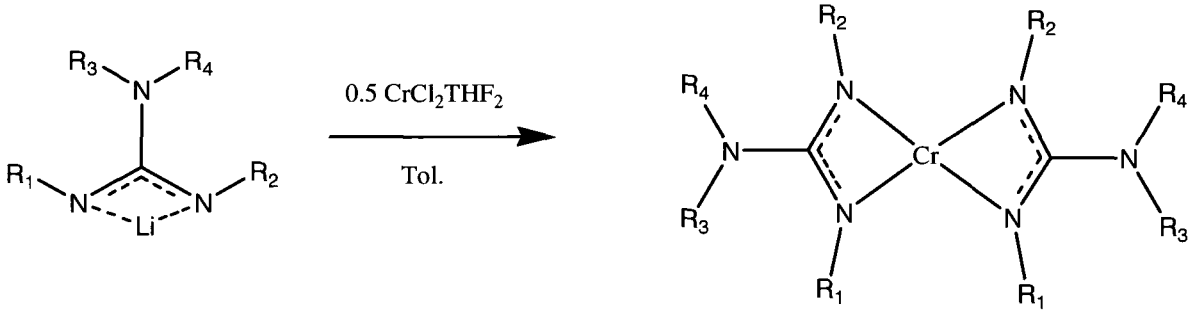

3: $R_1 = R_2 = Cy$, $R_3 = R_4 = TMS$
4: $R_1 = R_2 = {}^{i}Pr$, $R_3 = R_4 = TMS$
6: $R_1 = R_2 = R_3 = R_4 = Cy$
8: $R_1 = R_2 = R_3 = Cy$, $R_4 = H$
9: $R_1 = R_3 = {}^{i}Pr$, $R_2 = 2,6$-dimethylphenyl, $R_4 = H$

Figure 2.4.4 Synthesis of Bis-guanidinate Chromium (II) complexes.

Crystallization of **1** and **2** proved to be particularly tedious. This is most likely due to the large distortions in the molecule which cause the crystal lattice to be deformed and results in poor overall crystallinity. The magnetic susceptibility measurements for compounds **1** and **2** gave values of $\mu_{eff} = 8.79\ \mu_B$ and $\mu_{eff} = 8.78\ \mu_B$ respectively. These values are as to be expected as there are four d^4 chromium atoms held in close proximity and therefore most likely antiferromagnetically coupled.

Compounds **3** and **4** are also easy to prepare and crystallize quite readily from toluene. These compounds are monomeric and adopt a square-planar geometry as it can be expected for a Cr(II) atom in a low spin ligand field. Their magnetic moment were found in the expected range [μ_{eff} = 4.77 μ_B for **1** and μ_{eff} = 4.76 μ_B for **2**].

Reaction of either one or two equivalents of $(Cy)_2NC(NCy)_2Li$ with $CrCl_2THF_2$ in toluene afforded **5** and **6** respectively. Suitable single crystals could not be grown for these compounds and so their structure is based on the similarities with previous findings and other methods of characterization. The magnetic moment of complexes **5** and **6** are μ_{eff} = 8.83 μ_B and μ_{eff} = 4.73 μ_B respectively, elemental analysis also confirms this structural assignment as well.

Reaction of one or two equivalents of $(HNCy)C(NCy)_2Li$ with $CrCl_2THF_2$ in toluene generated compounds **7** and **8**. Crystals of compound **7** could not be grown to allow X-ray diffraction structural assignment which relied on the similarity of the values of the magnetic moment, μ_{eff} = 8.79 μ_B, and consistent elemental analysis data.

Compound **8** crystallized nicely from toluene thus allowing full characterization. This compound was found to posses the expected square planar geometry. The replacement of one cyclohexyl group on the amido nitrogen for a hydrogen atom did not alter the bite angle of the ligand. This substitution is in principle promising since that this amido nitrogen may be deprotonated and then functionalized further using a number of possible reagents. Unfortunately, attempts of deprotonating the ligand to form the dianionic congener prior to complexation were unsuccessful. Additionally, attempts at reacting complex **8** with either MeLi, ^nBuLi, or $AlMe_3$ yielded materials that could not be characterized.

The reaction of two equivalents of $(HN^iPr)C(ArN)(N^iPr)Li$ [Ar = 2,6-dimethylphenyl] with $CrCl_2THF_2$ in toluene provided the expected complex **9**. The reaction carried out with one equivalent of the lithium guanidinate salt did not produce the expected tetrameric cluster obtained in all the other cases. The complex is always formed in disregard of the stoichiomeric ratio including the use of excess of guanidinate ligand. The magnetic moment of **9** [μ_{eff} = 4.79 μ_B] was as expected for a chromium metal center in a square-planar ligand field.

In complexes **1-4** the bulkiness of the TMS, cyclohexyl or isopropyl groups made the angle between the "$(TMS)_2N$" and "RNCNR" moieties nearly 90 °. In turn, this prevents π-conjugation between the lone pair of the amido nitrogen and the sp^2 hybridized C atom. The presence of the less bulky 2,6-dimethylphenyl substituent to the "NCN" moiety of the ligand widened the bite angle and allowed for a greater amount of π conjugation to occur between the N amido atom and the sp^2-hybridized carbon atom. Using less sterically demanding substituents on the nitrogen atoms allows for more rotation to occur along the N-C bonds. The substituents can then come into plane and delocalization of charge can occur by increasing the π conjugation between atoms.

The guanidinato complexes of Cr(III) were also synthesized to eventually explore the effect of the oxidation state on catalytic behavior. The chromium starting material of preference was always $CrCl_3THF_3$ since the same metathesis reactions could thus be readily carried out. It should be noticed that reaction of one equivalent of lithium guanidinate with one equivalent of $CrCl_3THF_3$ did not yield any crystalline material or material that was sufficiently pure for analysis. As a result a confident structural assignment could not be made for the product of this reaction and therefore the reaction will not be any further discussed.

The reaction of two equivalents of $(Me_3Si)_2NC(NR)_2Li$ with $CrCl_3THF_3$ in toluene provided good yields of the complexes **10** and **11** shown in Figure 2.3.5. These complexes are interesting as they offer insight into the differences between Cr(II) and Cr(III) guanidinate complexes and can be useful starting materials for subsequent reactions (see chapter 3). The same reactions were attempted with the other guanidinate ligands but only an oily material was obtained that could not be further characterized. The use of the bulky TMS groups instead improved the crystallinity of the final products. Both complexes adopt the same distorted trigonal bipyramidal geometry as expected since the only difference between the two complexes is the cyclohexyl substituents in **10** being replaced by isopropyl substituents in **11**. These two groups have in fact a very similar cone angle. This geometry can also be expected since the two chelating ligands have the tendency to position themselves with their "CN_3" units perpendicular to each other. The chlorine atom then occupies one axial position. Both **10** and **11** had magnetic

moments [μ_{eff} = 3.49 μ_B and μ_{eff} = 3.51 μ_B] as expected for the high spin d^3 electronic configuration of monomeric Cr(III).

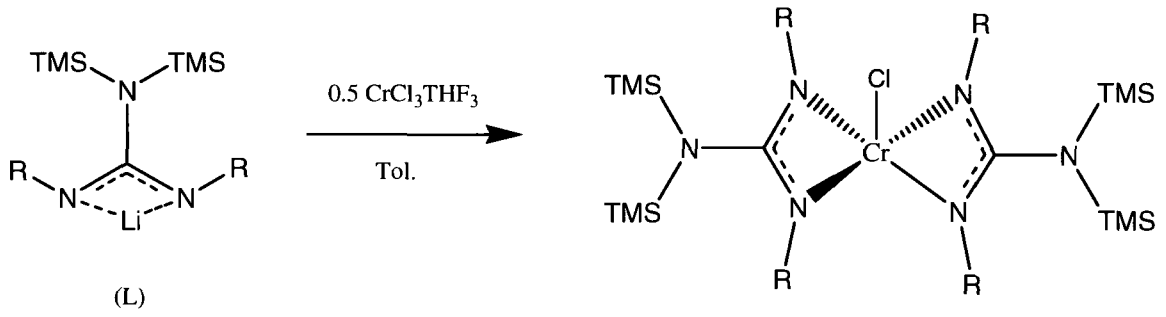

Figure 2.3.5 Synthesis of Complexes **10** and **11**.

For the sake of completeness the reaction with three equivalents of $(Me_3Si)_2NC(NR)_2Li$ was examined. The reactions in THF afforded complexes **12** and **13** (Figure 2.3.6). If toluene or hexanes were used as the solvent, a large amount of intractable material precipitated out of the solution and whose elemental analysis and magnetic moment is inconsistent with the structures of **12** and **13**. These complexes adopt a distorted octahedral geometry and show the expected value of the magnetic moments [μ_{eff} = 3.79 μ_B and μ_{eff} = 3.73 μ_B for **12** and **13** respectively].

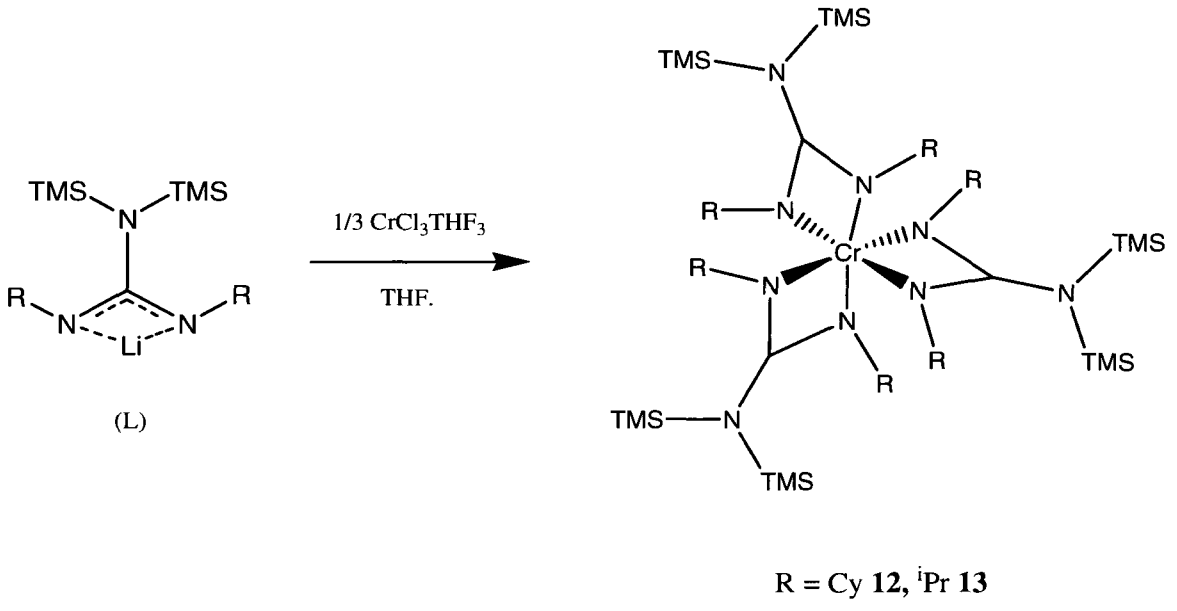

Figure 2.3.6 Synthesis of Complexes **12** and **13**.

Replacement of the two nitrogen donor atoms with sulfur is a reasonable strategy to investigate the influence of electronic parameters within the same ligand scaffold. For this purpose the reaction of one equivalent of tetraethylthiuram disulfide with two equivalents of $CrCl_2THF_2$ in THF was attempted (Figure 2.3.7). From this reaction complex **14** precipitates and was readily crystallized from a concentrated solution upon slow evaporation.

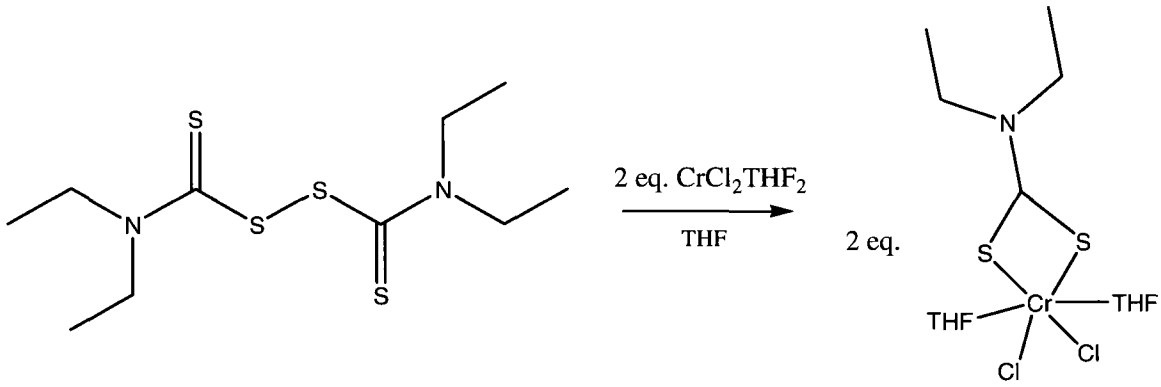

(14)

Figure 2.3.7 Synthesis of Complex **14** Method A.

The reaction is easily rationalized in terms of cooperative two electron attacks of two Cr(II) atoms to the anti-bonding oribital of the S-S bond. The cleavage of the S-S bond is accompanied by one electron oxidation of each Cr(II) atom. The anionic sulfur atoms then coordinate the metal center in a chelating fashion (Figure 2.3.7). The compound retains two equivalents of THF *trans* to each other in the coordination sphere and two *cis* positioned chlorine atoms. The presence of the two chlorine atoms makes this complex an attractive starting material for subsequent metathesis reaction with lithium alkyls or Grignard reagents. Compound **14** can also be synthesized in the more straightforward manner shown in Figure 2.3.8.

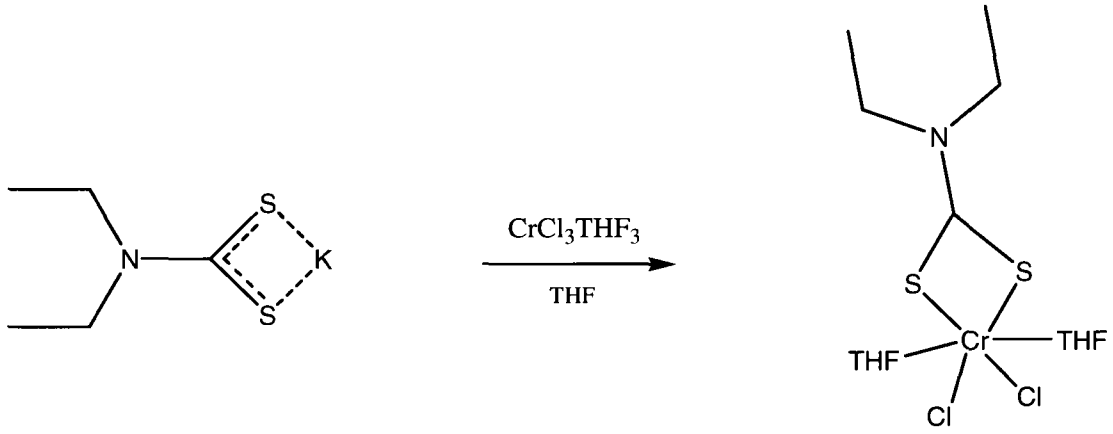

(14)

Figure 2.3.8 Synthesis of Complex **14** Method B.

The potassium dithiocarbamate salt was prepared according to a literature procedure.[7] Diethylamine was added to a solution of KOH in ethanol. The mixture was cooled to 0 °C and then carbon disulfide was added. The reaction was allowed to warm back to room temperature and stirred for 4 hours. The solvent was then removed under reduced pressure and replaced by anhydrous ether. The compound precipitated out of the solution was filtered and used without further purification. The alternative synthesis of **14** (Method B), involves the metathesis reaction of the potassium dithiocarbamate salt with $CrCl_3THF_3$ in THF. The reaction mixture was stirred overnight and centrifuged to remove KCl. Compound **14** crystallized after two days at -37 °C. The magnetic moment, μ_{eff} = 3.70 μ_B, and elemental analysis were both in agreement with the proposed formulation. One characteristic of compound **14** that was somewhat surprising was its remarkable stability towards O_2 and H_2O. The compound does not change color or seem to react in air or water.

One nickel guanidinate complex was also synthesized. This reaction was carried out because of the relationship between the electronic configuration of Ni(II) and Cr(II). The reaction of two equivalents of $(Me_3Si)_2NC(NCy)_2Li$ with $NiCl_2THF_2$ in toluene provided complex **15**, shown in Figure 2.3.9. The compound precipitates readily from toluene after 3 days at -37 °C. Compound **15** was found to be paramagnetic with a magnetic moment of μ_{eff} = 2.84 μ_B, corresponding to two unpaired electrons in the tetrahedral coordination environment. The tetrahedral geometry of this species has been

confirmed by the X-ray structure and is in striking contrast with the square planar geometry observed in the case of the chromium analogue.

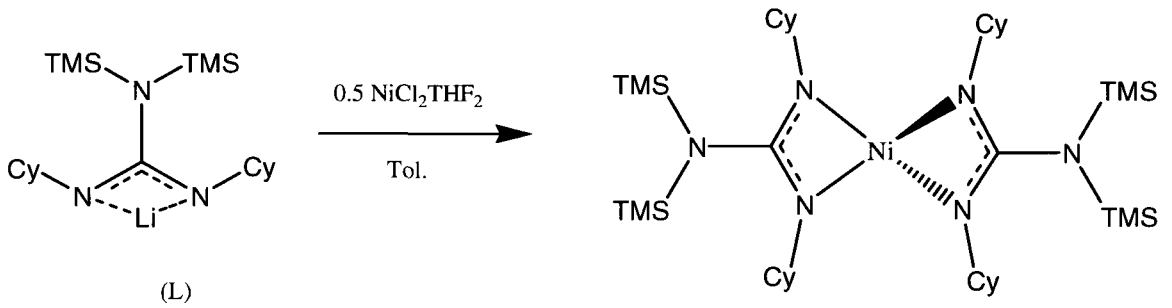

(**15**)

Figure 2.3.9 Synthesis of Complex **15**.

2.5 Conclusions

Guanidinate ligands have proven versatile for the preparation of a class of new Cr(II/III) complexes whose structures have been confirmed by X-ray crystallography studies.

The lithium salts of a number of guanidinate ligands, both tri- and tetrasubstituted, were found to react in a straightforward manner with $CrCl_2THF_2$ and $CrCl_3THF_3$ at room temperature. These reactions provided convenient yields of the corresponding complexes for further studies. As such, this chapter was intended to introduce the reader to the complexes that will now be used for the studies highlighted in chapter 3 and 4.

The use of bulky substituents on the guanidinate ligand has resulted in the formation of mainly mononuclear complexes. In the case of $CrCl_2THF_2$ when one equivalent of ligand was used, a novel tetrameric cluster with a cuboid core was obtained.

Additionally, the possibility of replacing the two donor nitrogen atoms for sulfur was also examined and one Cr(III) complex was synthesized and characterized. A Ni(II) guanidinate complex was also synthesized and characterized crystallographically.

2.6 X-Ray Crystallography Section

Table 2.6.1. Crystal data and structure refinement for complexes **1-4**.

	1	3	4
Formula	C49.25 H106.25 Cl2 Cr2 N6 Si4	C38 H80 Cr N6 Si4	C27.87 H66.13 Cr N6 Si4
FW	1069.91	785.44	649.76
space group	Tetragonal, I4(1)/a	Orthorhombic, Pbcn	Monoclinic, C2/m
a (Å)	21.778(2)	24.801(11)	39.889(8)
b (Å)	21.778(2)	13.745(6)	14.307(3)
c (Å)	32.073(4)	14.110(6)	27.887(5)
α (deg)	90	90	90
β (deg)	90	90	128.673(2)
γ (deg)	90	90	90
V ($Å^3$)	15211(3)	4810(4)	12426(4)
Z	8	4	12
radiation (Kα, Å)	0.71073	0.71073	0.71073
T (K)	200(2)	203(2)	200(2)
D_{calcd} ($g\ cm^{-3}$)	0.934	1.085	1.042
μ_{calcd} (mm^{-1})	0.447	0.368	0.415
F_{000}	4654	1720	4264
R, R_w [2a]	0.0767, 0.2386	0.0481, 0.1704	0.0533, 0.1643
GoF	1.024	1.171	1.052

[a] $R = \Sigma||Fo| - |Fc||/\Sigma|F|$. $Rw = [\Sigma(|Fo| - |Fc|)^2/\Sigma wFo^2]^{1/2}$.

Table 2.6.2. Crystal data and structure refinement for complexes **8-10**.

	8	**9**	**10**
Formula	C45 H76 Cr N6	C30 H48 Cr N6	C38 H80 Cl Cr N6 Si4
FW	753.12	544.74	820.89
space group	Triclinic, P1	Monoclinic, P2(1)/c	Monoclinic, C2/c
a (Å)	10.799(5)	7.9265(11)	14.180(2)
b (Å)	12.799(3)	11.4027(16)	23.582(3)
c (Å)	16.252(4)	17.957(3)	29.736(4)
α (deg)	95.711(4)	90	90
β (deg)	91.828(4)	99.171(2)	101.774(2)
γ (deg)	94.863(4)	90	90
V ($Å^3$)	2225.3(10)	1602.3(4)	9734(2)
Z	2	2	8
radiation (Kα, Å)	0.71073	0.71073	0.71073
T (K)	202(2)	205(2)	203(2)
D_{calcd} ($g\ cm^{-3}$)	1.124	1.129	1.120
μ_{calcd} (mm^{-1})	0.293	0.384	0.419
F_{000}	824	588	3576
R, R_w [2a]	0.0553, 0.1549	0.0605, 0.1671	0.0577, 0.1651
GoF	1.040	1.073	1.080

[a] $R = \Sigma||Fo| - |Fc||/\Sigma|F|$. $Rw = [\Sigma(|Fo| - |Fc|)^2/\Sigma wFo^2]^{1/2}$.

Table 2.6.3. Crystal data and structure refinement for complexes **11-15**.

	11	**14**	**15**
Formula	C26 H64 Cl Cr N6 Si4	C13 H26 Cl2 Cr N O2 S2	C38 H80 N6 Ni Si4
FW	660.64	415.37	792.13
space group	Triclinic, P-1	Monoclinic, P2(1)/c	Orthorhombic, Fddd
a (Å)	8.939(4)	8.014(6)	9.8605(17)
b (Å)	9.391(4)	12.273(9)	30.230(5)
c (Å)	26.760(13)	19.487(15)	31.891(5)
α (deg)	80.002(7)	90	90
β (deg)	85.411(9)	99.392(11)	90
γ (deg)	62.249(6)	90	90
V ($Å^3$)	1957.9	1891(2)	9506(3)
Z	2	4	8
radiation (Kα, Å)	0.71073	0.71073	0.71073
T (K)	218(2)	203(2)	203(2)
D_{calcd} ($g\ cm^{-3}$)	1.121	1.459	1.107
μ_{calcd} (mm^{-1})	0.506	1.110	0.540
F_{000}	718	868	3472
R, R_w [2a]	0.0513, 0.1378	0.0426, 0.1135	0.0551, 0.1659
GoF	1.050	1.060	1.067

[a] $R = \Sigma||Fo| - |Fc||/\Sigma|F|$. $Rw = [\Sigma(|Fo| - |Fc|)^2/\Sigma wFo^2]^{1/2}$.

2.7 References

1. For example: (a) P.J. Bailey, S. Pace, *Coordination Chemistry Reviews.* **2001**, *214*, 91. (b) A.L. Brazeau, G.A. DiLabio, K.A. Kreisel, W Monillas, G.P. A. Yap, S.T. Barry *Dalton Trans.*, **2007**, 3297. (c) A.P. Kenney, G. P. A. Yap, D.S. Richeson, S.T. Barry,† *Inorg. Chem.* **2005**, *44*, 2926. (d) M.K.T. Tin, G. P. A. Yap, D.S. Richeson *Inorg. Chem.* **1999**, *38,* 998-1001. (e) P. Bazinet, D.Wood, G. P. A. Yap, D. S. Richeson *Inorg. Chem.* **2003**, *42*, 6225-6229. (f) M.K.T. Tin, N. Thirupathi, G. P. A. Yap, D. S. Richeson *J. Chem. Soc., Dalton Trans.*, **1999**, 2947. (g) S.R. Foley, G. P.A. Yap, D.S. Richeson *Inorg. Chem.* **2002**, *41*, 4149. (h) A.A. Trifonov, D.M. Lyubov, G.K. Fukin, E.V. Baranov, Y.A. Kurskii *Organometallics* **2006**, *25,* 3935. (i) D.M. Lyubov, G.K. Fukin, A.A. Trifonov *Inorg. Chem.* **2007**, *46*, 11450. (j) A.A. Trifonov, G.G. Skvortsov, D.M. Lyubov, N.A. Skorodumova, G.K. Fukin, E.V. Baranov, V.N. Glushakova *Chem. Eur. J.* **2006**, *12*, 5320.

2. For example: (a) Hao, S.; Gambarotta, S.; Bensimon, C.; Edema, J. J. H. *Inorganica Chimica Acta.* **1993**, *213*, 65. b) Harder, S.; Boersma, J.; Brandsma, L. *Organometallics.* **1990**, *9*, 515. c) Jiabi, C.; Guixin, L.; Weihua, X.; Xianglin, J.; S. Meicheng; Youqi, T. *J. Organomet. Chem.* **1985**, *286*, 66. d) Eapen, K. C.; Tamborski, C. *J. Fluorine Chem.* **1980**, *15*, 241. e) Pornet, J.; Miginiac, L. *Bull. Soc. Chimi. Fra.* **1974**, *5-6*, 997. (f) S. Patai, Z. Rappoport, The Chemistry of Amidines and Imidinates, vol. 2, Wiley, New York, **1991** (Chapter 10).

3. For example: (a) Peter Gantzel[‡] and Patrick J. Walsh *Inorg. Chem.*, **1998**, *37*, 3450. (b) Cristina Tejel,*[‡] Miguel A. Ciriano,[‡] Gustavo Ríos-Moreno,[‡] Isabel T. Dobrinovitch,[‡] Fernando J. Lahoz,[‡] Luis A. Oro,[‡] and Miguel Parra-Hake *Inorg. Chem.*, **2004**, *43*, 4719. (c) Gabriele Albertin, Stefano Antoniutti, Marco Bedin, Jesús Castro, and Soledad Garcia-Fontán*Inorg. Chem.*, **2006**, *45*, 3816. (d) John T. Leman, Janet Braddock-Wilking, Alanna J. Coolong, Andrew R. Barron *Inorg. Chem.*, **1993**, *32*, 4324. (e) Anthony G. M. Barrett, Mark R. Crimmin, Michael S. Hill, Peter B. Hitchcock, Gabriele Kociok-K◊hn and Panayiotis A. Procopiou *Inorg. Chem.*, **2008**, *47*, 7366.

4. (a) F. Hein, D. Tille *Z. Anorg. Allg. Chem* **1964**, *329*, 72; (b) L. H. Gade *Koordionationchemie*, Wiley-VCH, Weinheim, **1998.**

5. (a) J. Klein, *Tetrahedron* **1983**, *39*, 2733. (b) I. Agranat, W.C. Hernden, T.P. Radhakrishnan, A. Skancke, *Chem. Phys. Lett.* **1991**, 117. (c) A. Skancke, *J. Chem. Phys.* **1994**, 5234.

6. M.P. Coles, P.B. Hitchcock, *Organometallics.* **2003**, *22*, 5201-5211

7. P.J. Bailey, K.J. Grant, L.A. Mitchell, S. Pace, A. Parkin, S. Parsons, *J. Chem. Soc. Dalton Trans.* **2000**, 1887.

8. (a) L.Coghi, M.Nardelli, G.Pelizzi, *Acta Crystallogr.,Sect B: Struct.Crytallogr.Cryst. Chem.* **1976**, *32*, 842. (b) G.R. Brubaker, L.E. Webb, *J.Am.Chem.Soc.* **1969**, *91*, 7199. (c)

F.A. Cotton, L.M. Daniels, P Huang, C.A. Murillo *Inorg Chem.* **2002**, *41*, 317. (d) A.E. Ceniceros-Gomez, N Barba-Behrns, M.E. Quiroz-Castro, S Bernes, H. Noth, S.E. Castillo-Blum *Polyhedron* **2000**, *19*, 1821. (e) T.Irrgang, R. Kempe *Eur.J.Inorg.Chem* **2005**, 4382. (f) F.A. Cotton, D.J. Timmons *Polyhedron* **1998**, *17*, 179. (g) A. Noor, G. Glatz, R. Müller, M. Kaupp, S. Demeshko, R. Kempe *Angew. Chem. Int. Ed.* **2009**, *8*, 1149.

9. Guzel, O; Salman, A. *Bioorganic and Medical Chemistry.* **2006**, *14*, 7804.

10. (a) Regan, W. K.; Freeman, J. W.; Conroy, B. K.; Pettijohn, T. M.; Benham, E. A. US Pat. 5 451 645 (Phillips Petroleum Company), **1995**. (b) Sugimura, K.; Nitabara, T. S.; Fujita, T. Jap. Pat. (Mitsui Chemical Incorporated), **1998**.

11. Richeson, D.; Yap, G.P.A.; Wood, D. *Inorg. Chem.* **1999**, *38,* 5788.

12. A. Jabri, C. Temple,P. Crewdson, S. Gambarotta,I. Korobkov, R.Duchateau. *J.Am.Chem.Soc.* **2006**, *128*, 9238.

13. J.M. Hope, R.L. Martin, D. Taylor, A.H. White. *Chem Commun.* **1977**, 99.

3 Chromium Guanidinate Complexes as Precursors

Table of Contents

Chapter 3

3.1 Introduction

Isolating active intermediates of the oligomerization or polymerization catalytic cycles is central to the clarification of a mechanistic puzzle. Besides the obvious convenience provided by the ability of these species to perform catalytic transformations without the use of co-catalyst (single component catalyst), their characterization allows for a great deal of understanding to be gained about the metal oxidation state, role of co-catalyst, and geometry around the metal center.

In this chapter, I describe the several attempts that were carried out with the goal of obtaining catalysts that do not require the use of co-catalyst. A number of compounds discussed in this chapter do not contain any metal-carbon bond or alkyl aluminum moiety but are still discussed as they are the product of a reaction between the chromium guanidinate precursors discussed in chapter 2 with standard activators. During the course of this work, two novel metal-metal multiply bonded complexes of record-short distances were obtained. In order to place these results in their appropriate perspective, a brief summary on metal-metal bonding will be presented in this Introduction.

The guanidinate ligand has been shown to promote metal-metal bonding in a variety of transition and non-transition metals.[1] Additionally, complexes of chromium have long been known to form metal-metal bonds of unusual shortness when three-center chelating ligands (such as the guanidinate monoanion) are employed.[2] Therefore, formation of dimers with exceedingly short metal-metal bonds was in fact anticipated.

A rich chemistry has developed around the metal-metal bond since the early discovery of a quadruple bond in $[Re_2Cl_8]^{2-}$ in 1964.[3] The quadruple bond between the two metal centers was used to account for the observed diamagnetism of the dinuclear frame as generated by the perfect pairing of the *d* electrons.

This overview will include all key elements in most other multiple bonds between metal atoms. In order to simplify the situation we shall only consider compounds with two metal atoms forming a square or square pyramidal MX_4 arrangement. This arrangement is often referred to as the paddlewheel as a result of its shape.

Quadruple bonds can only be made between transition metals since d-orbitals or higher (f, g-orbitals) are required.[3] A molecular orbital (MO) diagram of the overlaps of d^4-orbitals and their resulting energy levels as involved in metal-metal bonding is shown in Figure 3.1.1.

Each d-orbital on the metal atom interacts with the corresponding d-orbital on the adjacent metal atom to form 4 bonding and 4 anti-bonding MO's. The interaction of $d_{z2}^{(1)}$ with $d_{z2}^{(2)}$ gives rise to a bonding and anti-bonding pair of σ-orbitals. The $d_{xz}^{(1)} + d_{xz}^{(2)}$ and $d_{yz}^{(1)} + d_{yz}^{(2)}$ bonding and anti-bonding interactions give rise to two degenerate sets of π-orbitals. Finally the d_{xy} orbitals form bonding and anti-bonding δ-orbitals.

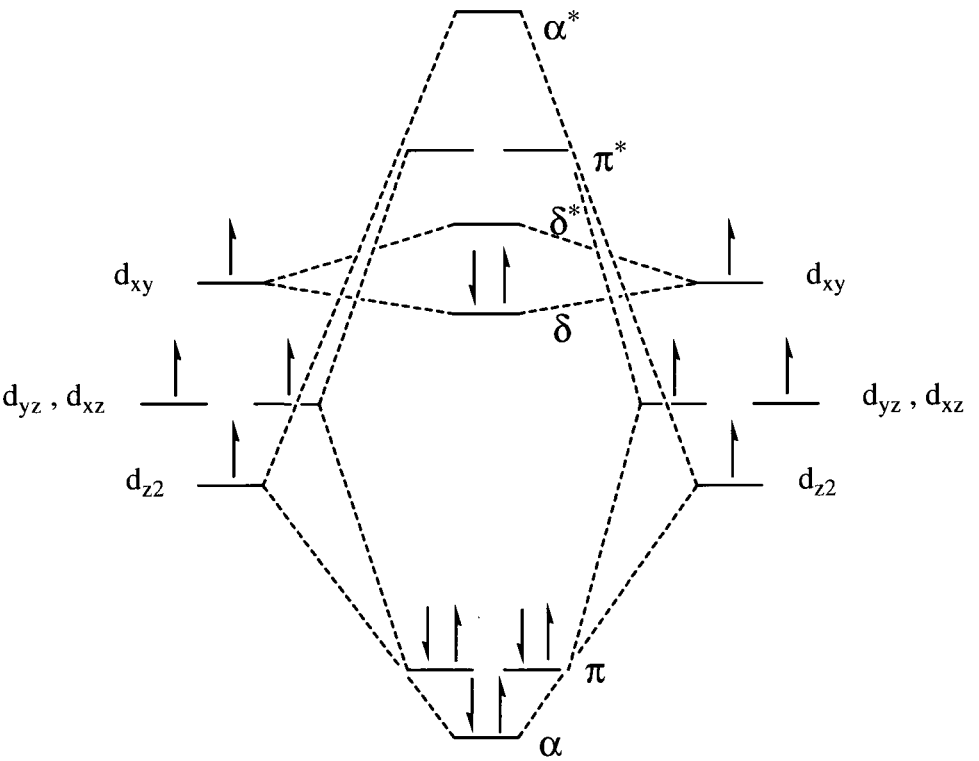

Figure 3.1.1 MO diagram of d^4-orbitals and their resulting energy levels as involved in metal-metal bonding.

The d_{x2-y2} orbitals can also form δ orbitals but are mostly involved in metal-ligand bonding and hence don't contribute much to the metal-metal bonding. The orbital energies can be ordered $\sigma < \pi << \delta < \delta^* << \pi^* < \sigma^*$ based on the simple Huckel concept.[3]

The eight electrons involved in the quadruple bond can be placed in orbitals to give the following configuration $\sigma^2\ \pi^4\ \delta^2$. According to conventional MO theory, bond order = $(n_b - n_a)/2$, where n_b is the number of electrons in bonding orbitals and n_a is the number of electrons in anti-bonding orbitals. This would lead to a value of 4, a quadruple bond for any d^4- d^4 paired system. This description of the quadruple bond can both account for its unusual shortness and eclipsed conformation of the ligands. It also explains why the quadruply bonded chromium (II) systems are diamagnetic.

Some weak paramagnetism can still arise in these systems from temperature independent paramagnetism at low temperature and paramagnetism arising from a slight population of a triplet state at higher temperature (room temperature).

Chromium(II)-chromium(II) interactions can be regarded as consisting of σ, π, and δ components. The strength of these interactions is dependent on the distance between the two metal atoms. The distance can be affected by the donor power of the ligand and basic strength of any axially bound ligands. The remarkable shortness of these metal metal bonds had initially led workers to believe that a strong Cr-Cr interaction exists in these systems.[4] On the other hand, experimental work has clearly demonstrated the surprising weakness of these bonds.[5] The paradoxical dichotomy of supershort-superweak quadruple bonds [6] can be only reconciled if we regard the Cr-Cr interaction not as a multiple chemical bond in its classical sense but as a ligand artefact instead.[7] Among the several dozen existing Cr-Cr "multiple bonds", the short contacts between divalent atoms have been exclusively observed in the presence of bridging metal-ligand interactions, with only one exception.[8] This at least has been the case in complexes where the Cr-Cr distance remains in the range of 1.90 Å and higher.

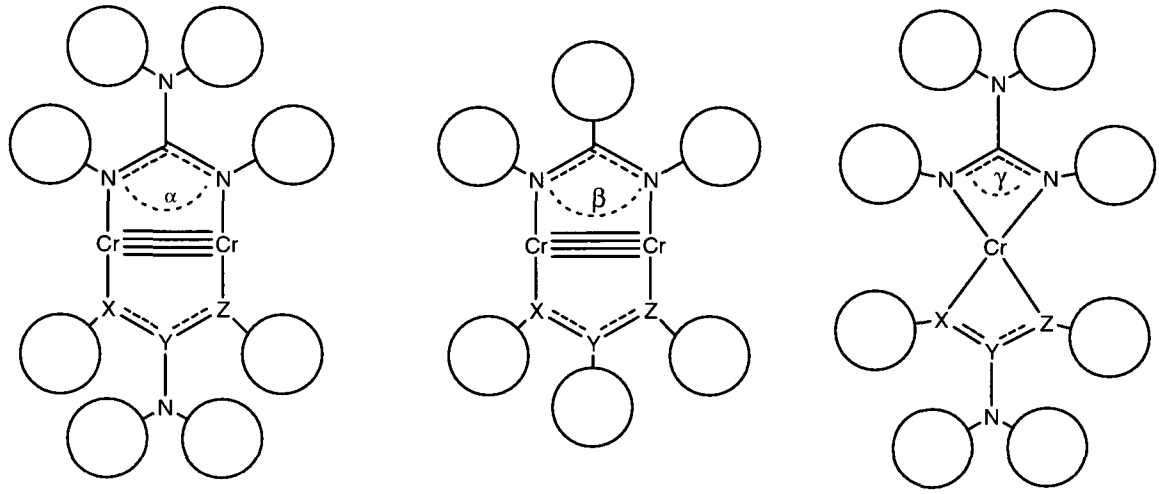

Figure 3.1.2 The role of the ligand is stabilizing ultra short metal metal bonds: guanidinate and amidinate with appropriate bite to accommodate two metals (left and center respectively), guanidinate with small bite angle resulting in monomeric species (right).

The recent discovery of Cr^{I}-Cr^{I} formally quintuply bonded systems of variable shortness (1.73-1.83Å) is a new landmark in this chemistry.[9] The monovalent state and the consequent presence of only one counter-anion obviously makes these systems ideal for the occurrence of exceedingly short Cr-Cr contacts.

An important aspect in the context of metal-metal bonds is the Hein-Cotton principle, that is the X-Y-Z-ligand arrangement shown in Figure 3.1.2, which brings the two metal atoms into close proximity in the first place.[9] The guanidinate ligand can be conveniently tuned in this regard. The bite angle, N-C-N angle, of the ligand can be widened, if the appropriate choice of substituents is made, to accommodate a dimeric structure, also shown in Figure 3.1.2. It has been recently reconfirmed with the guanidinate system that by making the appropriate choice of substituent on the non bonding nitrogen atom, a Cr(I) dimer with an ultra short metal metal bond can be made.[10]

3.2 Experimental Section

All reactions were carried out under a dry nitrogen atmosphere. Solvents were dried using an aluminum oxide solvent purification system. $CrCl_2THF_2$ was synthesized according to standard procedure. All AlR_xCl_{3-x} reagents were purchased from Strem and used as received. ^nBuLi and MeLi were purchased from Aldrich and used as received. Infrared spectra were recorded on an ABB Bomem FTIR instrument from Nujol mulls prepared in a drybox. Samples for magnetic susceptibility were pre-weighed inside a drybox equipped with an analytical balance and measured on a Johnson Matthey Magnetic Susceptibility balance. NMR data was collected on an INOVA Varian 300 or 500 MHz instrument in the deuterated solvent of choice. Elemental analysis was carried out with a Perkin-Elmer 2400 CHN analyzer. Data for X-ray crystal structure determination were obtained with a Bruker diffractometer equipped with a 1K Smart CCD area detector.

Synthesis of $[(Me_3Si)_2NC(NCy)_2]Cr(DMF)_2Cl(II)$ (16): A sample of crystalline **1** (500 mg, 0.27 mmol) was dissolved in anhydrous DMF (~ 10 mL). Long blue needle crystals, suitable for X-ray diffraction, precipitated out of the resulting solution after 2 days at -37 °C. (126 mg, 0.21 mmol, 78%). IR (Nujol, cm^{-1}): 1669 (m), 1482 (w), 1386 (s), 1345 (s), 1302 (s), 1250 (m), 1206 (m), 1142 (s), 1100 (m), 1045 (s), 1009 (s), 965 (s), 945 (m), 898 (s), 867 (s), 838 (w), 756 (m), 689 (s), 641 (s). Elemental Analysis calcd (found) for $C_{25}H_{54}ClCrN_5O_2Si_2$: C 50.02 (49.33), H 9.07 (9.28), N 11.67 (10.70). ($\mu_{eff} = 4.93\ \mu_B$)

Synthesis of $[(Me_3Si)_2NC(NCy)_2CrMe]_2(II)$ (17) (Method A): A solution of **3** (200 mg, 0.25 mmol) in toluene (10 mL) was cooled to -37 °C and a solution of trimethylaluminum (45 mg, 0.62mmol) in toluene (10 mL) was added. The solution changed color from red to dark red immediately upon addition of trimethylaluminum. The reaction mixture was stirred for 4 hours at which point the color had completely changed to dark green/brown. The reaction mixture was then centrifuged to remove any insoluble impurities. Green plate crystals of **5**, suitable for X-ray crystallography, precipitated out of the solution upon standing for 5 days at -37 °C (104 mg, 0.12 mmol,

48%). H^1 NMR (d_8-THF, ppm): δ = -0.782 (s, 6H, Cr-CH_3), 0.506 (s, 36H, Si-CH_3), 1.0-1.8 (40H, CH2), 3.972 (m, 4H, CH). C^{13} NMR (d_8-THF, ppm): δ = 123.22, 55.13, 36.85, 23.14, 22.61, 0.48, -0.63. IR (Nujol mull, cm-1): 2921 (s), 2855 (s), 1451 (m), 1344 (s), 1297 (s), 1253 (s), 1174 (m), 1136 (s), 1076 (s), 1009 (m), 967 (s), 935 (w), 840 (w), 756 (m), 689 (m), 641 (s). Elemental Analysis calcd (found) for C_{40} H_{86} Cr_2 N_6 Si_4: C 55.38 (55.03), H 9.99 (9.86), N 9.69 (9.70).

Synthesis of [$(Me_3Si)_2NC(NCy)_2CrMe]_2$(II) (17) (Method B): A solution of **1** (450 mg, 0.25 mmol) in THF (15 mL) was cooled to -37 °C and 1 eq. of MeLi (1.6 M in Et_2O, 0.16 mL, 0.25mmol) was added. The color of the solution changed from blue to dark blue and then green over 24 hours. The reaction mixture was then centrifuged to remove LiCl. A green powder precipitates out of solution after 3 days at -37 °C (182 mg, 0.21 mmol, 84%). H^1 NMR and IR both confirm this green powder being **17**.

Synthesis of [$(Me_3Si)_2NC(NCy)_2]AlMe_2$(III) (18): A solution of **3** (200 mg, 0.25 mmol) in toluene (10 mL) was cooled to -37 °C and combined with a solution of trimethylaluminum (90 mg, 1.25 mmol) in toluene (10 mL). The solution changed the color from red to dark red immediately upon addition of trimethyaluminum. The reaction mixture was stirred for 24 hours at which point the reaction mixture had completely changed to dark brown/black. The reaction mixture was then centrifuged to remove any insoluble impurities. A black solid was isolated but could not be characterized due to its low solubility. Clear block crystals, suitable for x-ray crystallography, precipitated out of the solution upon standing for 30 days at -37 °C (98 mg, 0.23 mmol). ^1H NMR (d_6-benzene, ppm): δ = 0.45 (s, 18H, Si-CH_3), 1.0-2.6 (22H, cyclohexyl CH_2, 2.63 (m, 2H, CH), -0.45 (s, 6H, Al-CH_3). ^{13}C NMR (d_6-benzene, ppm): δ = 119.23, 56.19, 37.65, 22.04, 21.51, 2.45, -4.63.IR (Nujol, cm^{-1}): 1430 (w), 1260 (m), 1205 (m), 1192 (s), 1177 (m), 1010 (m), 956 (m), 760 (s), 742 (m), 720 (w), 695 (m), 689 (s), 641 (s). Elemental Analysis calcd (found) for C_{21} H_{46} Al N_3 Si_2: C 59.52 (60.11), H 10.94 (11.23), N 9.92 (9.97).

Synthesis of $[(Me_3Si)_2NC(NCy)_2Cr^nBu]_2$(II) (19): A solution of **1** (7.264 g, 4 mmol) in THF (50 mL) was cooled to -37 °C. A cooled solution (-37 °C) of ^{n}BuLi (2.5 M in hexanes, 1.6 mL, 4 mmol) was added. The mixture immediately changed color from blue to dark blue. Stirring was continued for 24 hours at which time the solution had become completely green. The reaction mixture was then centrifuged to remove any LiCl. Green plate crystals of **19**, suitable for x-ray diffraction, precipitated out of the resulting solution after 4 days at -37°C. (2.642 g, 2.77 mmol, 69%), H^1 NMR (d_6-benzene, ppm): δ = 0.55 (s, 36H, Si-CH_3), 1.0-2.6 (58H, cyclohexyl CH2, butyl CH2 and CH3), 4.04 (m, 4H, CH). C^{13} NMR (d_6-benzene, ppm): δ = 158.69, 57.81, 39.51, 35.75, 31.20, 27.40, 26.57, 25.79, 14.63, 3.78. IR (Nujol, cm^{-1}): 1667 (m), 1640 (m), 1447 (w), 1372 (m), 1348 (m), 1301 (m), 1248 (s), 1167 (m), 1135 (s), 1073 (s), 1008 (s), 968 (s), 932 (m), 863 (m), 834 (w), 805 (s), 756 (m), 687 (m), 642 (s). Elemental Analysis calcd (found) for C_{46} H_{98} Cr_2 N_6 Si_4: C 58.06 (55.04), H 10.38 (10.12), N 8.83 (8.07).

Synthesis of $[(Cy)_2NC(NCy)_2CrMe]_2$(II) (20): Solid $(Cy)_2NC(NCy)_2Li$ (788 mg, 2 mmol) was added to a suspension of $CrCl_2(THF)_2$ (266 mg, 1 mmol) in toluene (20 mL). The solution turned purple over 1 hour. The resulting mixture was stirred for 24 hours and centrifuged to remove LiCl. The solution was then cooled to -37 °C and a solution of trimethylaluminum (180 mg, 2.5 mmol) in toluene (10 mL) was added. The solution changed color from purple to dark green immediately upon addition of trimethylaluminum and stirring was continued for 4 hours, at which point the reaction mixture had completely changed the color to dark green/brown. The reaction mixture was then centrifuged to remove any insoluble impurities. Green plate crystals of **20**, suitable for X-ray crystallography, precipitated out of the solution after 3 days at -37 °C (560 mg, 0.62 mmol, 62 %). H^1 NMR (d_6-benzene, ppm): δ = -0.798 (s, 6H, Cr-CH_3), 0.452 (s, 36H, Si-CH_3), 1.0-1.8 (40H, CH2), 4.023 (m, 4H, CH). C^{13} NMR (d_6-benzene, ppm): δ = 122.22, 55.45, 36.98, 22.82, 22.31, 0.43, -0.59. IR (Nujol mull, cm-1): 1501 (m), 1444 (s), 1398 (m), 1293 (s), 1251 (s), 1191 (m), 1176 (s), 1136 (m), 1019 (m), 971 (s), 928 (w), 852 (m), 767 (m), 690 (m), 643 (s). Elemental Analysis calcd (found) for C_{52} H_{94} Cr_2 N_6: C 68.83 (68.89), H 10.44 (10.77), N 9.26 (9.32).

Synthesis of {[(Cy)$_2$NC(NCy)$_2$]$_2$Cr}$_2$ μ-O(III) (21): Solid (Cy)$_2$NC(NCy)$_2$Li (788 mg, 2 mmol) was added to a suspension of $CrCl_2(THF)_2$ (266 mg, 1 mmol) in toluene (20 mL). The solution turned purple over one hour and stirring was continued for 24 hours. After centrifugation to remove LiCl, the solution was stored at -37 °C for 1 month after which small brown crystals of **21**, suitable for X-ray diffraction, precipitated out of sthe olution (70 mg, 0.04 mmol, 4%). The amount of product formed for was unsufficient for a reliable magnetic moment measurement. IR (Nujol, cm^{-1}): 1659 (m), 1630 (m), 1587 (w), 1520 (w), 1479 (m), 1461 (w), 1420 (m), 1388 (s), 1356 (s), 1301 (m), 1209 (m), 1172 (s), 1097 (m), 1004 (m), 934 (s), 898 (m), 843 (m), 798 (m), 743 (s), 698 (s), 643 (s). Elemental Analysis calcd. (found) for C_{100} O Cr_2 N_{12} H_{176} : C 72.07 (73.24), H 10.65 (11.23), N 10.09 (10.73).

Synthesis of {[(^{i}PrNH)C(ArN)(^{i}PrN)]$_2$Cr }$_2$ μ-CrCl$_2$(II) (22): To a solution of **13** (545 mg, 1 mmol) in THF (15 mL) $CrCl_2(THF)_2$ (133 mg, 0.5 mmol) was added. The solution changed color from purple to blue over 24 hours. Small blue crystals of **22**, suitable for X-ray diffraction, are grown over three days at -37 °C (312 mg, 0.26 mmol, 52 %). IR (Nujol, cm^{-1}): 1599 (s), 1536 (w), 1461 (w), 1376 (m), 1275 (w), 1121 (m), 1083 (s), 1056 (m), 967 (s), 911 (s), 874 (s), 767 (m), 731 (s), 695 (s), 665 (s), 609 (m). Elemental Analysis calcd (found) for C_{60} H_{96} Cl_2 Cr_3 N_{12}: C 59.44 (58.23), H 7.98 (8.15), N 13.86 (13.69). (μ_{eff} = 7.84 μ_B)

Synthesis of [(Me$_3$Si)$_2$NC(NCy)$_2$]$_2$CrMe(III) (23): A solution of **9** (400 mg, 0.49 mmol) in THF (15 mL) was cooled to -37 °C and treated with equimolar amount of MeLi (1.6 M in Et_2O, 0.31 mL, 0.49 mmol). The solution changed color from red to dark blue over 24 hours. The reaction mixture was then centrifuged to remove LiCl. Dark blue crystalline material of **23**, suitable for X-ray diffraction, appeared after 6 days at -37 °C (375 mg, 0.47 mmol, 96 %). IR (Nujol, cm^{-1}): 1504 (m), 1438 (s), 1401 (m), 1385 (m), 1329 (w), 1273 (m), 1261 (m), 1240 (m), 1203 (s), 1174 (m), 1099 (m), 1010 (s), 987 (m), 932 (m), 856 (m), 730 (m), 653 (s). Elemental Analysis calcd (found) for C_{39} H_{83} Cr N_6 Si_4: C 58.52 (59.12), H 10.45 (10.73), N 10.50 (10.61). (μ_{eff} = 3.65 μ_B).

Synthesis of $[(Me_3Si)_2NC(N^iPr)_2]_2CrMe$(III) (24): A solution of **10** (350 mg, 0.53 mmol) in THF (15 mL) was cooled to -37 °C and treated with equimolar amount of MeLi (1.6 M in Et_2O, 0.33 mL, 0.53 mmol. The solution changed color from red to dark blue over 24 hours. The reaction mixture was then centrifuged to remove LiCl. Dark blue crystalline material, suitable for X-ray diffraction, precipitated out of the solution after 6 days at -37 °C (332 mg, 0.52 mmol, 98 %). IR (Nujol, cm^{-1}): 1524 (m), 1501 (m), 1446 (s), 1385 (m), 1251 (m), 1234 (m), 1209 (s), 1181 (m), 1079 (m), 1017 (s), 981 (m), 965 (m), 932 (m), 860 (m), 729 (m), 643 (s). Elemental Analysis calcd (found) for C_{27} H_{67} Cr N_6 Si_4: C 50.66 (51.27), H 10.55 (10.77), N 13.13 (13.15). ($\mu_{eff} = 3.66\ \mu_B$)

3.3 Crystal Structure Descriptions

Complex **16** consists of a single chromium atom surrounded by the two nitrogen atoms of one chelating guanidinate ligand, one chlorine atom, and two oxygen atoms from two molecules of DMF (Figure 3.3.1). The chromium atom is in a distorted square pyramidal geometry with the two nitrogen atoms, chlorine atom, and oxygen from DMF defining the square base and one DMF molecule coordinated at the axial position. The bite angle of the ligand [N(1)-C(1)-N(2) = 111.2(7)°] accounts for the large deviation from the ideal trigonal planar geometry. The Cr-O bonds [Cr(1)-O(1) = 2.310(6) Å, Cr(1)-O(2) = 2.037(6) Å] are in the expected range. The Cr-Cl distance [Cr(1)-Cl(1) = 2.399(2) Å] is comparable to the Cr-Cl bond length found in **1**. The Cr-N bond lengths [Cr(1)-N(1) = 2.058(6) Å, Cr(1)-N(2) = 2.061(6) Å] are also comparable to those of the previously characterized complexes. The C-N bonds are [N(1)-C(1) = 1.320(9) Å, N(2)-C(1) = 1.325(9) Å] indicative of the partial double bond character of these bonds and very similar to the bond lengths found in **1**. The C-N bond to the non-coordinated nitrogen atom [N(3)-C(1) = 1.434(9) Å] indicates that little if any π conjugation is occurring between the amido N atom and the sp^2 carbon atom.

The structure of **17** (Figure 3.3.2) is shown to be dimeric containing two Cr^{II} atoms, two guanidinate ligands and two methyl ligands. The complex contains an exceptionally short Cr^{II}-Cr^{II} quadruple distance [Cr(1)-Cr(1a) = 1.7730(18) Å] longer only than three other recently reported Cr^{I}-Cr^{I} quintuple bonds.[11a-b,12] This structure is supported by the three-center chelating geometry of the guanidinate ligand. Each chromium atom is in a distorted square planar geometry with the adjacent chromium atom occupying the axial position. The bite angle of the chelating ligand [N(1)-C(3)-N(3) = 115.7(3)°] has been widened from what it was in **1** and **3** to accommodate a dimeric structure. Each methyl group is placed in a terminal position and disordered with equal occupancy on the two sides of each metal. Although terminally bonded, the methyl groups show a curious orientation towards the second chromium atom, possibly suggesting the presence of a four-center agostic, Cr–(CH2_H)–Cr interaction. The Cr-C distances [Cr(1)-C(1) = 2.192(7) Å, Cr(1)-C(2a) = 2.181(7) Å] are only slightly longer than those found in other complexes with a terminal Cr-C bond as a result of the bridging

agostic interaction taking place with the adjacent Cr atom.[11] The Cr-N distances [Cr(1)-N(1) = 2.019(3) Å, Cr(1a)-N(3) = 2.020(3) Å] are very similar to those found in complexes **1** and **3**. The C-N bonds of the central CN_3 unit [N(1)-C(3) = 1.337(4) Å, N(3)-C(3) = 1.337(4) Å, N(2)-C(3) = 1.446(4) Å] are also similar to those found in the precursors and again are a result of the presence of bulky substituents at the nitrogen atoms.

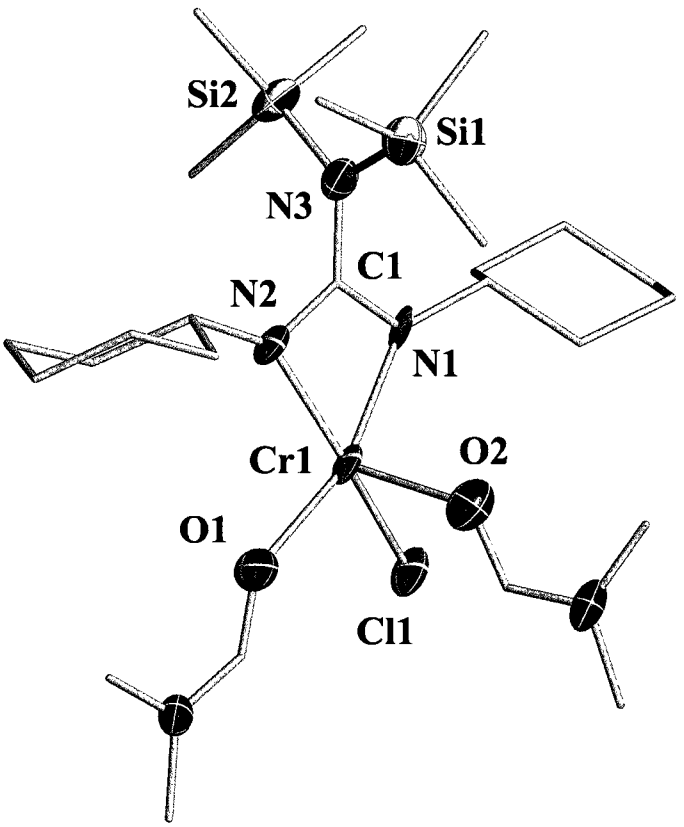

Figure 3.3.1 ORTEP representation of **16**, with thermal ellipsoids set at 50% probability and hydrogen atoms emitted for clarity. Atoms labeled with "a" are generated by the symmetry operation. Selected bond lengths (Å) and angles (°): Cr(1)-O(1) 2.310(6), Cr(1)-O(2) 2.037(6), Cr(1)-Cl(1) 2.399(2), Cr(1)-N(1) 2.058(6), Cr(1)-N(2) 2.061(6), N(1)-C(1)-N(2) 111.2(7).

Complex **18** (Figure 3.3.3) contains one aluminum metal center surrounded by two methyl groups and one chelating guanidinate ligand in a distorted tetrahedral geometry. The bite angle of the ligand [N(1)-C(1)-N(2) = 109.2(3)°] is responsible for the deviation from ideality. The Al-N bonds [Al(1)-N(1) = 1.954(3) Å, Al(1)-N(2) = 1.953(5)

Å] and Al-C bonds [Al(1)-C(2) and Al(1)-C(3) = 1.987(6) Å] are comparable to those found in other aluminum guanidinate complexes.[12] The C-N bonding within the CN_3 network [N(1)-C(1) = 1.356(3) Å, N(2)-C(1) = 1.355(5) Å, N(3)-C(1) = 1.433(5) Å] is also consistent with what has already been reported for this bulky ligand.

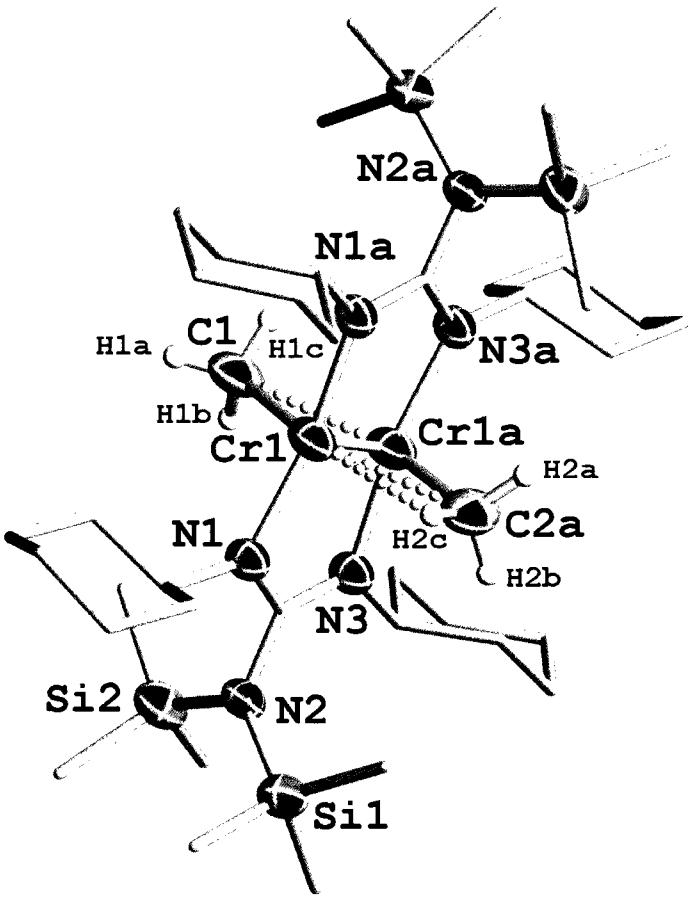

Figure 3.3.2 ORTEP representation of **17**, with thermal ellipsoids set at 50% probability and hydrogen atoms emitted for clarity. Atoms labeled with "a" are generated by the symmetry operation. Selected bond lengths (Å) and angles (°): Cr(1)-Cr(1a) 1.7730(18), Cr(1)-C(1) 2.192(7), Cr(1)-C(2a) 2.181(7), Cr(1)-N(1) 2.019(3), N(1)-C(3)-N(3) 115.7(3).

Complex **19** (Figure 3.3.4) was characterized by single crystal X-ray diffraction and found to be structurally analogous to compound **17**. This species adopts a dimeric structure with the intermetallic distance [Cr(1)-Cr(1a) = 1.8094(17) Å] being slightly longer than that found in the methyl analogue **17**. The bite angle of the ligand [N(1a)-

C(1)-N(1) = 116.1(5)°] has again been widened from what it was in the precursor to accommodate the two metal atoms. The Cr-N bonds [Cr(1)-N(1) = 2.030(3) Å] are all equal by symmetry operation. The Cr-C bond to the butyl group [Cr(1)-C(2) = 2.108(6) Å] is slightly shorter than that found in **17** possibly because of the absence of the agostic interactions each carbon atom is more tightly bound to its chromium atom. Once again the bonding within the CN_3 core is as expected [N(1)-C(1) and N(1a)-C(1) = 1.348(4) Å, N(2)-C(1) = 1.440(7) Å] showing the partial double bond character of the N(1)-C(1) and N(1a)-C(1) bonds and the lack of conjugation from the lone pair of the amido nitrogen with the sp^2 hybridized carbon.

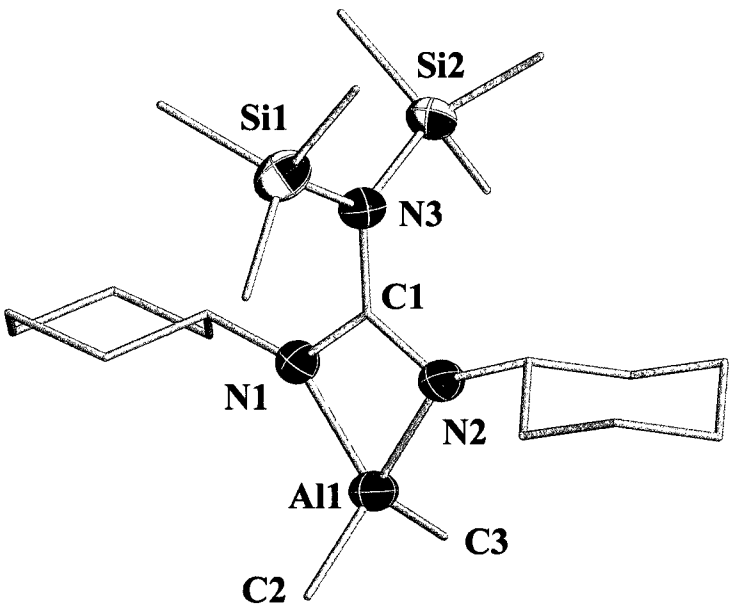

Figure 3.3.3. ORTEP representation of **18**, with thermal ellipsoids set at 50% probability and hydrogen atoms emitted for clarity. Atoms labeled with "a" are generated by the symmetry operation. Selected bond lengths (Å) and angles (°): Al(1)-N(1) 1.954(3), Al(1)-N(2) 1.953(5), Al(1)-C(2) and Al(1)-C(3) 1.987(6), N(1)-C(1)-N(2) 109.2(3).

Compound **20** (Figure 3.3.5) is also structurally related to **17,** the only difference is the replacement at the amido nitrogen atoms of the TMS by cyclohexyl groups. As in complex **17** the bite angle of the ligand [N(1)-C(2)-N(2a) = 115.0(3)°] has been widened to accommodate the two metal centers. The substitution of the bulky TMS for cyclohexyl groups reduces the amount of steric stress on the ligand. As a result, the two chromium atoms are not "pushed" as close to each other and forming a metal-metal bond [Cr(1)-

Cr(1a) = 1.7801(11) Å] that is slightly longer than in **17**. The Cr-N bonds [Cr(1)-N(1) = 2.011(3) Å] were all found to be equal by symmetry operation and fall in the expected range. The Cr-C bond [Cr(1)-C(1) = 2.115(4) Å] is slightly shorter than that found in **17**. The bonding within the CN_3 core of the ligand is also as expected [N(1)-C(2) and N(2a)-C(2) = 1.337(4) Å, N(3)-C(2) = 1.431(4) Å].

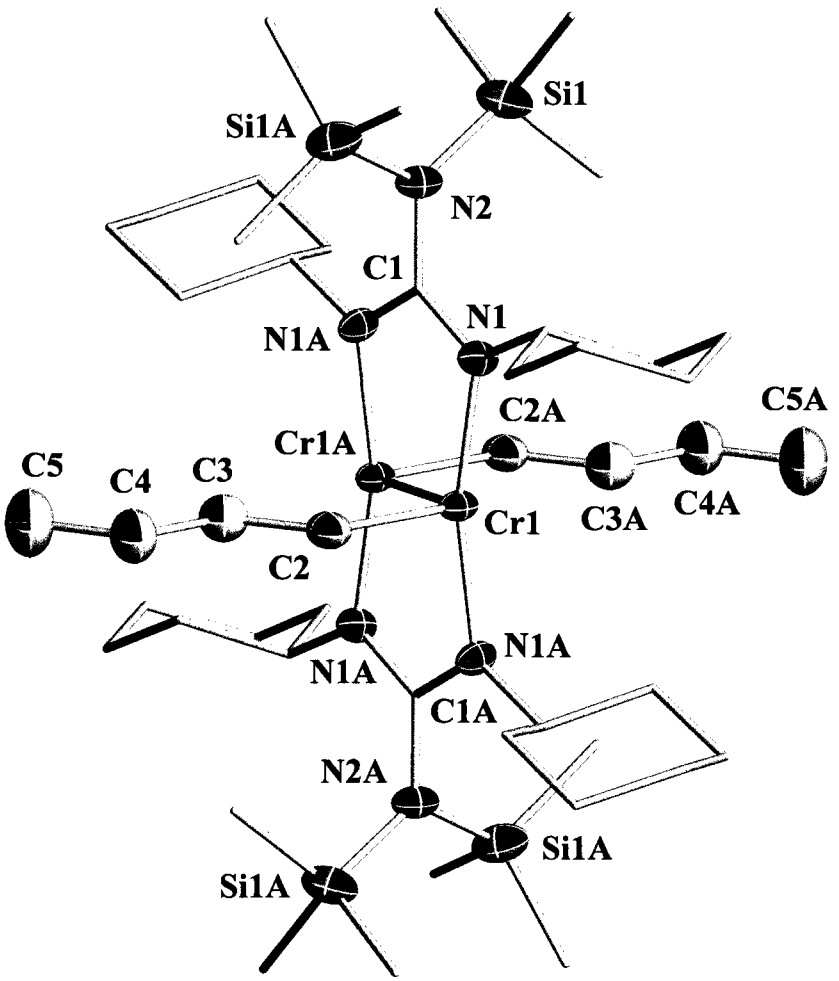

Figure 3.3.4. ORTEP representation of **19**, with thermal ellipsoids set at 50% probability and hydrogen atoms emitted for clarity. Atoms labeled with "a" are generated by the symmetry operation. Selected bond lengths (Å) and angles (°): Cr(1)-Cr(1a) 1.8094(17), Cr(1)-N(1) 2.030(3), Cr(1)-C(2) 2.108(6), N(1a)-C(1)-N(1) 116.1(5).

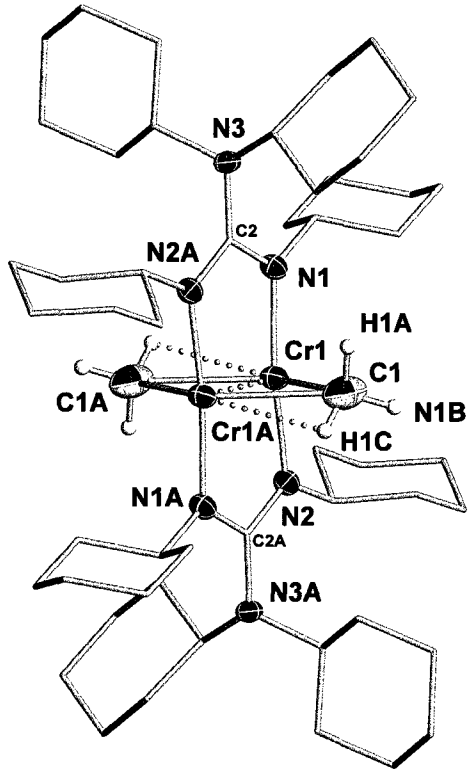

Figure 3.3.5. ORTEP representation of **20**, with thermal ellipsoids set at 50% probability and hydrogen atoms emitted for clarity. Atoms labeled with "a" are generated by symmetry. Selected bond lengths (Å) and angles (°): Cr(1)-Cr(1a) 1.7801(11), Cr(1)-N(1) 2.011(3), Cr(1)-C(1) 2.115(4), N(1)-C(2)-N(2a) 115.0(3).

Complex **21** is an oxo-bridged dimer with two chromium atoms being bonded by the oxygen atom, shown in Figure 3.3.6. Each chromium atom is surrounded by two chelating guanidinate ligands and a single bridging oxygen atom in a distorted trigonal bipyramidal geometry. The distortion is caused by the small bite of the guanidinate ligand [N(1)-C(1)-N(2) = 109.7(6)°]. The Cr-N bond lengths [Cr(1)-N(1) = 2.062(6) Å, Cr(1)-N(2) = 2.079(6) Å] are as expected and are all quite similar. The Cr-O bonds [Cr(1)-O(1) = 1.815(5) Å, Cr(2)-O(1) = 1.814(5) Å] are much shorter than those found in previously characterized complexes and are indicative of double bond character between the chromium and oxygen atoms.[13] The double bond is also evidenced by the Cr-O-Cr linear array [Cr(1)-O(1)-Cr(2) = 173.7(3)°]. The bonding within the CN_3 core [N(1)-C(1) = 1.355(8) Å, N(2)-C(1) = 1.344(8) Å, N(9)-C(1) = 1.423(8) Å] is in the expected range.

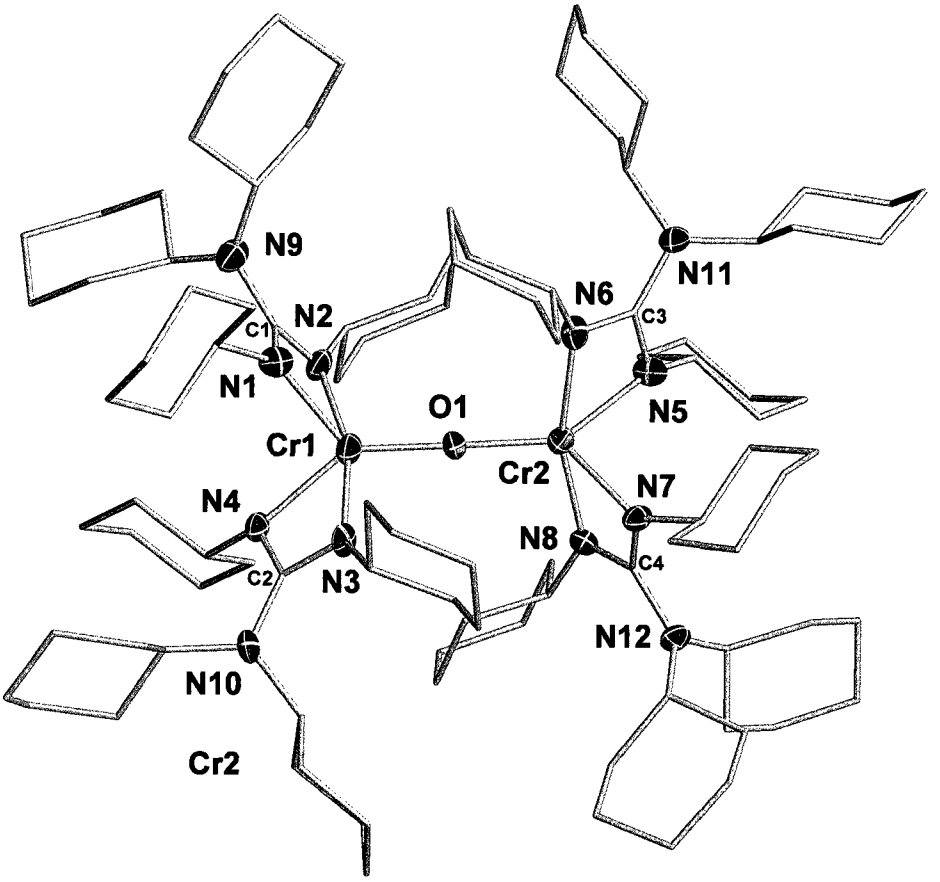

Figure 3.3.6. ORTEP representation of **21**, with thermal ellipsoids set at 50% probability and hydrogen atoms emitted for clarity. Atoms labeled with "a" are generated by the symmetry operation. Selected bond lengths (Å) and angles (°): Cr(1)-N(1) 2.062(6), Cr(1)-N(2) 2.079(6), Cr(1)-O(1) 1.815(5), Cr(2)-O(1) 1.814(5), Cr(1)-O(1)-Cr(2) 173.7(3), N(1)-C(1)-N(2) = 109.7(6).

Complex **22** (Figure 3.3.7) contains three chromium atoms is an unusual arrangement albeit strikingly similar to complex **9** (chapter 2). Complex **22** can be regarded as consisting of two symmetrically equivalent complex **9**'s trapping a single $CrCl_2$ unit between them. This forms two four-membered rings consisting of two chromium atoms, one chlorine and one nitrogen atom. The central chromium atom, Cr(2), is slightly distorted square planar as evidenced by the internal bond angles [Cl(1a)-Cr(2)-N(7a) = 88.76(18)°, Cl(1)-Cr(2)-N(7a) = 91.24(18)°]. The Cr-N bond lengths [Cr(2)-N(7a) and Cr(2)-N(7) = 2.114(6) Å] of the central chromium atom are symmetrically equivalent along with the Cr-Cl bonds [Cr(2)-Cl(1) and Cr(2)-Cl(1a) = 2.365(2) Å]. The Cr-N bonds [Cr(1)-N(1) = 2.101(7) Å, Cr(1)-N(3) = 2.046(7) Å, Cr(1)-N(7a) = 2.159(6)

Å, Cr(1)-N(4) = 2.088(7) Å] to the guanidinate ligand are in the expected range. The Cr(1)-N(7a) bond is slightly longer due to the fact that it is also bonded to the Cr(2) atom. The Cr-Cl bonds [Cr(1)-Cl(1) and Cr(1)-Cl(1a) = 2.710(3) Å] are slightly longer than those to the Cr(2) atom. The bonding within the CN_3 unit [N(1)-C(1) = 1.367(11) Å, N(3)-C(1) = 1.340(11) Å, N(6)-C(1) = 1.384(11) Å] has not been significantly changed from that found in **9**.

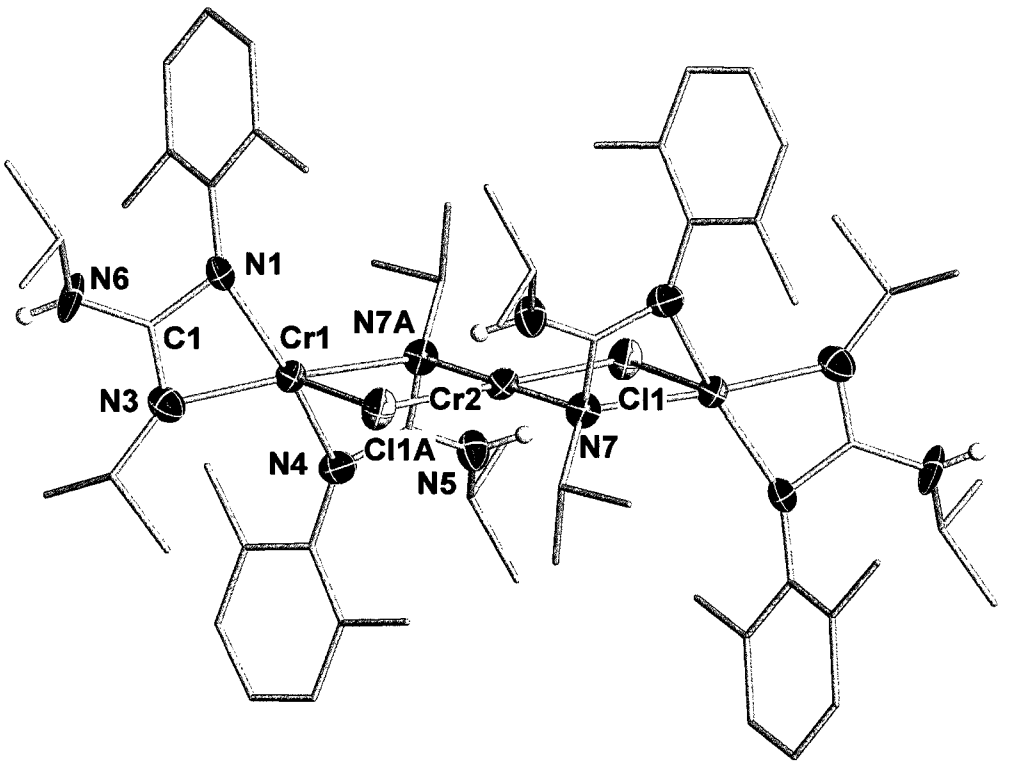

Figure 3.3.7. ORTEP representation of **22**, with thermal ellipsoids set at 50% probability and hydrogen atoms emitted for clarity. Atoms labeled with "a" are generated by the symmetry operation. Selected bond lengths (Å) and angles (°): Cr(2)-N(7a) and Cr(2)-N(7) 2.114(6), Cr(2)-Cl(1) and Cr(2)-Cl(1a) 2.365(2), Cr(1)-N(1) 2.101(7), Cr(1)-N(3) 2.046(7), Cr(1)-N(7a) 2.159(6), Cr(1)-N(4) 2.088(7), Cr(1)-Cl(1) and Cr(1)-Cl(1a) 2.710(3), Cl(1a)-Cr(2)-N(7a) 88.76(18), Cl(1)-Cr(2)-N(7a) 91.24(18).

Complex **23** contains one chromium atom surrounded by two chelating guanidinate ligands and one methyl group in a distorted square-pyramidal geometry, shown in Figure 3.3.8. The distortion once again arises from the narrow bite angle of the ligand [N(1)-C(3)-N(2) = 112.5(7)°]. The angles around the chromium metal center

[N(1)-Cr(1)-N(2) = 65.4(3)°, N(1)-Cr(1)-N(4) = 111.9(3)°, N(2)-Cr(1)-C(1) = 98.4(3)°, N(1)-Cr(1)-C(1) = 102.3(3)°] show quite clearly that the deviation is indeed arising from the bite of the ligand. The Cr-N bond lengths [Cr(1)-N(1) and Cr(1)-N(2) = 2.072(6) Å, Cr(1)-N(3) and Cr(1)-N(4) = 2.094(6) Å] have not changed from what was observed in the starting material. The Cr-C bond [Cr(1)-C(1) = 2.056(8) Å] is in the expected range for a single bond to a sp^3 hybridized carbon atom. The bonding within the CN_3 unit is the same as observed in the starting material.

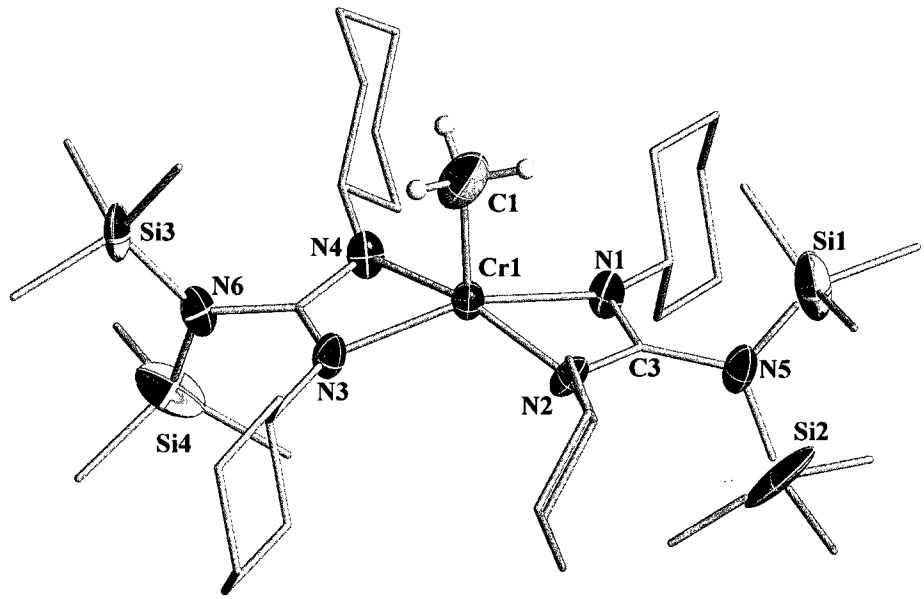

Figure 3.3.8. ORTEP representation of **23**, with thermal ellipsoids set at 50% probability and hydrogen atoms emitted for clarity. Atoms labeled with "a" are generated by the symmetry operation. Selected bond lengths (Å) and angles (°): Cr(1)-N(1) and Cr(1)-N(2) 2.072(6), Cr(1)-N(3) and Cr(1)-N(4) 2.094(6), Cr(1)-C(1) 2.056(8), N(1)-C(3)-N(2) 112.5(7), N(1)-Cr(1)-N(2) 65.4(3), N(1)-Cr(1)-N(4) 111.9(3), N(2)-Cr(1)-C(1) 98.4(3), N(1)-Cr(1)-C(1) 102.3(3).

Complex **24** (Figure 3.3.9) is structurally similar to complex **23** with the only difference being the substitution of the cyclohexyl groups by isopropyl groups on the ligand backbone. One chromium atom is surrounded by two chelating guanidinate ligands and one methyl group in a distorted square pyramidal geometry. The small bite angle of the ligand [N(1)-C(1)-N(2) = 111.7(3)°] reflects in narrow internal bond angles [N(2)-Cr(1)-N(1) = 64.36(12)°, N(2)-Cr(1)-N(2a) = 112.92(12)°, N(2)-Cr(1)-C(3) = 99.97(9)°,

N(1)-Cr(1)-C(3) = 97.18(9)°]. The Cr-N bonds [Cr(1)-N(1) = 2.072(6) Å, Cr(1)-N(2) = 2.057(3) Å] are as expected and similar to that of the starting material and compound **23**. The Cr-C bond length [Cr(1)-C(3) = 2.020(5) Å] is also within the expected range. The bonding within the CN_3 will not be discussed as it does not differ from what was found in the starting material and therefore does not warrant any further discussion.

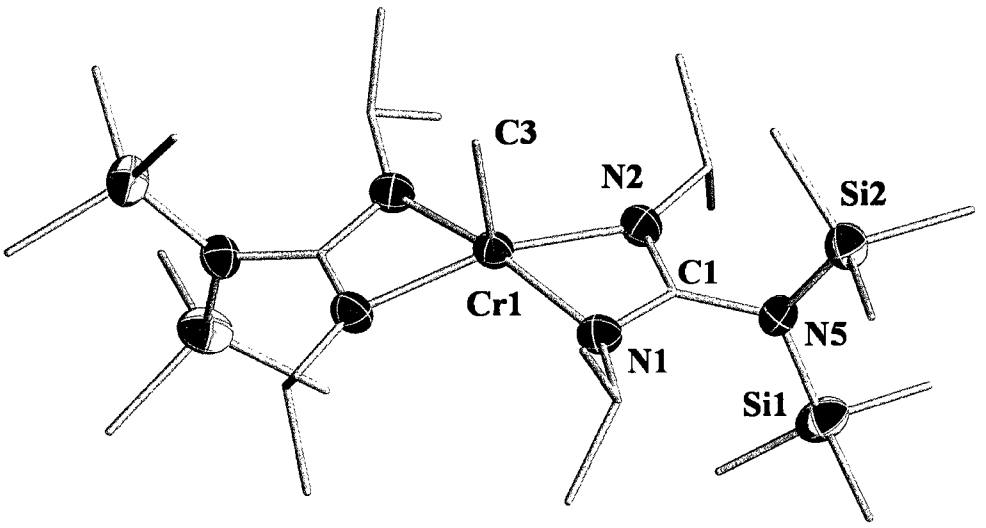

Figure 3.3.9. ORTEP representation of **24**, with thermal ellipsoids set at 50% probability and hydrogen atoms emitted for clarity. Atoms labeled with "a" are generated by the symmetry operation. Selected bond lengths (Å) and angles (°): Cr(1)-N(1) 2.072(6), Cr(1)-N(2) 2.057(3), Cr(1)-C(3) 2.020(5), N(1)-C(1)-N(2) 111.7(3), N(2)-Cr(1)-N(1) 64.36(12), N(2)-Cr(1)-N(2a) 112.92(12), N(2)-Cr(1)-C(3) 99.97(9), N(1)-Cr(1)-C(3) 97.18(9).

3.4 Results and Discussion

Many of the results obtained in this chapter were not anticipated at the beginning of the research project. It had been hoped that heterobimetallic complexes containing a chromium metal center and alkyl aluminum residues could be isolated. To this extent a large amount of reactions were carried out using a wide range of alkyl aluminum compounds containing different chain length, alkyl groups and a number of chlorine atoms. It was observed that alkyl aluminum reagents prefer to react through ligand exchange mechanisms with the chromium guanidinate complexes and do not form heterobimetallic species. This resulted in the formation of chromium alkyl complexes and in some cases these complexes could be isolated. Additionally, a number of complexes were obtained inadvertently through interaction with solvent, adventitious molecular oxygen and even $CrCl_2THF_2$ starting material. Herein, all these results will be reviewed in detail.

During the synthesis and characterization of compound **1** many different solvents were used in an attempt to obtain crystals of sufficient quality for X-ray diffraction. To this end, the use of anhydrous DMF (not desirable in the view of possible reactivity with alkyl aluminum) allowed to isolate complex **16** in crystalline form (Figure 3.4.1). It is clear that the strongly coordinating DMF molecule cleaved the tetrameric structure generating monomers containing one chromium atom surrounded by a single guanidinate anion, one chlorine atom and two DMF molecules coordinated through their oxygen atoms.

Reactions were carried out between all the compounds characterized in chapter 2 and a wide range of alkyl aluminum reagents, $AlMe_3$, $AlEt_3$, Al^iBu_3, $AlMe_2Cl$, $AlMeCl_2$, $AlCl_3$ in various stoichiometries. Unfortunately, only a small number of reactions yielded material that could be sufficiently characterized. In most cases an oily material or black solid was isolated which could not be fully characterized and often decomposed violently in air due to the presence of excess alkyl aluminums. However a few reactions were optimized and crystalline material of sufficient quality to undertake X-ray analysis was obtained.

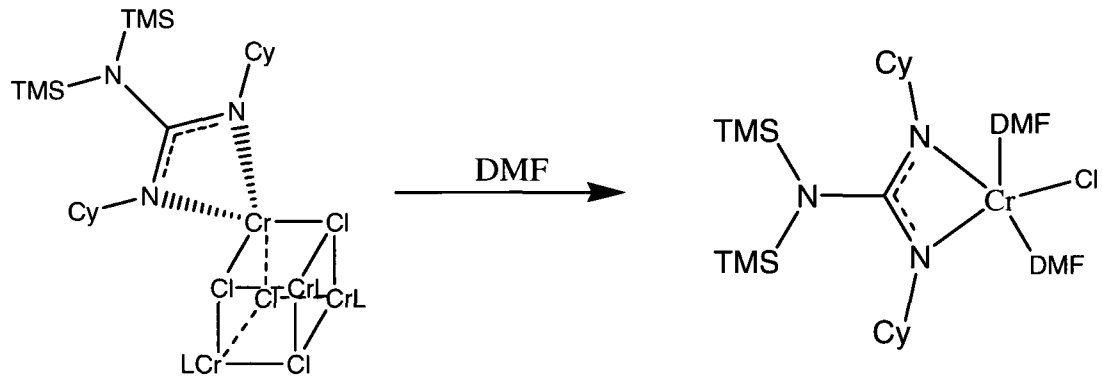

(1) (16)

Figure 3.4.1. Synthesis of Complex **16**.

The reaction of complex **3** with 2.5 eq. of $Al(Me)_3$, if conducted at low temperature and only for about 4 hours, yielded pure **17** (Figure 3.4.2). If the reaction is carried out at room temperature and allowed to stir for too long only an oily material was isolated. The other product of the reaction is the aluminum containing compound **18** where the chromium atom has been clearly leached out (Figure 3.4.3). It should be noticed that if an excess greater than 2.5 equivalents of AlR_xCl_{3-x} is used, chromium metal starts to precipitate out of solution as a black solid. Moreover, the unreacted starting material precipitates with the product in case not insufficient amount of $Al(Me)_3$ was used.

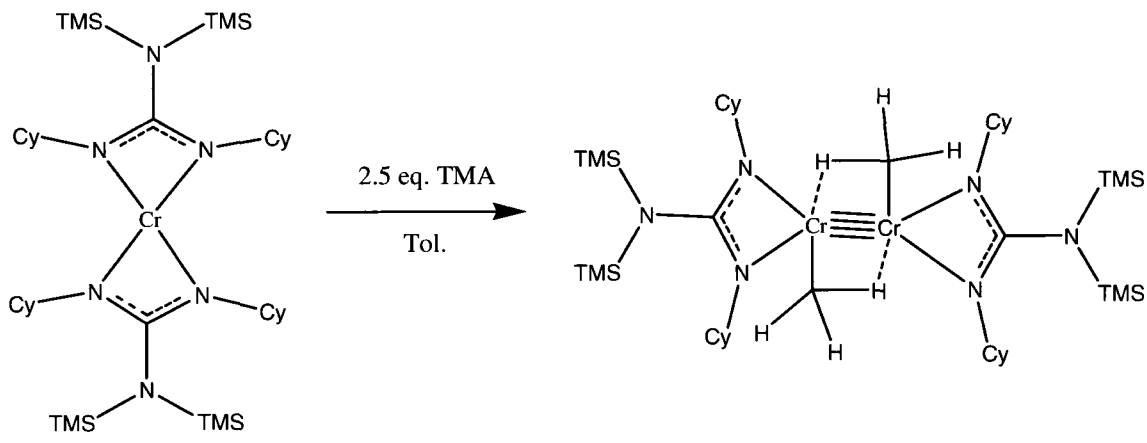

(3) (17)

Figure 3.4.2 Synthesis of Complex **17** (Method A).

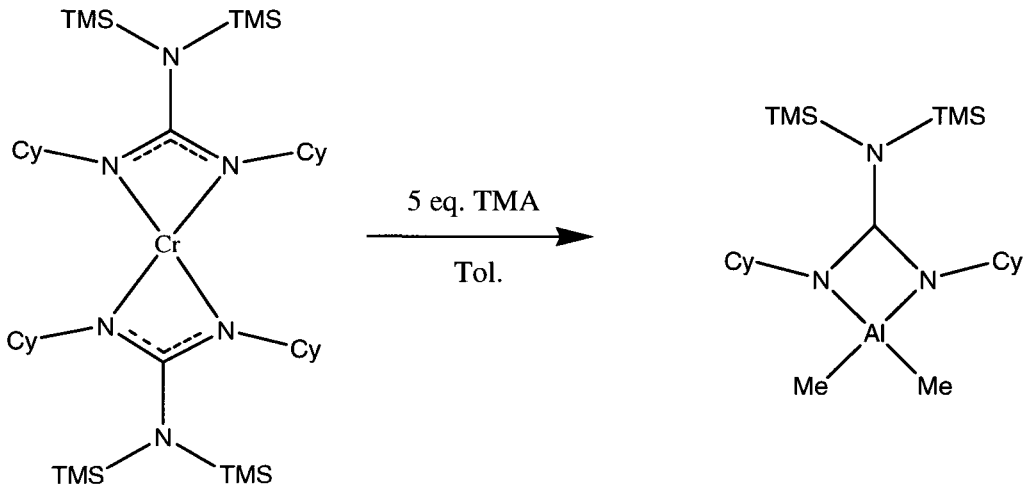

(3) (18)

Figure 3.4.3 Synthesis of Complex **18**.

Complex 17 contains an exceedingly short Cr-Cr contact. In order to elucidate the nature of the intermetallic interaction, a DFT study was done on the multiple bonding in complex **17.**[14]

DFT calculations (found in section 3.7) on both the non-truncated and truncated models (where the Cy and Me_3Si groups in **17** were replaced by the Me and H_3Si groups respectively, Figure 3.7.1) yielded geometrical parameters in good agreement with the experimental values. The calculated Cr-Cr distance for the non-truncated model (1.782Å) is in excellent agreement (0.009Å) with the experimental value (1.773Å). The predicted Cr-Cr distance in the truncated model (1.791Å) is only slightly longer. Calculations also predicted the presence of 4-center agostic interaction and the inward orientation of the two Me groups. The results are summarized in Figure 3.4.4 showing that symmetrization to regular bridging methyl groups, as expected during the Me exchange between the two Cr atoms, would require a non-negligible amount of energy ($\Delta G^{\ddagger}$ = 15.3 kcal/mol).

Among the possible spin states which have been used for calculation (Figure 3.4.5), the singlet states, both open- and closed-shell, displayed the lowest energies with a difference of only 0.5 kcal/mol in favour of the open-shell, broken-symmetry[18] configuration. The lowest excited state (~20 kcal/mol above the ground state) in both

models (truncated and non-truncated) is a triplet state with a slightly longer Cr-Cr bond distance (Figure 3.4.5). In comparison, the similar triplet excited state of the Cr^{II}-Cr^{II} complexes with weaker Cr-Cr interaction lies at much lower energy (~1-3 kcal/mol), thus accounting for their ubiquitously observed temperature-dependent paramagnetism.[2a,g] Consistent with this indicator of stronger Cr-Cr interaction in **17**, the potential energy profile shows a well defined minimum corresponding to a Cr-Cr bond energy of at least 40 kcal/mol. As it can be expected for the Cr^{II} dimers, the open-shell distances at the singlet and the nonet state (S=4) become degenerate at long Cr-Cr limit of the dimer dissociation (Figure 3.4.5). The calculated Cr-Cr bond order for the ground electronic state of **17** is 3.25. As expected, the frontier molecular orbitals of **17** are mainly Cr-centered with high 3*d*-character (Tables 3.7.1 and 3.7.2). The HOMO-LUMO gap (1.8 eV or 42 kcal/mol) is substantial and accounts for the observed diamagnetism. One Me group generates a 4-center agostic Cr-(CH_2-H)-Cr interaction (C-H = 1.117-1.124Å, Figure 3.4.4) with the second Cr atom (Cr..H = 2.26-2.38Å) therefore narrowing the Me-Cr-Cr bonding angle to 82.2° and 78.8° in non- and truncated models respectively [exp 78.2(2)°].

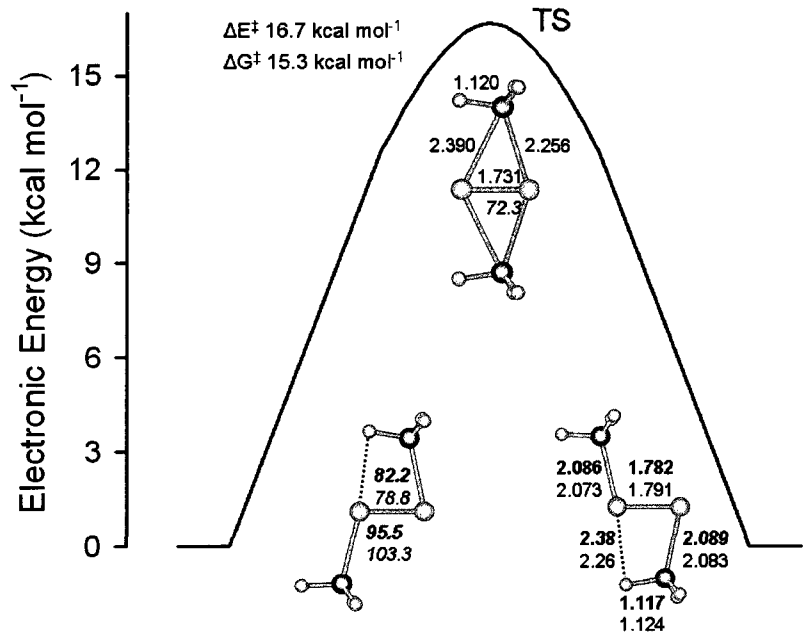

Figure 3.4.4 The DFT optimized structures of non- and truncated models (only the Cr_2Me_2 fragments are shown for clarity) and their relative energies. The interatomic distances (Å) for the two models are shown in bold and regular fonts respectively, bond angles (deg.) are shown in Italics).

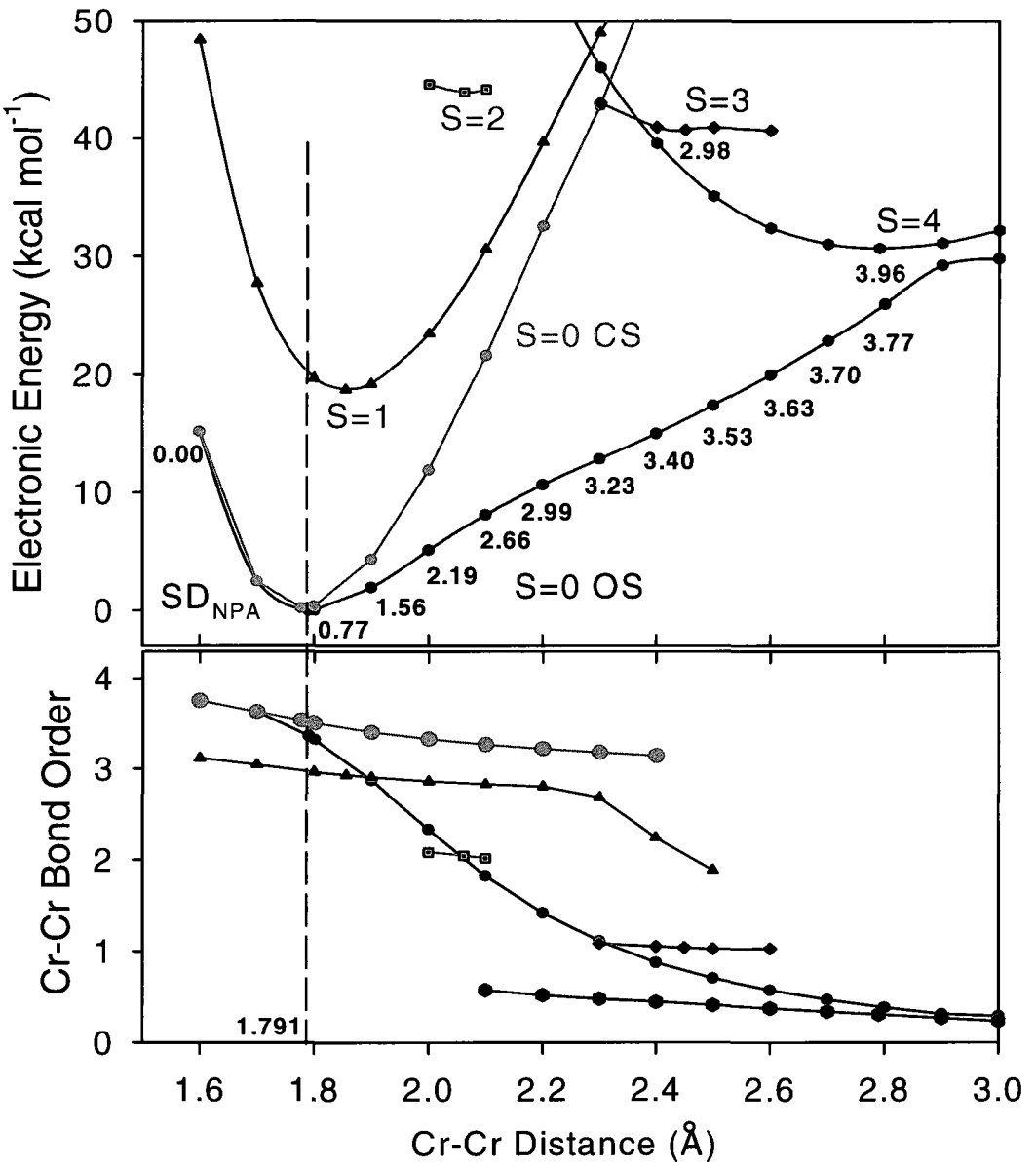

Figure 3.4.5 (Upper) Potential energy surfaces and (lower) Cr-Cr bond orders for different spin states (S=0 OS: open-shell singlet, black; S=0 CS: closed-shell singlet, grey; S=1: triplet, red; S=2: pentet, pink; S=3: septet, green; S=4: nonet, blue) for the truncated model as a function of the Cr-Cr internuclear distance (Å). The NPA-derived atomic spin density of the broken-symmetry wave function for the open-shell singlet state is indicated as well. The vertical dash line indicates the position of the energy minimum for the ground state.

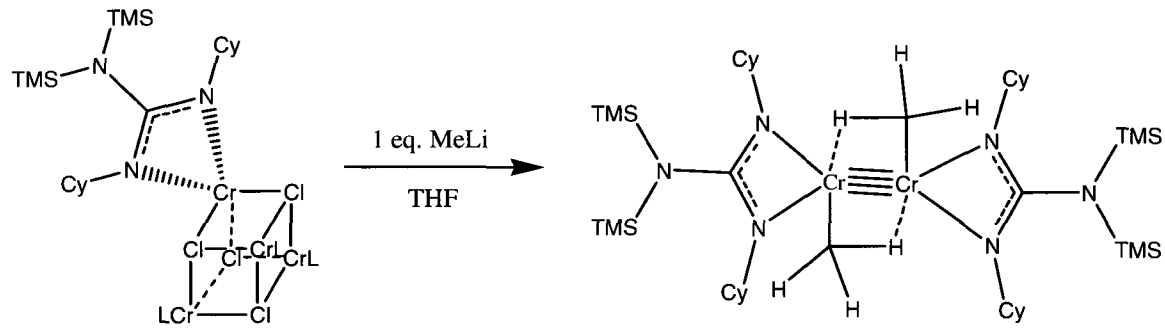

(1) (17)

Figure 3.4.6 Synthesis of Complex **17** (Method B).

To circumvent the difficulty in the synthesis of complex **1** an alternative more straightforward approach has been probed. Complex **1** which contains one guanidinate and one chlorine atom per chromium can be reacted through a salt metathesis reaction with MeLi to yield **17** in much better yield (Figure 3.4.6).

When the same salt metathesis reaction was carried out using ^{n}BuLi instead of MeLi, Figure 3.4.7, a structurally similar chromium dimer was obtained with ^{n}butyl groups in place of the methyl groups. To the best of my knowledge this is the first example of a chromium atom with a terminally bonded ^{n}butyl group. The same metathesis reactions were carried out with the other chromium guanidinate chlorides discussed in chapter 2 but none of these reactions yielded sufficiently pure crystalline material.

A number of reactions were attempted in situ in order to accelerate the screening process in case the reactivity could be screened with species generated in a "one pot" synthesis. Most of these reactions yielded materials insufficiently pure for characterization. Only in the case of the cyclohexylguanidinate anion, the corresponding complex **20** was successfully isolated in crystalline form (Figure 3.4.8). This complex is structurally analogous to **17**. It also contains an exceptionally short metal-metal bond and bridging methyl groups.

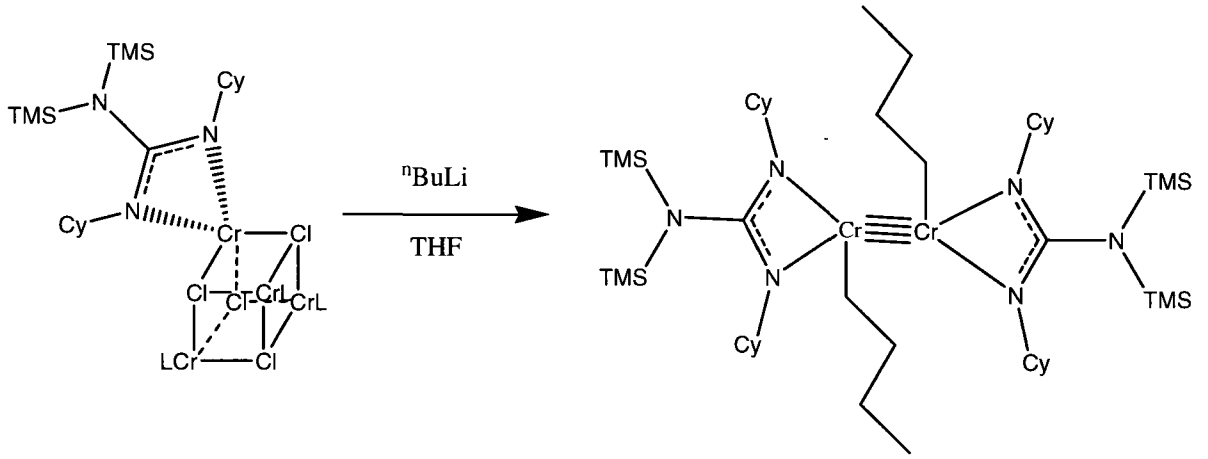

(1) (19)

Figure 3.4.7 Synthesis of Complex **19**.

The one-electron reduction of complex **1** to form a Cr^{I} complex with a quintuple bond was an obvious next step in the development of this chemistry. However as it can be seen in Figure 3.4.9 a Cr^{I} complex was never obtained. As strange as this seems, the reaction was repeated with a number of reducing agents, KC_8, K, Na, K/Na alloy always obtaining the same disappointing result. One plausible explanation for this phenomenon is that a disproportionation pathway may intervene once the initial reduction takes place. Assuming the much expected dinuclear structure, simple extrusion of metallic, colloidal chromium will afford the previously characterized divalent **3** (Figure 3.4.9). The inclination of Cr(I) towards disproportionative oxidation has been observed before.[15]

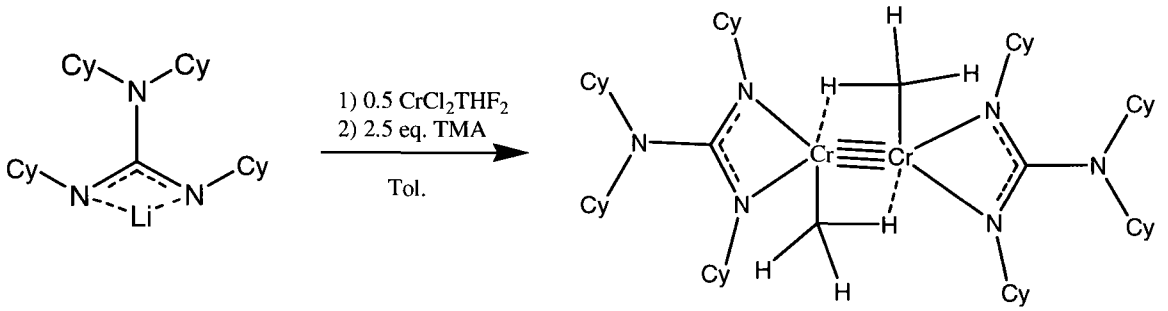

(20)

Figure 3.4.8 Synthesis of Complex **20**.

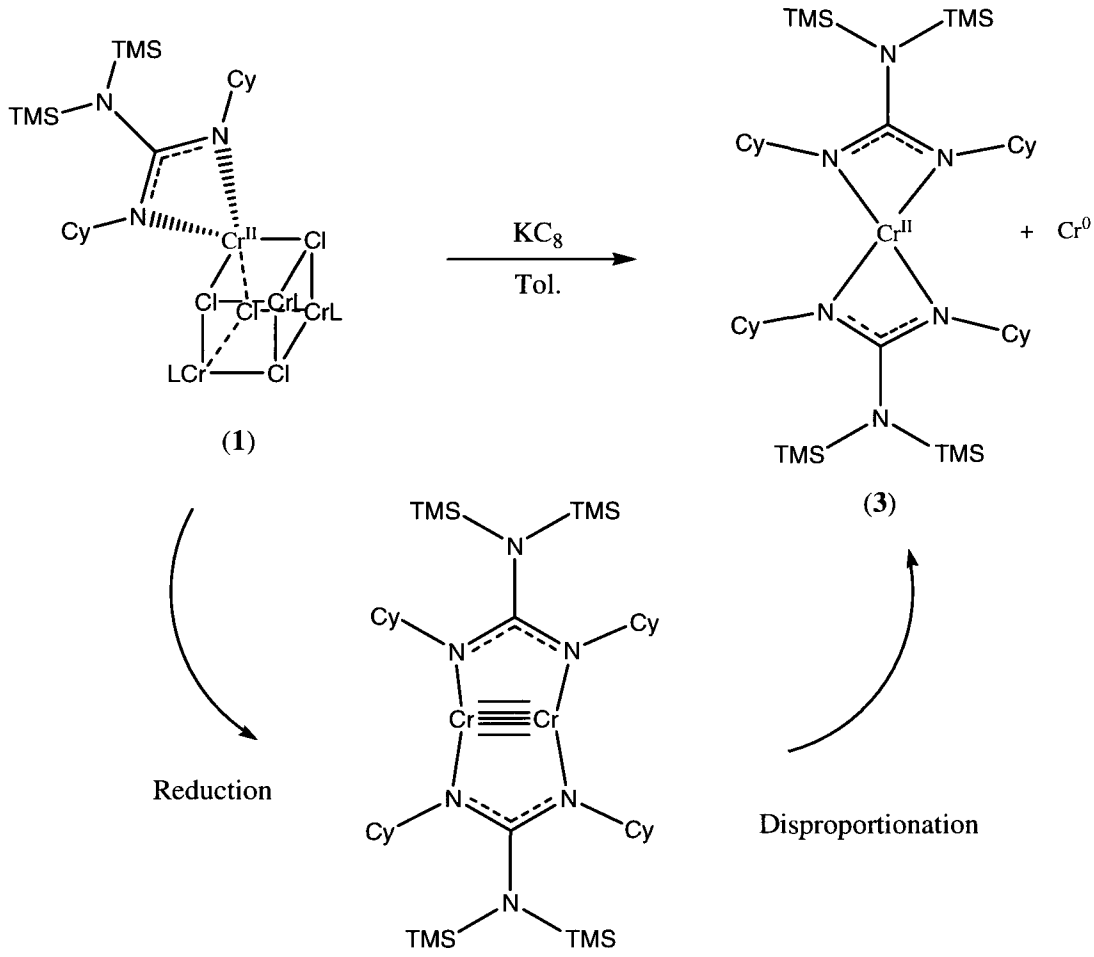

Figure 3.4.9 Reduction of **1** by KC_8 and possible explanation for result obtained.

From the above observations, it became apparent that the guanidinate ligands chosen for this thesis work are not capable of stabilizing the monovalent state of chromium. We argued that the ability of the guanidinate anions to stabilize low valent transition metal complexes is related to the presence of the lone pair on the amino nitrogen and which is used for donation (Figure 2.1.3). The consequent increase of electron density at the two nitrogen donor atoms used for coordination to the metal centre makes guanidinate ligands electronically flexible, a characteristic which indeed could be particularly versatile for stabilization of exceedingly low oxidation states. In agreement with this idea, the only monovalent chromium complex reported in the literature which contains a guanidinate ligand[10] has methyl substituents on the amido nitrogen and 2,6-

diisopropylphenyl groups which permits significant delocalization of the π-system over the three nitrogen atoms. Instead, the crystallographic analysis of the bond lengths and angles of the guanidinate anions used in this thesis clearly showed that the amino nitrogens of these guanidinate ligands are not conjugated to the sp^2 hybridized carbon atom because of steric crowding. We ascribe to this particular behavior the failure of these guanidinates to stabilize Cr(I).

As it was previously mentioned a few compounds in this chapter were serendipitously obtained. Nonetheless, given the dinuclear structures, we became interested in testing the catalytic behavior. During one attempt to crystallize complex **6**, the oxo-bridged dimer **21** was obtained (Figure 3.4.10). As the solvent used in the preparation was toluene, it is apparent that adventitious amount of moisture or oxygen could have been the only source of the oxygen atom. Although unintended, the formation of such a complex is interesting because it gives some information on how these chromium guanidinates may react with O_2. Thus, a more rational synthesis of **21** was attempted through two different routes but each to no avail. The first attempt was done by reacting **6** with an excess of dry molecular oxygen, this yielded only brown oily material that could not be crystallized. The second attempt was done using N_2O but again no material that could be crystallized was obtained. Given the apparent impossibility of rationally preparing this species, only a limited amount of this complex was available for characterization and catalytic testing.

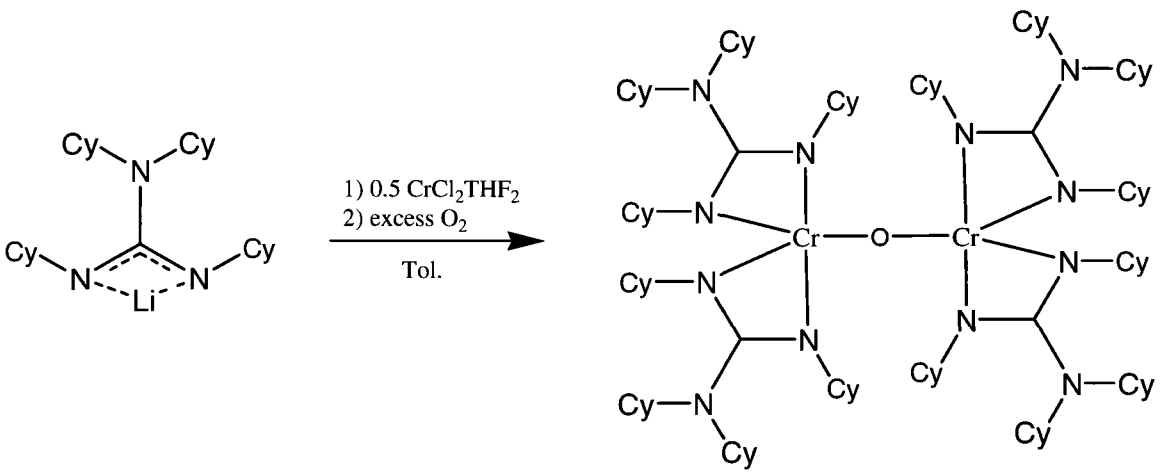

(21)

Figure 3.4.10 Attempted synthesis of **21**.

Similarly, complex **22** (Figure 3.4.11) was originally obtained during the preparation of **9**. A single crystal was picked from a heterogeneous crystalline mass. The crystal had the same color as complexes **1**, **2**, **5**, and **7.** It also scattered poorly. Nonetheless, the crystal structure was successfully solved revealing a trinuclear structure as formally arising from the aggregation of two molecules of **9** with a $CrCl_2$ unit. When the deliberate synthesis of this compound was attempted, **22** was again obtained (Figure 3.4.9). When the same preparation was attempted using the other chromium guanidinates obtained in chapter 2 no reaction was observed. Therefore, the presence of the electron withdrawing phenyl group on the nitrogen atom of the guanidinate ligand in this complex is necessary for the formation of this species.

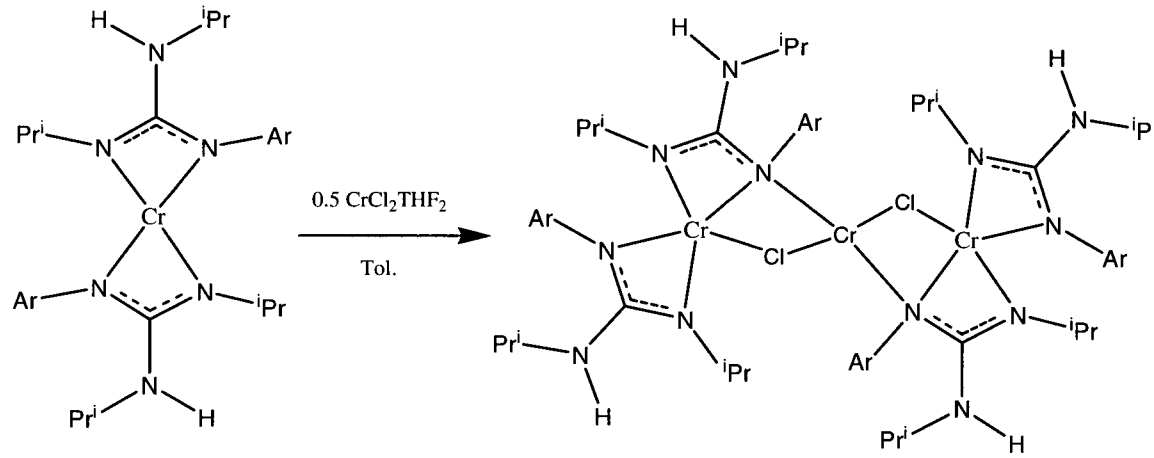

(**9**) (**22**)

Figure 3.4.11 Synthesis of Complex **22**.

The Cr(III) complexes **10**, **11**, **12**, and **13** were also reacted with the same range of aluminum alkyls in various stoichiometries listed earlier but no characterizable material could ever be obtained. When **10** and **11** were reacted with MeLi, complexes **23** and **24** were isolated respectively (Figure 3.4.10). The replacement of the chlorine atom with a methyl group induced substantial electronic change and/or steric hindrance at the metal center to modify the geometry from distorted trigonal bipyramidal to distorted square pyramidal.

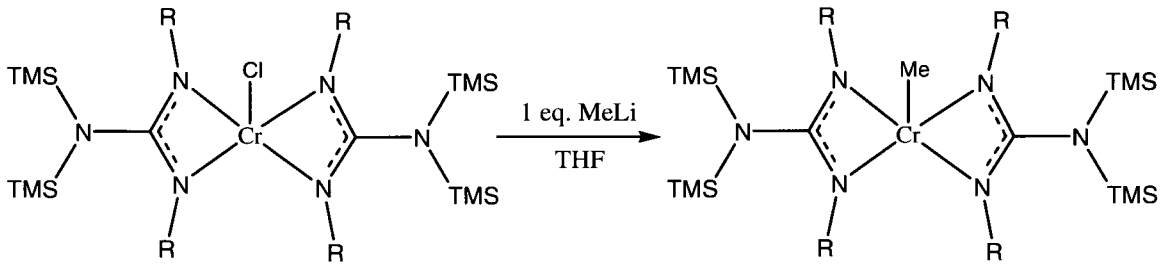

R = Cy **10**, ^{i}Pr **11**

R = Cy **23**, ^{i}Pr **24**

Figure 3.4.10 Synthesis of Complexes (**23**) and (**24**)

3.5 Conclusions

The main goal of the reactions above was to isolate organo-chromium guanidinate complexes that could be used for catalytic testing. It had been hoped that complexes could be isolated that would have the characteristics of a single component catalyst, such as retaining an alkylaluminum residue in the ligand backbond or containing a preformed metal-carbon bond. To this end a number of Cr(II) and Cr(III) complexes with terminally bonded alkyl groups have been obtained.

The Cr(II) guanidinates discussed in chapter 2 were reacted with a number of alkylating agents and three novel metal-metal bonded complexes **17**, **19**, and **20** were obtained. One of these complexes, **17**, contained the shortest known Cr^{II}-Cr^{II} quadruple bond to date. The reduction of the Cr(II) complexes to Cr(I) was unsuccessful as the bisguanidinate chromium complex was always isolated as the product of the reaction.

A series of Cr(III) complexes was also obtained. One complex was inadvertently obtained through reaction with adventitious molecular oxygen and it could not be deliberately prepared. However two other Cr(III) complexes , **23** and **24**, containing two guanidinate ligands and one terminally bonded methyl group could be synthesized in good yield for further use.

The results obtained within this chapter highlight the remarkable ability of the guanidinate ligand to stabilize complexes with ultra short metal-metal bonds and terminal alkyl groups of varying length. A number of these complexes showed great promise to be highly active single component catalysts, as they contained preformed metal-carbon bonds. The catalytic behavior of these species will be presented and discussed in Ch 4.

3.6 Crystallographic Data Section

Table 3.6.1. Crystal data and structure refinement for complexes **16-18**.

	16	**17**	**18**
Formula	C25 H54 Cl Cr N5 O2 Si2	C43.94 H78 Cr2 N6 Si4	C21 H46 Al N3 Si2
FW	600.36	906.73	423.77
space group	Orthorhombic, Pbca	Tetragonal, I4(1)/a	Orthorhombic, Pbca
a (Å)	8.779(2)	14.2723(12)	17.84(5)
b (Å)	20.925(5)	14.2723(12)	17.24(5)
c (Å)	37.388(8)	54.693(10)	18.67(5)
α (deg)	90	90	90
β (deg)	90	90	90
γ (deg)	90	90	90
V ($Å^3$)	6868(3)	11141(2)	5742(28)
Z	8	8	8
radiation (Kα, Å)	0.71073	0.71073	0.980
T (K)	203(2)	202(2)	203(2)
D_{calcd} ($g\ cm^{-3}$)	1.161	1.081	0.980
μ_{calcd} (mm^{-1})	0.508	0.508	0.164
F_{000}	2592	3901	1872
R, R_w [2 a]	0.0850, 0.2416	0.0724, 0.1726	0.0618, 0.1792
GoF	1.042	1.062	1.088

[a] $R = \Sigma|Fo| - |Fc|/\Sigma|F|$. $Rw = [\Sigma(|Fo| - |Fc|)^2/\Sigma wFo^2]^{1/2}$.

Table 3.6.2. Crystal data and structure refinement for complexes **19-21**.

	19	**20**	**21**
Formula	C46 H98 Cr2 N6 Si4	C66 H110 Cr2 N6	C106.30 H188.60 Cr2 N12 O2.58
FW	951.66	1091.60	1780.09
space group	Monoclinic, C2/m	Monoclinic, P2(1)/c	Triclinic, P-1
a (Å)	14.177(2)	13.922(2)	14.701(15)
b (Å)	25.767(4)	12.1326(17)	18.940(19)
c (Å)	9.2162(15)	19.389(3)	22.48(2)
α (deg)	90	90	88.914(17)
β (deg)	124.107(2)	105.806(2)	79.346(18)
γ (deg)	90	90	70.134(18)
V ($Å^3$)	2787.5(8)	3151.2(8)	5779(10)
Z	2	2	2
radiation (Kα, Å)	0.71073	0.71073	0.71073
T (K)	203(2)	203(2)	203(2)
D_{calcd} ($g\ cm^{-3}$)	1.134	1.150	1.023
μ_{calcd} (mm^{-1})	0.510	0.387	0.236
F_{000}	1040	1193	1958
R, R_w [2a]	0.0620, 0.1613	0.0539, 0.1482	0.0796, 0.1533
GoF	1.081	1.048	1.013

[a] $R = \Sigma||Fo| - |Fc||/\Sigma|F|$. $Rw = [\Sigma(|Fo| - |Fc|)^2/\Sigma wFo^2]^{1/2}$.

Table 3.6.3. Crystal data and structure refinement for complexes **22-24**.

	22	**23**	**24**
Formula	C60 H96 C12 Cr3 N12	C49.29 H94.76 Cr N6 Si4	C27 H70 Cr N6 Si4
FW	1212.39	935.91	643.25
space group	Triclinic, P-1	Monoclinic, C2/c	Monoclinic C2/c
a (Å)	10.575(4)	28.429(18)	24.300(3)
b (Å)	13.572(5)	20.193(13)	14.803(3)
c (Å)	14.700(5)	32.26(2)	12.128(2)
α (deg)	83.485(6)	90	90
β (deg)	76.829(6)	116.009(10)	114.246(3)
γ (deg)	69.315(5)	90	90
V ($Å^3$)	1920.7	16642(18)	3977.8(13)
Z	1	12	4
radiation (Kα, Å)	0.71073	0.71073	0.71073
T (K)	203(2)	203(2)	203(2)
D_{calcd} ($g\ cm^{-3}$)	1.048	1.121	1.074
μ_{calcd} (mm^{-1})	0.525	0.329	0.432
F_{000}	646	6150	1416
R, R_w [2 a]	0.0980, 0.2537	0.1467, 0.4079	0.0483, 0.1372
GoF	1.070	1.397	1.054

[a] $R = \Sigma||Fo| - |Fc||/\Sigma|F|$. $Rw = [\Sigma(|Fo| - |Fc|)^2/\Sigma wFo^2]^{1/2}$.

3.7 Computational Details

All density functional calculations were performed at the PBE[16]/TZVP[17] level using the Gaussian 03 package.[18] Spin-unrestrictred treatment was used for open-shell singlets and the electronic states of higher multiplicity. Spin-restricted treatment was used for closed-shell singlet states. Tight SCF convergence criteria were used for all calculations. The converged wave functions were tested to confirm that they corresponded to the ground-state surface. The second-order derivative of the energy with respect to nuclear positions was evaluated to determine the nature of the stationary points. Gibbs free energy of species was evaluated at 298 K and 1 atm. Initial guess wave functions for broken symmetry[19] calculations, calculation of bond orders and the analysis of molecular orbitals in terms of atomic orbital contributions were done using the AOMix package.[20] Atomic spin density was calculated using the natural population analysis (NPA).[21]

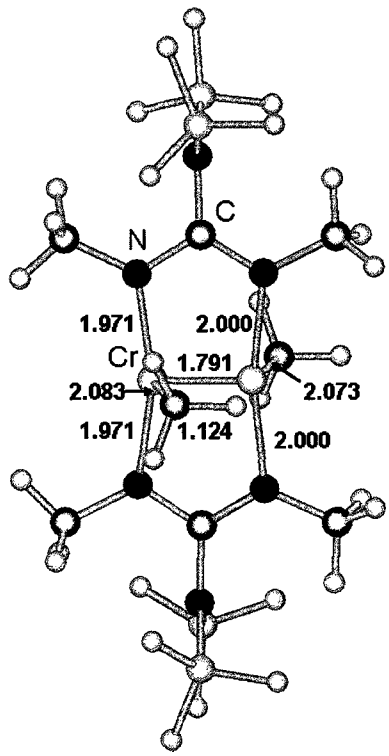

Figure 3.7.1 Optimized structure of the ground state of **17** (Cy and TMS groups have been replaced with Me and H_3Si) from the PBE/TZVP calculations. The internuclear distances (Å) are shown for relevant bonds.

Table 3.7.1 Energies, MPA[a]-derived compositions and Cr-Cr overlap populations (OP)[b] of α-spin frontier orbitals for the spin-singlet ground state of complex **2**.

	ε (eV)	% Cr_a	% Cr_b	OP(Cr_a-Cr_b)
LUMO+3	-0.48	32	44	-1.78
LUMO+2	-1.09	48	38	-0.36
LUMO+1	-1.16	21	37	-0.15
LUMO	-1.25	20	63	-0.08
HOMO	-3.24	62	19	0.05
HOMO-1	-4.25	32	25	0.04
HOMO-2	-4.48	46	36	0.00
HOMO-3	-4.64	10	8	0.01
HOMO-4	-4.72	27	18	0.05
HOMO-5	-5.09	37	27	0.09
HOMO-6	-5.35	34	17	-0.03

a) Mulliken population analysis[22]. b) Positive value for the overlap population indicates bonding Cr-Cr interactions for a given molecular orbital, negative value indicates antibonding Cr-Cr interactions.

Table 3.7.2 Energies, MPA-derived compositions and Cr-Cr overlap populations (OP) of α-spin frontier orbitals for the spin-singlet ground state of complex **3**.

	ε (eV)	% Cr_a	% Cr_b	OP(Cr_a-Cr_b)
LUMO+3	-0.96	7	18	-0.11
LUMO+2	-1.23	58	17	-1.32
LUMO+1	-1.59	57	26	-0.08
LUMO	-1.69	8	57	-0.33
HOMO	-3.51	24	55	0.06
HOMO-1	-4.61	30	33	0.06
HOMO-2	-4.81	33	48	0.02
HOMO-3	-5.04	11	13	0.02
HOMO-4	-5.20	40	47	0.13
HOMO-5	-5.33	7	14	0.01
HOMO-6	-5.44	24	20	0.02

3.8 References

1. (a) John F. Berry, F. Albert Cotton, Sergey A. Ibragimov, Carlos A. Murillo, and Xiaoping Wang *Inorganic Chemistry*, **2005**, *44*. (b) John F. Berry, Eberhard Bothe, F. Albert Cotton, Sergey A. Ibragimov, Carlos A. Murillo, Dino Villagra´n, and Xiaoping Wang *Inorganic Chemistry*. **2006**, *45* (c) F. Albert Cotton, Carlos A. Murillo, Xiaoping Wang, and Chad C. Wilkinson *Inorganic Chemistry,* **2006**, *45* (d) F. Albert Cotton, Sergey A. Ibragimov, Carlos A. Murillo, Pavel V. Poplaukhin, Qinliang Zhao *Journal of Molecular Structure* **2008**, *890*, 3. (e) Shaun P. Green, Cameron Jones, Andreas Stasch *Science* **2007**, 1754.

2. (a) Cotton, F. A.; Murillo, L. A.; Walton, R. A. *Multiple Bonds Between Metal Atoms*, 3rd ed.; Springer: Berlin, **2005** (b) Peligot, E.-M. *C.R. Acad. Sci.* **1844**, *19*, 609. (c) Peligot, E.-M. *Ann.Chim. Phys.* **1844**, *12*, 528. (d) van Niekerk, J. N.; Schoening, F. R. L. *Acta Crystallogr.* **1951**, *4*, 35. (e) van Niekerk, J. N.; Schoening, F. R. L. *Acta Crystallogr.* **1953**, *6*, 501. (f) van Niekerk, J. N.; Schoening, F. R. L. *Nature* **1953**, *171*, 36.

3. Cotton, F. A.; Curtis, N. F.; Harris, C. B.; Johnson, B. F. G.; Lippard, S. J.; Mague, J. T.; Robinson, W. R.; Wood, J. S. *Science* **1964**, *145*, 1305.

4. (a) M. Guest, C. D. Garner, I. H. Hiller, I. B. Walton *J. Chem. Soc. Farady Trans. II* **1978**, *74*, 2092. (b) M. Benard *J. Am. Chem. Soc.* **1978**, *100*, 2354. (c) F. A. Cotton, G. G. Stanley *Inorg. Chem.* **1977**, *16*, 2671. (d) R. A. Kok, M. B. Hall *Inorg. Chem* **1985**, *24*, 1542. (e) R. D. Davy, M. B. Hall *J. Am. Chem. Soc. 1989*, *111*, 1268. (f) M. Benard *J. Chem. Phys.* **1979**, *71*, 2545. (g) P. C. de Mello, W. D. Edwards, M. C. Zerner *J. Am. Chem. Soc.* **1982**, *104*, 1440.

5. (a) J. Edema, S. Gambarotta, F. van Bolhuis, A.L. Spek *J. Am. Chem. Soc.* **1989**, *111*, 2142; (b) J. Edema, S. Gambarotta, A. Meetsma, F. van Bolhuis, A. Spek *Inorg. Chem.* **1990**, *29*, 2147. (c) J.J. Edema, S. Gambarotta, A. Meetsma, A.L. Spek *Organometallics* **1992**, *11*, 2452. (d) S. Hao, J-I. Song, P. Berno, S. Gambarotta *Organometallics* **1994**, *13*, 1326. (e) M. El Kadri, M. J. Heeg, C. H. Winter *Inorg. Chem.* **2006**, *45*, 5278; (f) A. R. Sadique, M. J. Heeg, C. H. Winter *J. Am. Chem. Soc.* **2003**, *125*, 7774; (g) S. Hao, J.J.H. Edema, S. Gambarotta, C. Bensimon *Inorg. Chem.* **1992**, *31*, 2676.

6. M. B. Hall *Polyhedron* **1987**, *6*, 679

7. J. J. H. Edema, S. Gambarotta *Comments Inorg. Chem.* **1991**, *11*, 195.

8. J. Edema, S. Gambarotta, A. Spek, W. Smeets *Inorg. Chem.* **1989**, *28*, 3782.

9. (a) Y. C. Tsai, C. W. Hsu, G. S. K. Yu, G. H. Lee, Y. Wang, T. S. Kuo *Angew. Chem. Int. Ed. Engl.* **2008**, *ASAP*. (b) A. Noor, F. R. Wagner, R. Kempe *Angew. Chem. Int. Ed. Engl.* **2008**, *ASAP* (c) G. Frenking *Science* **2005**, *310*, 796; (d) M. Brynda, L. Gagliardi,

P. O. Widmark, P. P. Power, B. O. Roos *Angew. Chem. Int. Ed. Engl.* **2006**, *45*, 3804; (e). T. Nguyen, A. D. Sutton, S. Brynda, J. C. Fettinger, G. J. Long, P. P. Power, *Science*, **2005**, *310*, 844.

10. Awal Noor [1], Germund Glatz [1], Robert Müller [2], Martin Kaupp, Prof. Dr. [*], Serhiy Demeshko [3], Rhett Kempe, Prof. Dr. [*] *Angew. Chem. Int. Ed. Engl.* **2009**, *8*, 1149

11. (a) Indu Vidyaratne,† Jennifer Scott,† Sandro Gambarotta,*,† and Robbert Duchateau *Organometallics* **2007**, *26,* 3201. (b) S. Hao, S. Gambarotta, C. Bensimon, J. Am. Chem. Soc. **1992**, *114*, 3556.

12. (a) C.-C. Chang, C.-S. Hsiung, H.-S. Su, B. Srinivas, M.Y. Chiang, G.-H. Lee, Y. Wang, *Organometallics* **1998**, *17*, 1595. (b) Amanda P. Kenney, Glenn P. A. Yap, Darrin S. Richeson, and Sean T. Barry, *Inorganic Chemistry*, **2005**, *44*.

13. Anthony Harton, Katisha Terrell, John C. Huffman, Chris MacDonald, Alicia Beatty, Sichu Li, Charles J. O'Connor, and John B. Vincent. *Inorg. Chem.* **1997**, *36,* 4875.

14. Steven Horvath, Serge I. Gorelsky, Sandro Gambarotta, Ilia Korobkov. *Angew. Chem. Int. Ed. Engl.* **2008**, *47*, 9937.

15. A. Jabri, C. Temple,P. Crewdson, S. Gambarotta,I. Korobkov, R.Duchateau. *J.Am.Chem.Soc.* **2006**, *128*, 9238.

16. J. P. Perdew, K. Burke, M. Ernzerhof *Phys. Rev.* **1996**, *77*, 3865.

17. A. Schafer, C. Huber, R. Ahlrichs *J. Chem. Phys.* **1994**, *100*, 5829.

18. M. J. Frisch, G. W. Trucks, H. B. Schlegel, G. E. Scuseria, M. A. Robb, J. R. Cheeseman, J. A. Montgomery, Jr., T. Vreven, K. N. Kudin, J. C. Burant, J. M. Millam, S. S. Iyengar, J. Tomasi, V. Barone, B. Mennucci, M. Cossi, G. Scalmani, N. Rega, G. A. Petersson, H. Nakatsuji, M. Hada, M. Ehara, K. Toyota, R. Fukuda, J. Hasegawa, M. Ishida, T. Nakajima, Y. Honda, O. Kitao, H. Nakai, M. Klene, X. Li, J. E. Knox, H. P. Hratchian, J. B. Cross, V. Bakken, C. Adamo, J. Jaramillo, R. Gomperts, R. E. Stratmann, O. Yazyev, A. J. Austin, R. Cammi, C. Pomelli, J. W. Ochterski, P. Y. Ayala, K. Morokuma, G. A. Voth, P. Salvador, J. J. Dannenberg, V. G. Zakrzewski, S. Dapprich, A. D. Daniels, M. C. Strain, O. Farkas, D. K. Malick, A. D. Rabuck, K. Raghavachari, J. B. Foresman, J. V. Ortiz, Q. Cui, A. G. Baboul, S. Clifford, J. Cioslowski, B. B. Stefanov, G. Liu, A. Liashenko, P. Piskorz, I. Komaromi, R. L. Martin, D. J. Fox, T. Keith, M. A. Al-Laham, C. Y. Peng, A. Nanayakkara, M. Challacombe, P. M. W. Gill, B. Johnson, W. Chen, M. W. Wong, C. Gonzalez, and J. A. Pople, Gaussian, Inc., Wallingford CT, **2004**.

19. L. Noodleman, D. A. Case *Adv. Inorg. Chem.* **1992**, *38*, 423.

20. S. I. Gorelsky. AOMix: Program for Molecular Orbital Analysis, version 6.36; University of Ottawa: Ottawa, Canada, 2007; http://www.sg-chem.net.

21. A. E. Reed, L. A. Curtis, F. Weinhold *Chem. Rev.* **1988**, *88*, 899.

22. R. S. Mulliken *J. Chem. Phys.* **1955**, *23*, 1833.

4 Catalytic Testing of Chromium Guanidinates

Table of Contents

Chapter 4

4.1 Introduction

This last chapter is an account of the catalytic behavior of the complexes prepared in this work. The catalytic activity will be placed in the perspective of the research rationale and critically evaluated. The main objective of this thesis was to test new oligomerization/polymerization catalysts of chromium. To this end a large number of chromium guanidinate complexes were synthesized and tested for catalytic activity. The rationale for embarking on this research and detailed arguments for the selection of the metal and ligand system have been widely discussed in the previous chapters. For this reason the introduction to this chapter will deal with the Anderson Shulz Flory model of polymerization as this is a topic that is repeatedly brought up in this chapter.

The first kinetic model for polymerization was proposed by Anderson.[1] This was derived from a polymerization model proposed by Schulz and Flory.[2, 3] The combination of these two models is now known as the Anderson Schulz Flory (ASF) model.

Starting from C_2, ethylene building blocks can be continuously added to this. This results in a C_n length chain. The polymer chain can then be terminated by β-hydride elimination generating the terminal alkene function. The probability of chain growth is given by (α). This is the chance that another ethylene molecule will be inserted into the growing chain over β-hydride elimination. This is defined as the ratio between propagation rate (k_p) and the sum of the propagation rate and termination rate (k_t). An equation for the alpha value (α) is shown below in equation 4.1.1.

It has been established that α is independent of the chain length. The one exception is for very short chains (such as C_4), where this is not always obeyed.

$$\alpha = \frac{k_p}{k_p + k_t}$$

α - Probability of chain growth
k_p - Rate of propagation
k_t - Rate of termination

Equation 4.1.1 Equation for the probability of chain growth (α).

The ASF distribution can be used to calculate the maximum amount of C_6 and C_8 (1-hexene and 1-octene) that can be produced in a Schulz-Flory distribution.[4] An example of the visualization of this can be seen in figure 4.1.1.

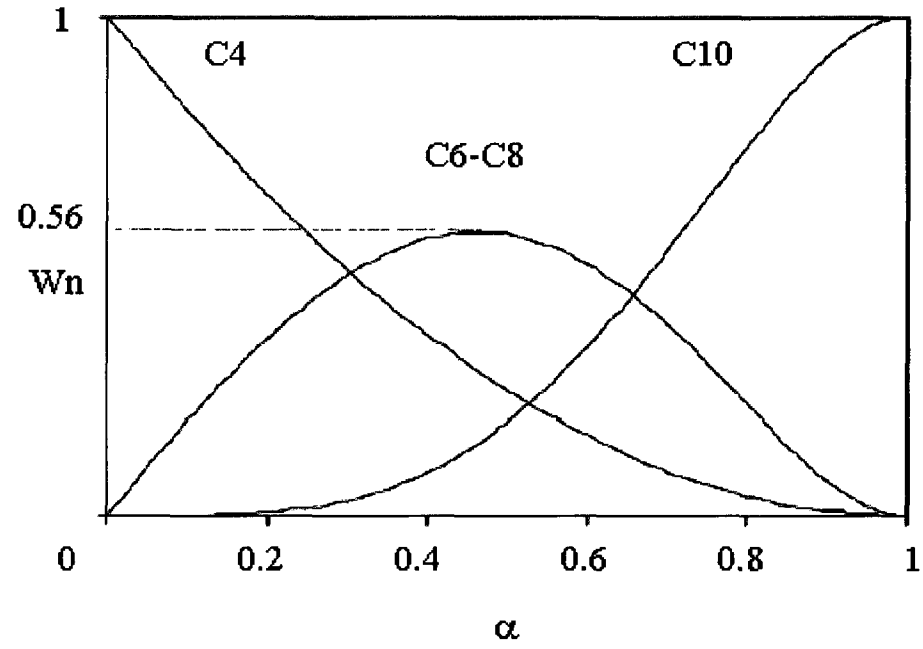

Figure 4.1.1 Visualization of Shultz-Flory distribution where α is the probability of chain growth and W_n is the weight fraction of chains with n carbons.

From figure 4.1.1, the maximum production of 1-hexene to 1-octene that can be produced in this example by a Schulz-Flory mechanism would be 56% of the total yield. As the α value is increased, the amount of higher oligomers produced increases, while the amount of lower weight oligomers decreases. This is then reversed for low values of α.

Many catalysts currently produce a Schulz-Flurry distribution of oligomers, which is a statistical distribution of oligomers.[5] Selective catalysts are instead rare and obviously of greater importance.[6] A catalyst is described as being selective if it is producing the required oligomer at greater than 80 mol%.[4] There should only be an acceptable (small) amount of polymer present, but the preference is that no polymer is formed since reactor fouling in large scale operation may significantly detract from the economic viability of the catalytic cycle.

4.2 Experimental Section

All reactions were carried out under dry nitrogen or argon atmosphere. Solvents were dried using an aluminum oxide solvent purification system. The Aluminum activators, MAO (Aldrich), TIBAO (Aldrich), $AlMe_3$ (Strem), $AlEt_3$ (Strem), Al^iBu_3 (Strem), and $AlEt_2Cl$ (Strem) were used as received. The chromium guanidinate complexes were prepared according to the procedures given in chapters 2 and 3. Polymerization/oligomerization reactions were carried out in either a 250 mL or 400 mL steel Büchi reactor equipped with mechanical stirrer and temperature probe. The larger 400 mL steel reactor had a cold water coil running inside the reactor for which cooling of the reaction mixture could be done, while the 250 mL steel reactor did not have this feature. Prior to each run the reactor would be dried in an oven at 150 °C for a minimum of 4 hours. The reactor would then be assembled and put under vacuum at 100 °C for an additional hour, after which it was flushed with 3 cycles of nitrogen/vacuum. A mixture of the solvent of choice and aluminum activator was added against a stream of nitrogen and the reaction mixture stirred at the desired reaction temperature for approximately 30 minutes. The catalyst was prepared inside a nitrogen filled drybox by dilution. Then the desired volume was taken up by syringe and plugged with a rubber stopper. This solution would then be injected against a flow of nitrogen into the steel reactor after which it was charged with the desired pressure of ethylene. After the reaction time had expired the reactor was quickly cooled to 5 °C to reduce the loss of 1-butene and depressurized. 50 mL of 10% HCl in methanol was added to quench the reaction mixture and any solid was filtered off. An aliquot of the toluene fraction was removed from the mother liquor and kept for NMR and GC analysis to determine the total volume of oligomers. Any insoluble polymer that was filtered was washed 3 times with 10% HCl in water and dried under vacuum overnight before shipped to Dr. Duchateau in Eindhoven for SEC analysis. NMR data was collected on an INOVA Varian 300 or 500 MHz instrument in $CDCl_3$ unless otherwise stated. The oligomer reaction mixtures were analyzed using a CP 9000 gas chromatograph (GC) fitted with a 30 m X 0.32 mm i.d. capillary CP volamine column, with an FID detector. An analysis of the low molecular weight polymer obtained in this

chapter was done by solid state and solution NMR, and size exclusion chromatography (SEC). NMR analysis was done by Dr. Glenn Facey at the University of Ottawa. SEC analysis was done at the Technical University of Eindhoven by Mr. Martin W.M. Fijten. All of these data are shown in Figures 4.3.1-4.3.4. A ^{13}C NMR simulation of branched and linear polyethylene is included, generated by Dr. Glenn Facey, for comparison to the polymer obtained.

Any additional details as related to the experimental procedure will be included in the results and discussion.

4.3 Results and Discussion

Some of the complexes were not tested as the only difference was the alkyl substituent in the ligand backbone. The choice of substituents in the ligand backbone was found early on not to have a large impact on the selectivity of this class of catalysts. It should be mentioned that during some catalytic tests it was observed that the reaction temperature rose spectacularly as the reactor was pressurized with ethylene and the catalytic run began. This was observed when MAO was used in large excess (>200 eq.). The exothermicity of the reaction made testing of these catalysts very difficult and controlling the temperature of the reaction mixture was a major challenge. In fact temperature control is indeed a major issue in the search for selective catalysts. The reader should be reminded about the interconvertibility of chromium oxidation states in its organometallics derivatives as a function of the temperature. Therefore, a number of setups were used to try to control the reaction temperature. Some tests were carried out at the Technical University of Eindhoven under the supervision of Dr. Rob Duchateau. The reactors used in Eindhoven had a cooling jacket that surrounded the reactor and cooled at a moderate rate as the flow of the cold ethanol through the jacket was not manually controlled. This setup did not afford sufficient cooling to the reaction mixture and the internal temperature of the reaction could not be maintained at the desired temperature even with this more sophisticated setup. The reproducibility of some catalytic runs was thus poor as the reactions would rise to a different temperature until stabilized. A setup in Ottawa was built which had a cooling coil run through the middle of the reactor essentially surrounding the stirring rod inside. The flow of cold water through the coil was controlled manually and could be increased to afford more cooling. This setup was found to be much more efficient at maintaining the reaction at the desired temperature. Using this setup the effect of temperature on the product distribution could be probed much more accurately.

Complex **1** was the first to be tested for catalytic activity and the results initially obtained were very encouraging. The catalyst showed a high activity when activated with an excess of MAO but the catalyst was unselective, producing a Shultz-Flory distribution of α-olefins and low molecular weight waxy polymer (Table 4.3.1). These were the first

experiments attempted and so the temperature and reaction time varies among the three tests as these were done more for screening purposes. As it was mentioned above the exothermicity of the reaction was found to be very high. Once the reaction temperature reaches 115-125 °C the catalytically active organochromium is believed to have been thermally decomposed and the temperature slowly drops back to the starting temperature. To circumvent this problem, lower catalyst loadings were used. The temperature spike did not occur as quickly and the reaction took longer to reach 115 °C or higher therefore allowing more product to form before decomposition of the catalyst. If loadings of less than 5 μmol are used the reactions become irreproducible and in some case no product is formed, for this reason most runs were done using either 5 or 10 μmols. This is well summarized in Table 4.3.1 showing that by decreasing the loading, lowering the initial temperature and even shortening the reaction time results in better productivity of oligomers and less polymer.

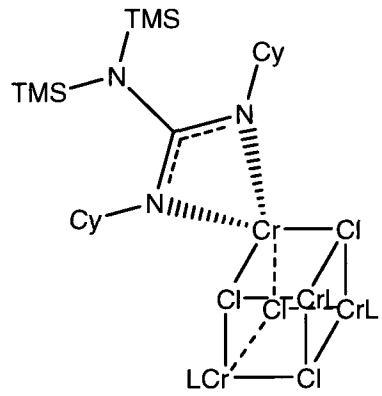

(**1**) L = Guanidinate ligand

Table 4.3.1. Effect of catalyst loading on catalyst 1[a]

Entry	Cat amt. (μmol)	Rxn time	Temp. (°C)	P.E. (g)	Alkenes (mL)	Activity (g/mmol·hr)
1	20	1 hr.	70 (125)	10	30	1500
2	10	30 min.	30 (115)	8	27	5329
3	5	1 hr.	30 (124)	6	35	12728

[a] Conditions : 1000 eq. MAO, 40 bar ethylene, 100 mL toluene used as solvent. Temperature in brackets is maximum temperature reached.

The effect of temperature and time on the catalytic behavior of **1** was probed once the reaction temperature could be controlled properly using the cooling coil, this data are offered in Table 4.3.2. Entries 4 and 5 clearly show that, by controlling the temperature and maintaining the temperature below ~100 °C, no polymer is formed and the main product is a Shultz-Flory distribution of α-olefins. If the temperature of the reaction is allowed to rise above 100 °C, large amount of a low molecular weight polymer is formed. In entries 6, 7, and 8 it is shown that by maintaining an overall higher temperature during the entire catalytic run but not allowing it to exceed 100 °C more α-olefins are produced. One catalytic run was carried out for a very short time (entry 9). The reactor was pressurized and allowed to warm to 100 °C over 3 minutes. Once the reaction mixture reached 100 °C the reaction was cooled quickly using an ice water bath. The reactor was depressurized once the time had reached 5 minutes. The reaction gave a large amount of α-olefins indicating that there is a very high activity at the beginning of the catalytic process. By comparing entries 4 and 9, it is clear that the catalyst does produce more product as time passes but the activity drops significantly. In turn this is a clear indication that the majority of the liquid α-olefins obtained are produced at the beginning of the reaction.

Table 4.3.2 Effect of temperature and time on catalyst 1[a]

Entry	Cat amt. (μmol)	Rxn time	Temp. (°C)	P.E. (g)	Alkenes (mL)	Activity (g/mmol·hr)
4	10	1 hr.	50 (77)[b]	trace	129	9142
5	10	30 min.	90 (122)	12[b]	15	6110
6	10	30 min.	30 (96)[b]	trace	26	3680
7	10	30 min.	50 (89)[b]	trace	39	5720
8	10	30 min.	70 (98)[b]	trace	44	6380
9	5	5 min.	25 (100)	trace	35	42910

[a] Conditions : 1000 eq. MAO, 40 bar ethylene, 100 mL toluene used as solvent. [b] water cooling used to control reaction temperature. Trace is less than 300 mg.

An analysis of the polyethylene formed and α-olefin distribution for entires 1-9 is given in Table 4.3.3. In all cases where only a very small amount of polyethylene was formed, no molecular weight or polydispersity is given. The polymer formed by catalyst

1 is a very low molecular weight polymer having average molecular weights between 500-700 g/mol. The PDI of this polymer is usually in the range of 1.3-1.7. The formation of the polymer also coincides with a shift in the α-olefin distribution to higher molecular weight α-olefins.

Table 4.3.3 Analysis of P.E. and α-olefin product distribution*

Entry	Mlclr Wt. (g/mol)	PDI	C4	C6	C8	C10	C12	C14	C16	C18 ≤
1	564	1.45	10.0	14.3	19.5	14.6	12.6	10.2	8.3	10.5
2	505	1.38	8.1	13	19.1	17.1	13.9	11.7	7.8	9.0
3	602	1.64	7.0	13.8	20.4	17.1	14.6	11.5	9.1	7.0
4	n/a	n/a	20.6	38.	17.1	11.7	6.0	3.7	1.9	1.0
5	697	1.51	13.0	11.6	19.3	14.9	12.4	10.1	7.8	11.3
6	n/a	n/a	5.1	22.5	26.0	17.6	13.0	7.9	4.7	3.2
7	n/a	n/a	2.5	23.2	20.3	17.3	14.5	10.4	7.1	4.6
8	n/a	n/a	7.0	30.7	21.4	17.0	11.3	7.2	4.6	2.8
9	n/a	n/a	8.4	25.9	24.6	15.8	10.6	6.9	4.6	3.1

* Oligomer distribution given in percentage.

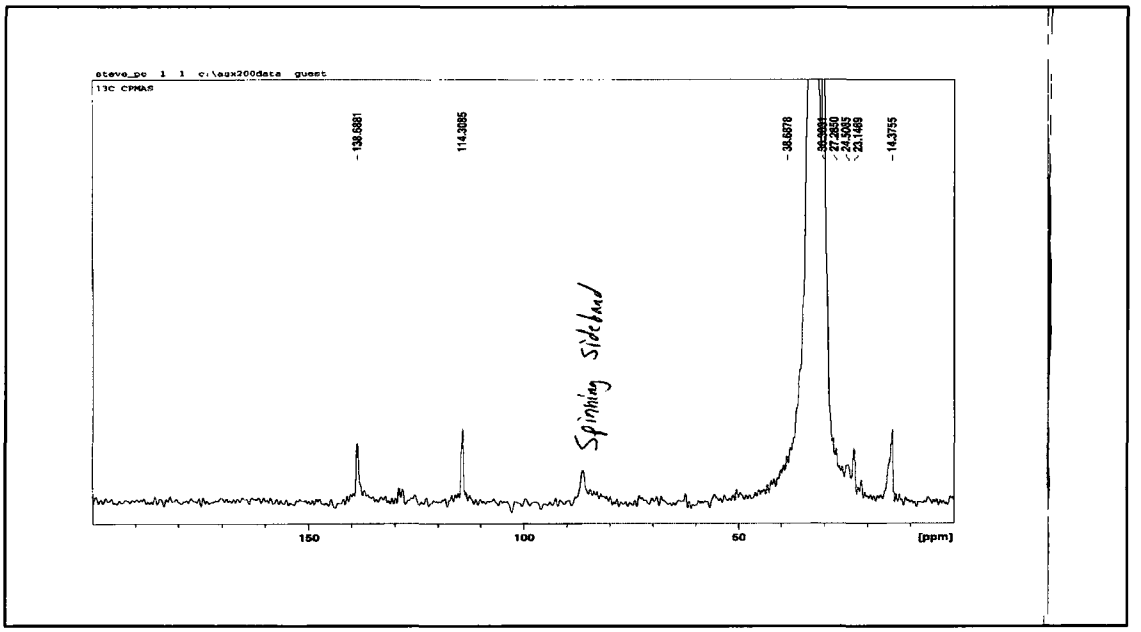

Figure 4.3.1 Solid State NMR of P.E. from entry 1

The solid state NMR and ^{13}C NMR shows the low molecular weight polymer to be a linear α-olefin with essentially no branching (Figure 4.3.1 and 4.3.2).

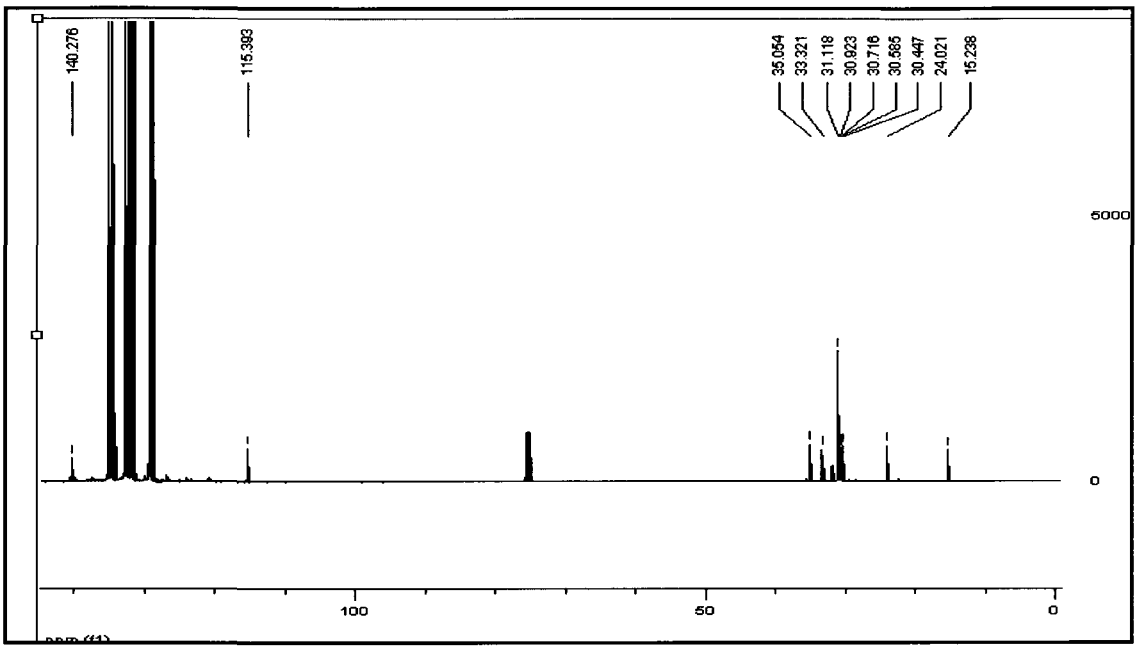

Figure 4.3.2 Solution ^{13}C NMR of P.E. from entry 1

This leads us to the conclusion that the wax is not necessarily the product of a different catalytically active species being formed in solution. Rather the increase in temperature shifts the distribution to much higher molecular weight α-olefins. During runs where the temperature increased significantly (entries 1, 2, 3, and 5 in Table 4.3.3), the amount of C6 in particular has been decreased and the amount of C18 that forms is significantly increased. This data supports the notion that the same catalytically active species is being generated despite the temperature control of the reaction and only the product distribution is being affected. However, the GPC analysis of the low molecular weight polymer, Figure 4.3.3, shows a slightly bimodal distribution which could indicate that two different catalytically active species are being formed.

The next variable to be probed was the amount of co-catalyst used. In Table 4.3.4 it is shown that using less MAO the activity decreases. What was also interesting about this series of experiments is that not only was the activity affected but the catalyst seemed to switch from a non-selective oligomerization catalyst with large excess of MAO to a genuine polymerization catalyst in low loadings of MAO. With an intermediate loading, entry 10, the catalyst produces a Shultz-Flory distribution of α-olefins and polymer.

Therefore, it was concluded that a large excess of MAO is thus necessary to form the highly active yet non-selective catalyst. Additionally, it should be noted that in entries 10 and 11 no water cooling was necessary to maintain the desired reaction temperature as the temperature spike was much more moderate.

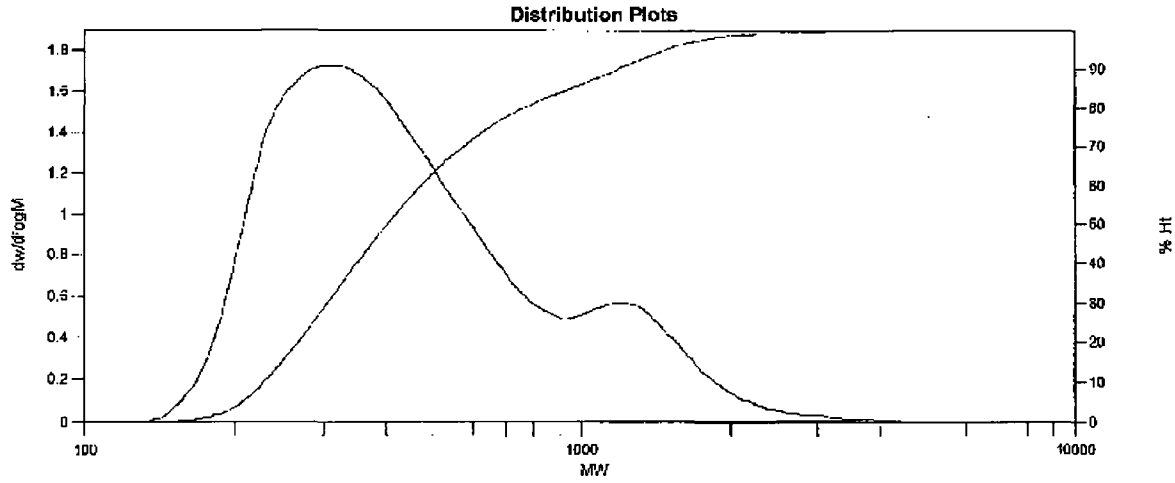

Figure 4.3.3 GPC Analysis of P.E. from entry 1

Table 4.3.4 Effect of MAO on catalyst 1[a]

Entry	Al:Cr (MAO)	Rxn time	Temp. (°C)	P.E. (g)	Alkenes (mL)	Activity (g/mmol·hr)
4	1000	1 hr.	50 (77)[b]	trace	129	9142
10	170	1 hr.	50 (70)	6.2	36	3320
11	10	1 hr.	50 (55)	2.3	0	230

[a] Conditions : 10 μmol catalyst loading, 40 bar ethylene, 100 mL toluene used as solvent.
[b] water cooling used to control reaction temperature. Trace is less than 300 mg.

The effect of pressure on the activity and selectivity of catalyst **1** was probed and the results shown in Table 4.3.5. At high pressure the activity of this catalyst was the highest ever reported in the literature (Entry 4). Decreasing the pressure of ethylene from 40 bar to 20 bar reduces the activity by about 70%. When the pressure is decreased further to 5 bar the activity is reduced once again. Finally a test was carried out at 1 bar of ethylene and the catalyst was found to be inactive. It is also important to note that in entry 12, water cooling was used to control the reaction temperature, while in entry 13 the temperature spike was not so drastic and no water cooling was necessary.

Catalyst loading, temperature, amount of co-catalyst, and pressure all seem to have major effects on the activity of catalyst **1** but not on the selectivity. In all cases highly active non-selective oligomerization catalysts are generated. With one of the major goals of the thesis being to obtain a selective catalyst for trimerization or tetramerization of ethylene the final parameter that was probed was the nature of the co-catalyst. It has been previously demonstrated that the co-catalyst can have a major effect on the selectivity of the catalyst.[7] Five of the most commonly used alkyl aluminum activators were screened as useful co-catalysts for the chromium guanidinate system, the results of the testing is shown in Table 4.3.6. Using alkyl aluminums such as TMA, TEAL, and TIBA as co-catalyst gave no activity of any sort. However when DEAC or TIBAO was used as the co-catalyst a small amount of polyethylene was formed. The polymer obtained in each case had similar properties and was a much higher molecular weight polymer than that obtained when using MAO. However the overall activity of the catalyst remained very poor and thus no more testing was carried out for this particular catalyst.

Table 4.3.5 Effect of pressure on catalyst 1[a]

Entry	Pressure (bar)	Rxn time	Temp. (°C)	P.E. (g)	Alkenes (mL)	Activity (g/mmol·hr)
4	40	1 hr.	50 (77)[b]	trace	129	9142
12	20	1 hr.	50 (65)[b]	trace	37	2640
13	5	1 hr.	50 (79)	trace	15	1090
14	1	1 hr.	50	0	0	0

[a] Conditions : 10 μmol catalyst loading, 1000 eq. MAO, 100 mL toluene used as solvent.
[b] water cooling used to control reaction temperature. Trace is less than 300 mg.

Table 4.3.6 Effect of co-catalyst on catalyst 1[a]

Entry	Co-Catalyst	Al:Cr	Rxn time	Temp. (°C)	P.E. (g)	Alkenes (mL)	Activity (g/mmol·hr)
15	TMA	200	1 hr.	50	0	0	0
16	TEAL	200	1 hr.	50	0	0	0
17	TIBA	200	1 hr.	50	0	0	0
18	TIBAO	500	30 min.	60 (70)	3.3	0	660
19	DEAC	200	1 hr.	50 (53)	4.0	0	400

[a] Conditions : 10 μmol catalyst loading, 40 bar ethylene, 100 mL toluene used as solvent.

Table 4.3.7 Analysis of P.E. and α-olefin product distribution*

Entry	Mlclr Wt. (g/mol)	PDI	C4	C6	C8	C10	C12	C14	C16	C18 ≤
10	19452	32.9	7.6	11.2	17.3	17.5	16.6	12.5	8.4	9.4
11	42968	3.45	0	0	0	0	0	0	0	0
12	n/a	n/a	7.6	27.3	24.6	16.8	11.4	6.7	4.4	1.2
13	n/a	n/a	8.4	28.1	25.3	15.4	10.5	6.9	3.9	1.5
18	41907	4.0	0	0	0	0	0	0	0	0
19	54752	3.61	0	0	0	0	0	0	0	0

* Oligomer distribution given in percentage.

Complex **2** was also tested for catalytic activity. Since the complex is so structurally similar to that of **1** the results were anticipated to be quite similar possibly affecting only the activity but not the selectivity. The results obtained are shown in Tables 4.3.8 and 4.3.9. The only exception was run 20 and which showed an intriguing small excess of 1-hexene being formed. Overall however, catalyst **2** does behave very similarly to catalyst **1** and thus this line of research was abandoned.

Complex **3** also is a Cr(II) complex but contains two guanidinate ligands per metal atom, no chlorine and is monomeric. Although a similar catalytic behavior was anticipated, a few runs were carried out to exclude possible effects arising from the structural differences. However, the catalytic runs confirmed a close similarity of behavior.

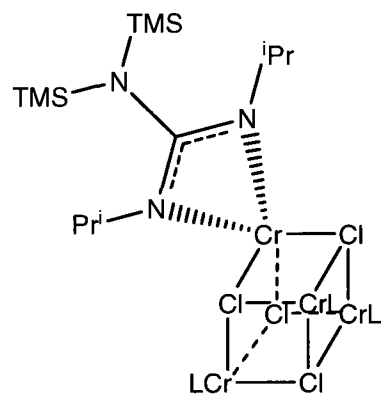

(**2**)

Table 4.3.8 Oligomerization/polymerization activity of catalyst 2[a]

Entry	Cat amt. (μmol)	Rxn time	Temp. (°C)	P.E. (g)	Alkenes (mL)	Activity (g/mmol·hr)
20	10	1 hr.	50 (82)	trace	124	8770
21	10	30 min.	50 (90)	trace	59	8560

[a] Conditions : 1000 eq. MAO, 40 bar ethylene, 100 mL toluene used as solvent.

Table 4.3.9 Analysis of P.E. and α-olefin product distribution*

Entry	Mlclr Wt. (g/mol)	PDI	C4	C6	C8	C10	C12	C14	C16	C18 ≤
20	n/a	n/a	10.1	41.0	18.4	11.2	8.0	5.2	2.8	3.5
21	n/a	n/a	4.8	26.1	21.8	17.8	12.3	8.3	5.5	3.5

* Oligomer distribution given in percentage.

Complex **3** was also extensively tested to see if any of the parameters could be fine tuned in search for selective oligomerization. However an inspection of the data collected in Tables 4.3.10-4.3.13 quickly revealed that this catalyst is well comparable to **1** or **2** although activity is slightly higher. The effect of temperature on **3** was found to be the same as for catalyst **1** with higher overall temperatures resulting in higher activities and large amounts of a low molecular weight polymer forming when reaction temperatures rise above 100 °C.

A series of experiments was carried out to study the effect of reaction time on the activity of catalyst **3** (entries 22-24). The catalyst produces more α-olefin as the reaction time is increased. As in the case of catalyst **1** the entry with the highest activity is the entry with the shortest reaction time. During the first 20 minutes of the reaction a substantial amount of product is being formed then the catalyst produces the remaining α-olefin with a relatively constant activity. This explains why the activity in entry 22 is slightly higher than the very similar activities in entries 23 and 24.

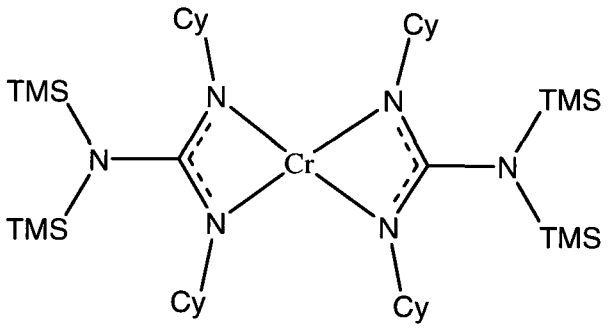

(**3**)

Table 4.3.10 Effect of temperature control and time on catalyst 3[a]

Entry	Cat amt. (μmol)	Rxn time	Temp. (°C)	P.E. (g)	Alkenes (mL)	Activity (g/mmol·hr)
22	5	20 min.	50 (70)[b]	trace	34	14727
23	5	40 min.	50 (65)[b]	trace	56	12060
24	5	1 hr.	50 (75)[b]	trace	85	12100
25	5	30 min.	50 (123)	17	21	13094
26	10	1 hr.	50 (89)[b]	trace	146	10340

[a] Conditions : 1000 eq. MAO, 40 bar ethylene, 100 mL toluene used as solvent. [b] water cooling used to control reaction temperature. Trace is less than 300 mg.

Table 4.3.11 Analysis of P.E. and α-olefin product distribution*

Entry	Mlclr Wt. (g/mol)	PDI	C4	C6	C8	C10	C12	C14	C16	C18 ≤
22	n/a	n/a	7.9	35.2	24.7	15.3	8.9	4.3	2.6	1.1
23	n/a	n/a	7.2	37.7	24.1	15.0	8.6	3.8	2.3	1.3
24	n/a	n/a	8.8	34.6	23.1	14.8	9.2	5.0	2.9	1.6
25	562	2.46	8.9	13.4	19.3	15.6	13.1	11.0	7.9	11
26	n/a	n/a	7.6	37.9	23.9	16.0	8.9	3.1	2	0.5

* Oligomer distribution given in percentage.

Catalyst **3** showed no catalytic activity when activated with TMA, TEAL, or TIBA, shown in Table 4.3.12. When activated with DEAC or TIBAO the activity was low and only a polymer with a relatively wide polydispersity was obtained. The most interesting result from the set of experiments shown in Table 4.3.12 is in entry 32. The MAO used in this experiment was mixed with 30% BHT, which is a bulky alcohol

commonly used to deplete residual TMA in MAO. It is known that about 30% of MAO contains pure TMA so by adding the bulky alcohol it can be more conclusively shown that it is indeed MAO alone and not the combination of MAO and TMA that is responsible for inducing the catalytic activity. The experiment yielded 32 mL of alkenes and the overall activity was slightly lower than that observed in entries 22-26. By adding the 30% BHT to the reaction mixture we may have "killed" some of the active catalyst through possible reaction with the alcohol or the products it forms with the TMA. What is interesting is that water cooling was not needed in this experiment to maintain the reaction temperature and no polymer is formed.

Table 4.3.12 Effect of co-catalyst on catalyst 3[a]

Entry	Co-Catalyst	Al:Cr	Rxn time	Temp. (°C)	P.E. (g)	Alkenes (mL)	Activity (g/mmol·hr)
27	TMA	200	1 hr.	50	0	0	0
28	TEAL	200	1 hr.	50	0	0	0
29	TIBA	200	1 hr.	50	0	0	0
30	TIBAO	500	1 hr.	50 (55)	2.8	0	280
31	DEAC	200	1 hr.	50 (55)	7	0	700
32	MAO[b]	1000	30 min.	50 (57)	trace	32	4617

[a] Conditions : 10 μmol catalyst loading, 40 bar ethylene, 100 mL toluene used as solvent.
[b] 30% BHT added to MAO to kill active TMA.

Table 4.3.13 Analysis of P.E. and α-olefin product distribution*

Entry	Mlclr Wt. (g/mol)	PDI	C4	C6	C8	C10	C12	C14	C16	C18 ≤
30	43875	4.32	0	0	0	0	0	0	0	0
31	356230	11.3	0	0	0	0	0	0	0	0
32	n/a	n/a	6.4	29.6	22.1	17.0	11.4	7.6	3.8	2.1

* Oligomer distribution given in percentage.

Complex **4** was screened to see if there was any substantial change in activity introduced by substitution of the cyclohexyl groups with isopropyl groups. Two experiments were performed and the results are shown in Tables 4.3.14 and 4.3.15. This catalyst unsurprisingly performed nearly identically to catalyst **3**. The lower activity in entry 34 is a result of using a higher catalyst loading.

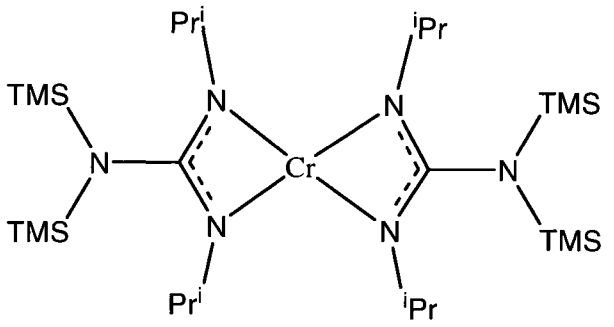

(**4**)

Table 4.3.14 Oligomerization/polymerization activity of catalyst 4[a]

Entry	Cat amt. (μmol)	Rxn time	Temp. (°C)	P.E. (g)	Alkenes (mL)	Activity (g/mmol·hr)
33	10	1 hr.	50 (78)[b]	trace	133	9417
34	10	30 min.	50 (124)	19	20	2967

[a] Conditions : 1000 eq. MAO, 40 bar ethylene, 100 mL toluene used as solvent. [b] water cooling used to control reaction temperature. Trace is less than 300 mg.

Table 4.3.15 Analysis of P.E. and α-olefin product distribution*

Entry	Mlclr Wt. (g/mol)	PDI	C4	C6	C8	C10	C12	C14	C16	C18 ≤
33	n/a	n/a	6.7	36.8	24.6	17.1	8.6	3.2	2.3	0.9
34	451	1.33	9.7	16.5	21.5	17.1	12.4	9.3	6.9	6.6

* Oligomer distribution given in percentage.

Complex **8** was screened because the ligand attached to chromium contains only three alkyl substituents and a hydrogen atom. Unlike the bulkier ligands in catalysts **1-4** it is also possible that the residual H atom might be removed by the activator, opening the door to formation of dianionic ligand or possible zwitteronic structures. The catalytic activity and selectivity however was not different than what was already observed for this class of compounds and it is shown in Tables 4.3.14 and 4.3.15. When activated with MAO a massive temperature spike occurs and a Shultz-Flory distribution of α-olefins and low molecular weight polymer were obtained. When activated with TIBAO a small amount of polymer was obtained which was also similar to that found for catalysts **1** and **3**.

Complex **9** is structurally similar to the other catalysts screened thus far, yet its activity and selectivity was still probed as the presence of the aromatic ring was thought

to possibly induce some substantial electronic change at the metal center. The results obtained when testing this catalyst with MAO were surprising and are shown in Tables 4.3.16 and 4.3.17.

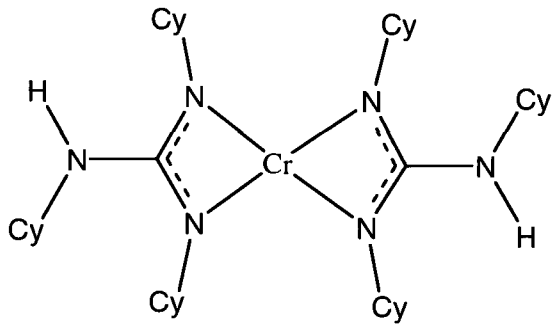

(**8**)

Table 4.3.16 Oligomerization/polymerization activity of catalyst 8[a]

Entry	Cat amt. (μmol)	Co-Catalyst	Al:Cr	Temp. (°C)	P.E. (g)	Alkenes (mL)	Activity (g/mmol·hr)
35	10	MAO	1000	50 (120)	15	42	4620
36	10	TIBAO	1000	50 (55)	1.5	0	150

[a] Conditions : 40 bar ethylene, 100 mL toluene used as solvent, 1 hr. reaction time. [b] water cooling used to control reaction temperature. Trace is less than 300 mg.

Table 4.3.17 Analysis of P.E. and α-olefin product distribution*

Entry	Mlclr Wt. (g/mol)	PDI	C4	C6	C8	C10	C12	C14	C16	C18 ≤
35	593	1.62	6.4	13.2	20.5	16.7	14.8	11.7	9.4	7.3
36	46324	4.21	0	0	0	0	0	0	0	0

* Oligomer distribution given in percentage.

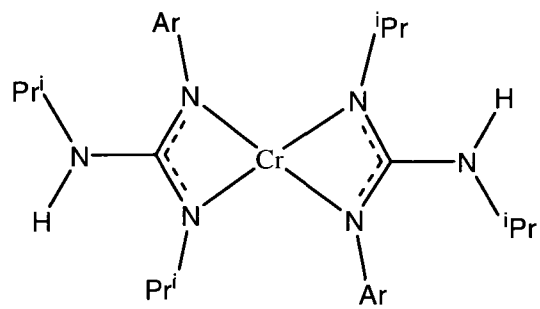

(**9**)

Table 4.3.18 Oligomerization/polymerization activity of catalyst 9[a]

Entry	Temp. (°C)	P.E. (g)	Alkenes (mL)	Activity (g/mmol·hr)
37	50 (58)	6	69	10980
38	50 (110)[b]	trace	22	3200

[a] Conditions : 5 μmol catalyst loading, 1000 eq. MAO, 40 bar ethylene, 100 mL toluene used as solvent, 1 hr. reaction time. [b] water cooling used to control reaction temperature. Trace is less than 300 mg.

Table 4.3.19 Analysis of P.E. and α-olefin product distribution*

Entry	Mlclr Wt. (g/mol)	PDI	C4	C6	C8	C10	C12	C14	C16	C18 ≤
37	543	1.67	13.1	34.9	24.5	12.2	8.2	4.1	2.0	1.0
38	n/a	n/a	6.4	27.1	25.9	16.3	11.2	7.4	3.8	1.9

* Oligomer distribution given in percentage.

The activity of catalyst **9** is very similar to the previous catalysts screened but the effect of temperature on the product distribution is entirely reversed. When the temperature was allowed to rise uncontrollably, a low molecular weight polymer was obtained with all the previous catalysts and the Shultz-Flory distribution was shifted to higher molecular weight α-olefins. In the case of **9** when the temperature rises uncontrolled no polymer is formed. When the reaction temperature is maintained around 60 °C however the same low molecular weight polymer is obtained. These results are surprising and the reasons why this particular catalyst would behave in a completely reversed manner have still not been elucidated. The presence of the aromatic ring clearly plays a significant role as this is the only catalyst to containing an aromatic ring in the ligand backbone.

Complex **10** was quickly screened for its catalytic activity to test the effect of the metal trivalent state. When activated with MAO only a small amount of polymer was obtained (4.3.20 and 4.3.21). A single reaction using TEAL as co-catalyst was performed but no product was formed. The further testing of this catalyst was abandoned as it showed no promise to be a selective trimerization or tetramerization catalyst.

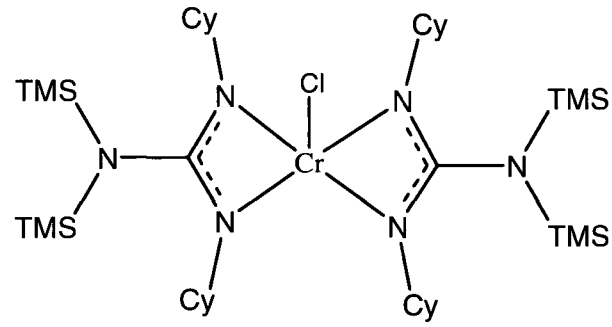

(**10**)

Table 4.3.20 Oligomerization/polymerization activity of catalyst 10[a]

Entry	Cat amt. (μmol)	Co-Catalyst	Al:Cr	Temp. (°C)	P.E. (g)	Alkenes (mL)	Activity (g/mmol·hr)
39	10	MAO	1000	50 (55)	1.5	0	150
40	10	TEAL	200	50	0	0	0

[a] Conditions : 40 bar ethylene, 100 mL toluene used as solvent, 1 hr. reaction time. [b] water cooling used to control reaction temperature. Trace is less than 300 mg.

Table 4.3.21 Analysis of P.E. and α-olefin product distribution*

Entry	Mlclr Wt. (g/mol)	PDI	C4	C6	C8	C10	C12	C14	C16	C18 ≤
39	56937	3.87	0	0	0	0	0	0	0	0

* Oligomer distribution given in percentage.

Complex **14**, containing the thiocarbamate ligand, was screened for catalytic activity to evaluate the effect of different donor atoms (Tables 4.3.22 and 4.3.23). The results were not encouraging and using MAO or TEAL as co-catalyst gave small amounts of a relatively useless polymer.

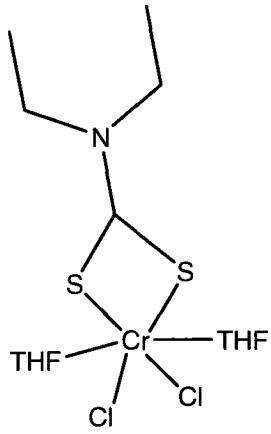

(**14**)

Table 4.3.22 Oligomerization/polymerization activity of catalyst 14[a]

Entry	Cat amt. (μmol)	Co-Catalyst	Al:Cr	Temp. (°C)	P.E. (g)	Alkenes (mL)	Activity (g/mmol·hr)
41	10	MAO	1000	50 (56)	2.1	0	210
42	10	TEAL	50	50 (59)	1.7	0	170

[a] Conditions : 40 bar ethylene, 100 mL toluene used as solvent, 1 hr. reaction time. [b] water cooling used to control reaction temperature. Trace is less than 300 mg.

Table 4.3.23 Analysis of P.E. and α-olefin product distribution*

Entry	Mlclr Wt. (g/mol)	PDI	C4	C6	C8	C10	C12	C14	C16	C18 ≤
41	287401	17.4	0	0	0	0	0	0	0	0
42	341131	13.0	0	0	0	0	0	0	0	0

* Oligomer distribution given in percentage.

The majority of the remaining catalytic testing was aimed at trying to elucidate the nature of the active species responsible for the high activities observed when the chromium (II) guanidinates are activated with MAO.

Complex **17** was tested for its catalytic activity. Since this complex already contains a metal-carbon bond it may act as a self-activating complex, which does not require use of co-catalyst. However, the lack of cationization in this species and the possible robustness of the exceedingly short Cr-Cr bond moderated our expectations. The results of the testing are summarized in Tables 4.3.24 and 4.3.25. Originally it was

thought that this complex was the active species responsible for the Shultz-Flory distribution of α-olefins and polymer obtained when **1** or **3** was activated with MAO. The testing proved conclusively that this is not the case as catalyst **17** does not produce any alkene or polymer when no co-catalyst is used (43 and 44). When activated with MAO (entries 45 and 46), the catalytic activity and selectivity were nearly identical to complexes **1** and **3**. No product was formed when activated with TEAL. BARF is a common reagent used to activate a complex that contains a metal-carbon bond. The role of BARF is to cationize the metal center by removing the alkyl ligand attached to the metal. In this case no product was formed when BARF was used. This could be due in part to the strong agostic interactions occurring between the metal center and the methyl group which does not allow abstraction of the methyl group.

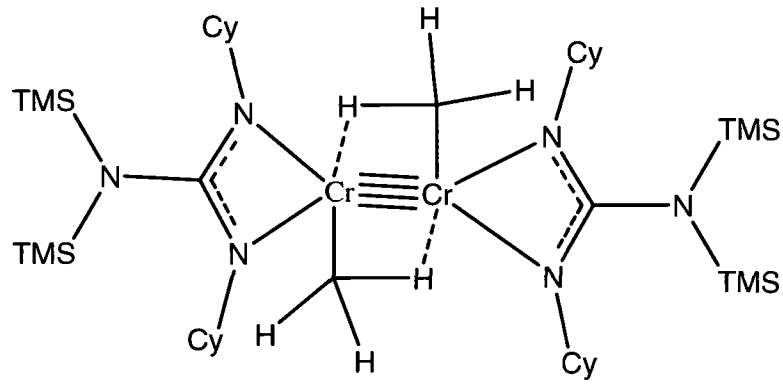

(**17**)

Table 4.3.24 Oligomerization/polymerization activity of catalyst 17[a]

Entry	Cat amt. (μmol)	Co-Catalyst	Al:Cr	Temp. (°C)	P.E. (g)	Alkenes (mL)	Activity (g/mmol·hr)
43	20	none	0	50	0	0	0
44	20	none	0	90	0	0	0
45	10	MAO	1000	50 (127)	10	58	5300
46	10	MAO	1000	50 (78)[b]	trace	132	9390

47	10	TEAL	200	50	0	0	0
48	10	BARF	0	50	0	0	0

[a] Conditions : 40 bar ethylene, 100 mL toluene used as solvent, 1 hr. reaction time. [b] water cooling used to control reaction temperature. Trace is less than 300 mg.

Table 4.3.25 Analysis of P.E. and α-olefin product distribution*

Entry	Mlclr Wt. (g/mol)	PDI	C4	C6	C8	C10	C12	C14	C16	C18 ≤
45	599	1.54	7.9	12.9	19.8	16.9	14.6	11.8	9.0	7.1
46	n/a	n/a	14.9	37.3	20.1	12.8	7.9	3.7	2.4	1.0

* Oligomer distribution given in percentage.

The results of the catalytic testing of **19** are shown in Tables 4.3.26 and 4.3.27. When no co-catalyst was used the catalyst still produced 1g of polyethylene. This polyethylene has the same properties as the polymer obtained when the other catalysts were activated with TIBAO. When this complex is activated with MAO a massive temperature spike occurs which was controlled with water cooling and a Shultz-Flory distribution of α-olefins was obtained. This is similar to all the other Cr(II) guanidinate complexes tested thus far and leads to the conclusion that MAO is still reacting further with these metal-metal bonded dimers to form the actual active catalytic species.

The second metal-metal bonded dimer to be tested was complex **20** (Tables 4.3.28 and 4.3.29). This catalyst again did not perform as a self-activating catalyst and needed co-catalyst to show any catalytic activity. When activated with MAO and the temperature allowed to rise uncontrolled a Shultz-Flory distribution of α-olefins and low molecular weight polymer was obtained with the typical very high activity.

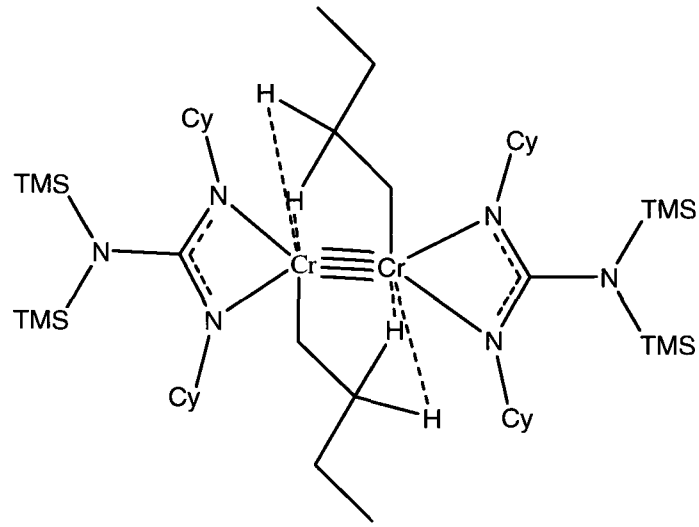

(**19**)

Table 4.3.26 Oligomerization/polymerization activity of catalyst 19[a]

Entry	Cat amt. (μmol)	Co-Catalyst	Al:Cr	Temp. (°C)	P.E. (g)	Alkenes (mL)	Activity (g/mmol·hr)
49	20	none	none	80	1	0	50
50	10	MAO	1000	50 (72)[b]	trace	137	9740

[a] Conditions : 40 bar ethylene, 100 mL toluene used as solvent, 1 hr. reaction time. [b] water cooling used to control reaction temperature. Trace is less than 300 mg.

Table 4.3.27 Analysis of P.E. and α-olefin product distribution*

Entry	Mlclr Wt. (g/mol)	PDI	C4	C6	C8	C10	C12	C14	C16	C18 ≤
49	52869	4.15	0	0	0	0	0	0	0	0
50	n/a	n/a	11.5	37.9	21.4	13.3	7.9	4.7	2.5	0.8

* Oligomer distribution given in percentage.

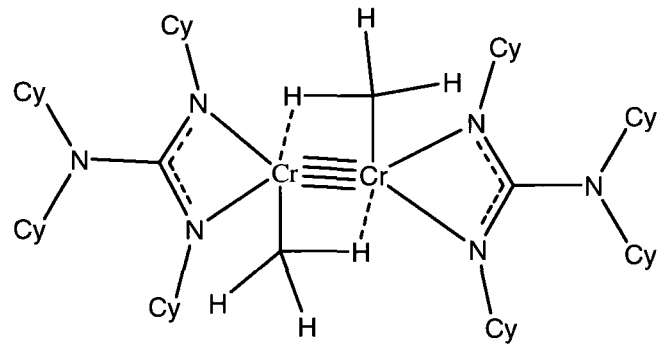

(**20**)

Table 4.3.28 Oligomerization/polymerization activity of catalyst 20[a]

Entry	Cat amt. (μmol)	Co-Catalyst	Al:Cr	Temp. (°C)	P.E. (g)	Alkenes (mL)	Activity (g/mmol·hr)
51	20	none	0	50	0	0	0
52	10	MAO	1000	50 (121)	12	45	3308

[a] Conditions : 40 bar ethylene, 100 mL toluene used as solvent, 1 hr. reaction time.

Table 4.3.29 Analysis of P.E. and α-olefin product distribution*

Entry	Mlclr Wt. (g/mol)	PDI	C4	C6	C8	C10	C12	C14	C16	C18 ≤
52	612	1.39	8.5	13.2	20.1	16.5	13.9	11.7	8.6	7.5

* Oligomer distribution given in percentage.

The oxygen bridged dimer **21** was accidentally obtained through reaction with adventitious oxygen. This small amount of crystalline material was not sufficient for a large scale investigation but it allowed for a small number of catalytic tests to be performed. When activated with MAO a small rise in temperaturewas observed and which stabilized around 75°C. A Shultz-Flory distribution of α-olefins was obtained in good yield. These results are significant since this is the first Cr(III) guanidinate complex that produced a Shultz-Flory distribution of α-olefins. Therefore, it cannot be ruled out that Cr(III) is responsible for the non-selective oligomerization of ethylene. Additionally, the oxygen bridging dimers may offer insight into the nature of the actual active species as MAO contains a large amount of oxygen atoms.

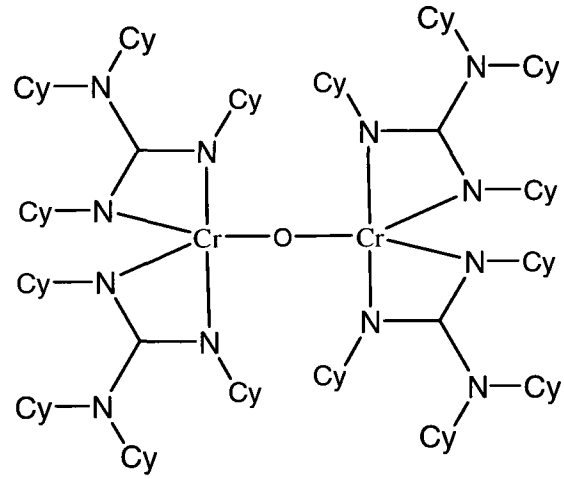

(**21**)

Table 4.3.30 Oligomerization/polymerization activity of catalyst 21[a]

Entry	Cat amt. (μmol)	Co-Catalyst	Al:Cr	Temp. (°C)	P.E. (g)	Alkenes (mL)	Activity (g/mmol·hr)
53	5	MAO	1000	60 (75)	trace	28	4020

[a] Conditions : 40 bar ethylene, 100 mL toluene used as solvent, 1 hr. reaction time.

Table 4.3.31 Analysis of P.E. and α-olefin product distribution*

Entry	Mlclr Wt. (g/mol)	PDI	C4	C6	C8	C10	C12	C14	C16	C18 ≤
53	n/a	n/a	18.7	29.8	20.6	12.1	8.3	6.0	3.0	1.5

* Oligomer distribution given in percentage.

Complex **22** was also tested for catalytic activity as this complex could be reproducibly obtained in good yield and may perform differently from the other Cr (II) guanidinates tested thus far because of the unusual arrangement of the three chromium atoms. The results obtained are shown in Tables 4.3.32 and 4.3.33. When activated using MAO a large temperature spike occurs. What was unusual is that whether or not the temperature was controlled both the low molecular weight polymer and Shultz-Flory distribution of α-olefins were obtained. This is possibly because a number of species are generated in solution. Some species may act in the expected manner where at high temperatures the polymer forms. Some of complex **9** may also be formed which has already been shown to perform in the reverse manner as the other catalyst producing the low molecular polymer at low temperatures.

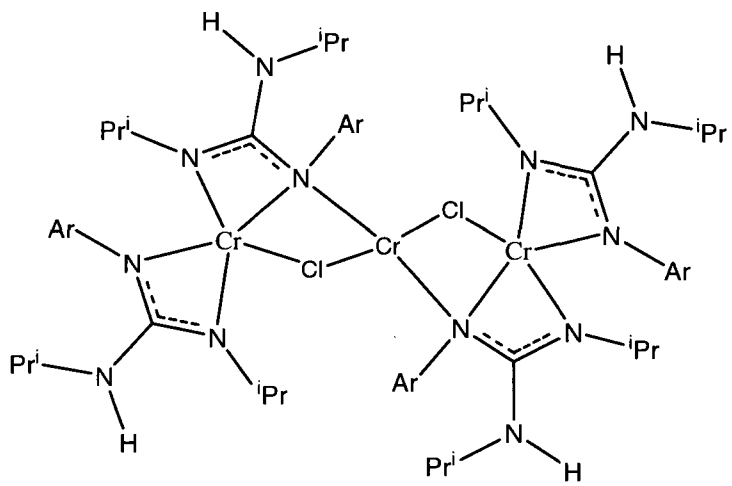

(**22**)

Table 4.3.32 Oligomerization/polymerization activity of catalyst 22[a]

Entry	Temp. (°C)	P.E. (g)	Alkenes (mL)	Activity (g/mmol·hr)
54	50 (86)[b]	3.1	54	8380
55	50 (107)	7.0	22	4560

[a] Conditions : 5 μmol catalyst loading, 1000 eq. MAO, 40 bar ethylene, 100 mL toluene used as solvent, 1 hr. reaction time. [b] water cooling used to control reaction temperature. Trace is less than 300 mg.

Table 4.3.33 Analysis of P.E. and α-olefin product distribution*

Entry	Mlclr Wt. (g/mol)	PDI	C4	C6	C8	C10	C12	C14	C16	C18 ≤
54	524	1.53	9	33.4	21.0	14.8	10.4	6.9	3.0	1.5
55	589	1.45	7.3	23.8	26.7	16.1	11.2	7.4	4.8	2.8

* Oligomer distribution given in percentage.

Complex **23** is a trivalent organochromium species. It was screened for catalytic activity and the results are summarized in Tables 4.3.34 and 4.3.35. No product of any kind was obtained when no co-catalyst was used to activate the complex. However when activated with MAO a low-temperature spike occurred which stabilized around 75°C. The reaction produced a Shultz-Flory distribution of α-olefins and only a trace amount of polymer.

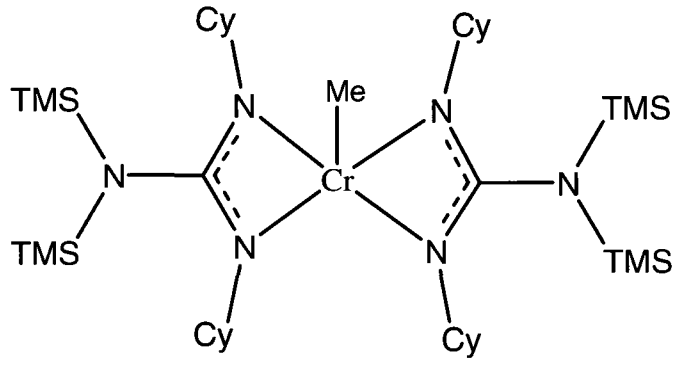

(**23**)

Table 4.3.34 Oligomerization/polymerization activity of catalyst 23[a]

Entry	Cat amt. (μmol)	Co-Catalyst	Al:Cr	Temp. (°C)	P.E. (g)	Alkenes (mL)	Activity (g/mmol·hr)
56	20	none	0	70	0	0	0
57	5	MAO	1000	60 (77)	trace	22	3200

[a] Conditions : 40 bar ethylene, 100 mL toluene used as solvent, 1 hr. reaction time. [b] water cooling used to control reaction temperature. Trace is less than 300 mg.

Table 4.3.35 Analysis of P.E. and α-olefin product distribution*

Entry	Mlclr Wt. (g/mol)	PDI	C4	C6	C8	C10	C12	C14	C16	C18 ≤
57	n/a	n/a	6.3	23.8	23.5	17.1	14.2	8.3	4.7	2.1

* Oligomer distribution given in percentage.

The nickel complex synthesized in Chapter 2, complex **15**, was tested for catalytic activity using the same reaction conditions as used above for the chromium complexes. Unfortunately the two runs attempted, one with MAO co-catalyst and one with TEAL, produced no polymer or short chain α-olefin. The testing of this complex is far from complete and a few more experiments may need to be performed to conclusively say this complex cannot perform as a catalyst.

4.4 Conclusions

The systematic testing carried out on the family of Cr(II) and Cr(III) guanidinate compounds with or without preformed organometallic function has yielded a rather precise picture of the chemical behavior of this family of catalysts. While blank reactions performed on simple ligand-free chromium salts showed a totally different behavior, it is true that all the complexes tested in these studies gave remarkably similar catalytic performances, regardless of the ligand substituents, metal oxidation states and presence/absence of preformed organochromium functions. In turn, this clearly indicates that the large variety of complexes prepared in this study simply provides different ways to feed the same catalytically active species into the catalytic cycle. Although this clearly frustrated the original quest for selective trimerization or tetramerization catalyst and even the search for single component catalysts, we were delighted to observe an unprecedentedly high catalytic activity for producing a statistical distribution of oligomers. The enormous reactivity observed in some of the runs as well as the very minor amount of solid residues makes our discovery promising for industrial applications.

The lack of selectivity in the oligomerization process speaks for the lack of ability of this ligand system to support monovalent chromium intermediates. Although this may seem to be contradicted by the recent crystal structure of Cr(I) guanidinates bearing the shortest ever observed Cr-Cr contact, the stabilization of these species is possible only via a delicate balance of ligand backbone steric repulsions. The ligands that we have employed are clearly too bulky to support *monovalent* dinuclear species. Multiplied bonded dimers can be obtained only with the additional presence of bridging alkyls and whose presence appears to be crucial to the stabilization of these systems. In the absence of those functions, disporportionation is most likely triggered towards metallic chromium and higher valent compounds ready to re-enter the catalytic cycle of unselective oligomerization. Furthemore, this suggests the intriguing idea that the quest for ligand systems capable of selective oligomerization should be directed towards the employment of neutral rather than anionic ligands, unless a zwitterionic structure may be introduced. Guanidinates clearly failed this second possibility by having shown the ability to be

extracted to some extent by alkyl alumiun reagents but not forming heterobimetallic structures.

Although the desirable monovalent state has not been achieved, yet, we have proven that divalent compounds are responsible for an enormous activity in cleanly producing a statistical distribution of oligomers. In turn, these findings have generated a new project aiming at the immobilization of guanidinate complexes on surfaces to build unprecedented heterogeous oligomerization catalysts. Therefore, we can confidently conclude that this master thesis has been crown with success.

4.5 References

1. Friedel, R.A. and R.B. Anderson. *Journal of the American Chemical Society*, **1950**. *72*, 2307.

2. Schulz, G.V., Z. *Phys. Chem*, **1935**, 379.

3. Flory, P.J. *Journal of the American Chemical Society*, **1936**, 58, 1877.

4. G.P. van der Laan and A.A.C.M. Beenackers, *Catal.Rev.-Sci.Eng.* **1999**, *41*, 255.

5. (a) Oguri, M.; Mimura, H.; Aoyama, H.; Okada, H.; Koie, Y. *JP* 11,092,407, Tosoh Corporation, **1999**. (b) Murakita, S.; Yamamoto, T.; Okada, H.; Osamu, Y. *JP* 2,001,149,788, **2001**. (c) Briggs, J. R. *US-A* 4,668,838, Union Carbide, **1987**. (d) Araki, Y.; Nakamura, H.; Nanba, Y.; Okano, T. *US-A* 5,856,612, Mitsubishi Chemicals, **1997**. (e) Kohn, R. D.; Haufe, M.; Kociok-Kohn, G.; Grimm, S.; Wasserscheid, P.; Keim, W. *Angew. Chem., Int. Ed.* **2000**, *39*, 4337. (f) Briggs, J. R. *J. Chem. Soc. Chem. Commun.* **1989**, 674. (g) Emrich, R.; Heineman, O.; Jolly, P. W.; Kruger, C.; Verhovnik, G. P. J. *Organometallics* **1997**, *16*, 1511.

6. (a) K. H. Theopold, *J. Am. Chem. Soc.* **2005**, *127*, 1082; P. A.White, J. Calabrese, K. H. Theopold, *Organometallics* **1996**, *15*, 5473. (b) K. Albahily, S. Gambarotta, et al. *Angew. Chem. Int. Ed.* **2008**, *47*, 5816 . (c) Amir Jabri, Chris B. Mason, Yan Sim, Sandro Gambarotta, Tara J. Burchell, and Robbert Duchateau *Angew. Chem. Int. Ed.* **2008**, *47*, 9717.

7. (a) E. Y.-X. Chen, T. J. Marks, *Chem. Rev.* **2000**, *100*, 1391 (b) J.-N. PMdeutour, K. Radhakrishnan, H. Cramail, A. Deffieux, *Macromol. Rapid Commun.* **2001**, *22*, 1095 (c) M. Bochmann, *J. Organomet. Chem.* **2004**, *689*, 3982.